Laboratory Characterization of Income Generating Appliances

A Study to Further Minigrid Development

Authors:
Factor[e] Ventures
The Energy Institute at Colorado State University

Contents

1. Executive Summary 1
2. Background 2
3. Purpose 4
4. Laboratory Test Results 8
   4.1. Stick Welder – A One Page Summary 8
   4.2. Detailed Stick Welder Results 10
   4.3. Multi-Purpose Mill – A One Page Summary 13
   4.4. Detailed Multi-Purpose Mill Results 15
   4.5. Solar Water Pump – A One Page Summary 18
   4.6. Detailed Solar Water Pump Results 20
5. Appendix 22
   5.1. Stick Welder Test Methods 22
   5.2. Stick Welder Test Report 39
   5.3. Multi-Purpose Mill Test Methods 72
   5.4. Multi-purpose Mill Test Report 101
   5.5. Solar Water Pump Test Methods 130
   5.6. Solar Water Pump Test Report 161

1. Executive Summary

Energy is central to human development and limited access to modern electricity remains a fundamental challenge to progress worldwide. Roughly three in ten people on the planet are unable to meet even their most basic needs like lighting, cooking, and phone charging let alone power productive activities to grow their incomes. Income generating appliances (IGAs) can be an important driver of rural development across off- and weak-grid environments. However, there are many differences in terms of technology, energy requirements, cost, and use between power and appliances that improve quality of life and power and appliances that generate income.

Both for this potential and because of the hope that IGAs can drastically improve the minigrid business model by increasing revenues, these appliances have generated particular interest among proponents of minigrids.

> *The minigrid business is challenging; no one has really quite figured it out yet. To boost average revenue per connection, we're doing some thinking about productive use appliances.*

Lean in to any conversation in the energy access sector and you have probably heard something like this sentence. The hope –that needs to be validated – is that increased revenues from IGAs will increase project profitability, which will make the minigrid sector more attractive for investment and, therefore, accelerate the pace of rural electrification around the world.

At the moment, however, these higher-power appliances are rarely connected to remote, renewable minigrids. Their technical characteristics, utilization patterns, and potential financial and technical impact on the minigrid are unknown or not well understood. In contrast, end users are generally familiar with consumer electronic appliances (lights, TVs, fans) and minigrid developers are comfortable deploying them. What do these appliances all have in common? They are low-cost and efficient thanks to advances in solid-state technology. These simple devices don't require much technical know-how, however the economic benefit of these appliances is often indirect.

In this study, Factor[e] Ventures and The Energy Institute at Colorado State University (CSU) sought to demystify appliances that have a *direct* economic benefit to the end user, because these appliances are often unelectrified even in villages where a minigrid is present. To begin unpacking the opportunity and challenge of IGAs, high fidelity laboratory testing and evaluations were conducted on three appliances; an informal stick welder, multi-purpose agricultural mill, and solar powered water pump.

Through this study, key attributes were discovered that influence how (or whether) these appliances should be incorporated into decentralized, renewable power systems and robust descriptions of their characteristics were created. Key performance characteristics were also identified that, along with appliances' energy requirements, factor into decision-making about supporting particular IGAs.

2. Background

There are several, technical concepts – expressed by minigrid developers and others that this study has identified independently – which the appliance testing aims to capture. The impacts of these technical concepts are applicable to the power system as well as the appliance itself. The concepts describe characteristics that generally make appliances less efficient and less friendly to a renewable energy system, which ultimately causes problems and economic drag for the appliance and/or power system operator.

Technical Concepts Applicable to Income-Generating Appliances:

1. *In-rush current:* Motor-driven appliances typically feature a significant and temporary current draw when the appliance is switched "on". This condition can last for less than a second and up to several seconds as the motor ramps up to its operational speed. The current drawn can be up to 6 times the value expected during operation, and therefore has potential to harm a power system in several ways, including:
    a. Exceeding a limit within a smart meter, which causes the appliance to shut off abruptly before it can start properly.
    b. Exceeding the time limit within which an inverter can sustain a maximum current output, which could cause the inverter to turn off and effectively shut the entire minigrid system down.
    c. Overheating the appliance motor, which – over repeated use – can cause degradation of internal insulation, poor efficiency, or even a short, which leads to motor and appliance failure.

2. *Peak Current (Generic):* All appliances have the potential for a maximum current draw that exceeds the current draw during "steady-state" operation. Peak currents can be caused by putting too much grain into a mill at one time or by a water pump sucking up muddy or silty waters. Whatever the event, the appliance will need to pull more current to achieve the task at hand. Appliances were tested for peak current conditions because peak currents occur frequently in real life. In certain instances, peak current may exceed the operating limits of power system equipment.

3. Power Factor: Power factor, a unitless value between 0 and 1, is a way to characterize the amount of electricity a grid needs to provide to an electrical device in order for that device to be functional. For basic electrical devices such as filament lightbulbs and resistive heating elements the amount of electricity that is converted into useful work is the same amount of electricity that is supplied by the grid. Using these types of devices does not lead to any 'waste' electricity. If a lightbulb operates at 10 watts, then the grid must provide only 10 watts. The total power consumed in this scenario is defined as 'Real Power' and always results in a power factor of 1. A power factor of 1 is the universal goal for all electrical devices.

    For electrical devices that have a motor, Real Power is consumed along with 'Reactive Power'. Reactive Power is wasted electricity that is required to magnetize a motor and get that motor started. Demonstrated in Figure 1, as Reactive Power increases, power factor moves closer to 0.

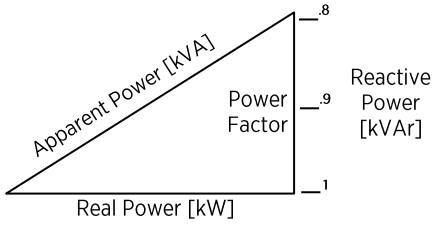

Figure 1. Power Factor Illustration

In summary, minimizing reactive power consumption by appliances will move power factor closer to 1 and reduce the amount of "extra" electricity a grid needs to provide to ensure appliance functionality.

4. Current Total Harmonic Distortion (THD): Current THD is a way to quantify an electrical device's impact on a grid's power quality. If an appliance's THD is above an acceptable threshold defined by the power system industry, then the grid could suffer. Localized current distortion at an appliance can cause distorted voltage drops all along the power system. Since voltage is common across all grid users, the distortion at a single appliance ripples outwards leading to losses and potential disruption of electrical devices. Over time, increased temperatures and interference can greatly shorten the life of electronic equipment and cause damage to power systems.[1]

   For example, a mill is designed to operate between 216-280 VAC, ± 10% of the nominal 240 VAC rating. When voltage is supplied to the appliance outside of that voltage range, the motor may run hotter, potentially reducing its operation and service life.

5. *Power consumption variability:* Over the period of operation, certain appliances will consume a relatively constant amount of power while others will consume varying amounts of power. To slowly irrigate a field, a pump may run for several hours, providing a constant flow rate of water and consumption of power. When running an agricultural mill, power consumption will dip between grain loadings, leading to moderate power consumption variability. Welders are an extreme case, where power consumption may jump from 0 to max power in a fraction of a second and back down to 0 within another second.

   Predictable and constant power consumption is preferred, allowing for the deployment of a combination of generation assets at different parts of the day. However, when extreme demand variability is introduced, a power system may struggle to respond quickly. While solid state power system equipment (solar panels and batteries) respond to power consumption nearly instantaneously, rotational assets (hydro, wind, diesel generators) take time to ramp up and respond. If relying only on the rotational assets to respond to high appliance loads that kick on, variability may cause specific appliance inoperability and potentially shut down of the grid.

6. *Overloading:* Overloading is an important issue to an appliance owner. It is the product of poor design or operation of an appliance. Often, an electrical motor is matched with hardware that leverages the motor to perform useful work. If the matched hardware or method of operation (often these two variables are directly linked) causes the motor to pull more current than the motor is rated for, the motor may generate excess heat, reducing its operation and service life.

7. *Efficiency:* An electrical device's efficiency can be defined by the ratio in which the device converts electrical power to useful work. For a pump, efficiency can be the conversion of electrical power to hydraulic power and for a mill, efficiency can be the conversion of electrical power to mechanical power. Low efficiency values demand a grid provide more power to complete the same amount of work. By improving electrical device efficiencies, a grid with a set amount of generation capacity can serve a larger number of appliances.

[1] Associated Power Technologies, *Total Harmonic Distortion and Effects in Electrical Power Systems*, source: https://www.aptsources.com/wp-content/uploads/pdfs/Total-Harmonic-Distortion-and-Effects-in-Electrical-Power-Systems.pdf, accessed November 2018.

3. Purpose

The purpose of identifying appliance characteristics is two-fold:

1. To establish an over-arching approach along with open-access test methods especially attuned to the technical concerns of minigrid developers and appliance retailers selling into the off-grid or weak grid market.
2. To test representative appliances and uncover critical technical information that has not been available to-date. These preliminary appliance characteristics should inform in-market pilots and can begin to fill in knowledge gaps currently preventing the sale or support of IGAs in the rural context.

At the beginning of this study, Factor[e] conducted 18 interviews on productive use appliances with minigrid developers and appliance manufacturers. These stakeholders indicated the appliances they support (depicted in blue in Figure 2 below) and the appliances they are seeking to support (in orange). The chart indicates the number of interview subjects supporting and expressing their desire to support each appliance. As a result of these interviews, the study paid special attention to appliances that interviewees indicated they wished to support and prioritized lab testing for these appliances in particular.

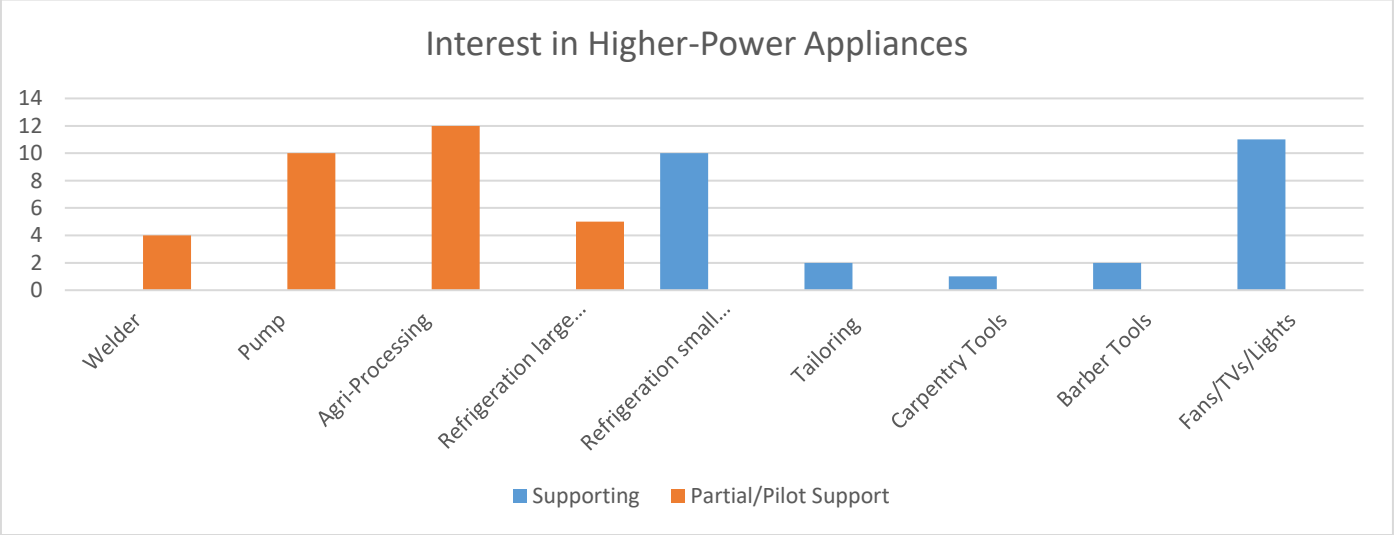

Figure 2. Interest in Higher-Power Appliances

In the course of interviews with minigrid and appliance developers, mills, welders, and water pumps were consistently raised as problematic to power. The following are testimonials and synthesized remarks from developers and appliance retailers.

Milling machines

> *To keep customers happy with the grinding/milling time at the posho mill, we ideally want to replace a diesel-powered mill with an electric mill of comparable size. However, the power requirement can be exceeded easily.* – East African Minigrid Developer

There is a large in-rush current associated with this type of mill. Is there anything we can do to innovate around the size, mechanical action, or power electronics to help make the operation straightforward? – Indian Minigrid Developer

Our system is a closed, off-grid system, and we want to know how a mill will perform in "weak grid" conditions before deploying in the field. – Stand-alone solar mill company

Milling activities usually happen in large business that are not close to the community. – Indian Minigrid developer

There is a steep learning curve when it comes to motors; that's why it's such a challenge to support the higher-power appliances – East African Minigrid Developer

Welders

The in-rush current and continuously varying arcing involved with this appliance prohibits us from powering it. – Multiple East African Minigrid Developers

Most of the welders in these communities don't have name plate ratings as they are handmade, which makes it very difficult for us to power them from our grid. – East African Minigrid Developer

After much trial and error, we finally found a productized welder that works on our grid. – East African Minigrid Developer

Pumps for drinking water or irrigation

Pumps have some in-rush current problems, but not as significant as welders or milling machines. However, they are often placed far away from the power supply, and the voltage drop over the distribution line results in poor voltage quality at the pump. We need to understand performance under these conditions. – East African Minigrid Developer

It's not clear if I need to spend more money on a well-established brand to achieve good efficiency; I would like to use a Variable Frequency Drive (VFD), but they are very expensive. – Sub-Sahara African Minigrid Developer

There is a 5HP pump I would like to power, but I have no idea how it will behave, and I cannot guarantee that it will not trip my grid. – India Minigrid Developer

I'm currently sourcing a pump locally, and it would be good to know what other types of pumps would be sufficiently efficient for our customers. – Appliance Distribution Company

What is the optimal configuration? A DC pump with a rectifier, or an AC pump with a VFD? – Question Posed Across the Energy Access Sector

In order to begin to answer some of these questions, Factor[e] looked for readily-available information about these sector-relevant appliances. However, for each category, major information gaps or barriers were found that created confusion or uncertainty around the procurement, sale, or electrification of such appliances.

Appliance	Main Barrier or Information Gap	Result
Hand-built welder	Un-rated, unknown characteristics.	Powered by diesel gensets; are not electrified and remain unconnected to minigrids.
Industrially-manufactured welder	Unclear performance comparison to existing hand-built welders; no established brand recognition or preference; unclear performance advantage over hand-built welders, unclear justification for price difference.	New welders would have to be procured specially, but customer acceptance and value proposition to minigrid developer is unclear. The result of this uncertainty and separate procurement process is that such welders generally don't reach rural communities.
Diesel-powered grain mill	Specifications and performance are relatively unknown except if measured at site.	Powered by diesel engines; are not electrified and remain unconnected to minigrid.
Electrically-powered grain mill	Largely absent from off-grid markets and so no brand or performance differentiation; most electric mills are manufactured in China and procurement is not obvious to minigrid operators and appliances suppliers; both Chinese and East African electric mills lack reliable performance characteristics.	Starting to see units in the field, but there is limited technical knowledge about sizing and operating machines effectively (trial and error, mostly error, approach at the moment); unclear what motors and mills should be procured.
Solar-powered water pump	Different or unknown testing methods for determining power/energy consumption at varying levels of pumping performance; installations are distributed and so generally require their own power source or robust transmission infrastructure.	Pumps are rarely connected to minigrids either because the services are hard to monetize without adopting the full business model of pump seller and financier, the required transmission infrastructure is not built out, and/or because the energy consumption, power required, and ancillary equipment (e.g., VFD) is not well-understood; stand-alone solar pumps are becoming more common, but require distribution, finance, and after sales support and meaningful behavior change.

Table 1. Table of Appliance Information Gaps

As a result of these information gaps, Factor[e] and The Energy Institute at CSU set out to shed some light on IGA information. The remainder of the report details the laboratory findings of appliance testing at both a consumable and detailed level. The test methods and corresponding test report for each of the three appliances were compiled and are located at the end of the report due to their length. The test reports contain reference information in the Appendix to a full record of raw data collected during testing.

4. Laboratory Test Results

4.1. Stick Welder – A One Page Summary

Stick Welder

(Shielded Metal Arc Welder)

Date of test:	7/2018
Lab Name:	CSU Energy Institute
Lab Location:	Fort Collins, Colorado

Appliance Description

This stick welder is a hand-built, step-down transformer acquired in Kigali, Rwanda, and is commonly found throughout SSA. The primary purpose of the welder is to aid in steel fabrication and assembly. The core consists of thin steel laminations pressed together with two wood blocks at the top and bottom. The windings are insulated using cellulose, such as electrical kraft or crepe paper. The primary winding is copper and the secondary winding is aluminum with a fixed turns ratio. Contrary to commercial stick welders with adjustable voltage and controllable air gap between windings, this welder's fixed turns ratio produces a constant voltage and variable current.

Key Appliance Manufacturer Ratings

List Price (Rwandan Francs/USD):	98,000/112
Input Supply Voltage (VAC):	Unrated
Average/Peak Current (A):	Unrated
Average/Peak Real Power (kW):	Unrated
Duty Cycle:	Unrated
Efficiency (%):	Unrated

Steel Laminations Average Length (mm) = **74.8**

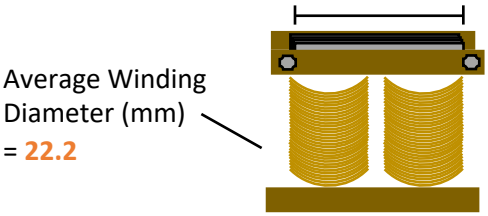

Modes of Operation Tested

Short Arc — Stronger Penetration

Long Arc — Weaker Penetration

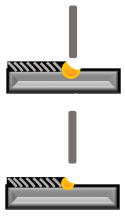

Lab Test Parameters	Short Arc	Long Arc
Supply voltage, avg [V]	208	208
Supply current, avg. [A_{RMS}]	24.1	18
Supply current peak [A]	62.8	60.1
Real power, avg [kW]	3.2	2.5
Reactive power, avg [kVAR]	3.8	2.6
THD, supply current (%)	8.8	6.5
Supply power factor	0.64	0.69
Throughput (Wh/cm)	3.8	2.7
Efficiency (%)	71.2	75.7
Turns Ratio	4.25	
Duty Cycle (% of 10 mins @ 25A)	25	

Short Arc Power

A short arc has a more consistent power profile and higher average and peak current. This is due to a stronger connection between the electrode and steel. Compared to longer arc welds, short arc welds demonstrate a more predictable load.

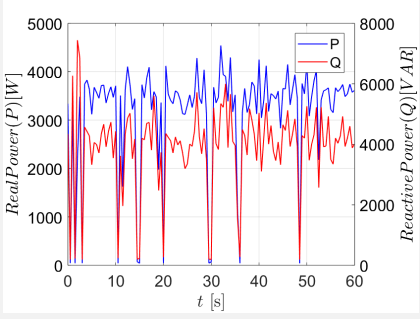

Long Arc Power

A long arc creates an intermittent connection between the electrode and steel, resulting in highly variable power. This can cause issues in power systems with inertial generation. Without proper visibility equipment, long arc welds may be more common.

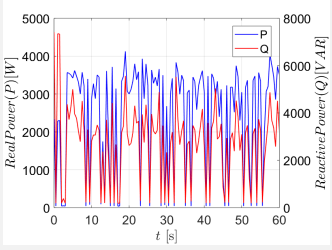

**The data and observations within this page are specific to informal hand-built welders and may not translate to commercial welders.*

4.2. Detailed Stick Welder Results

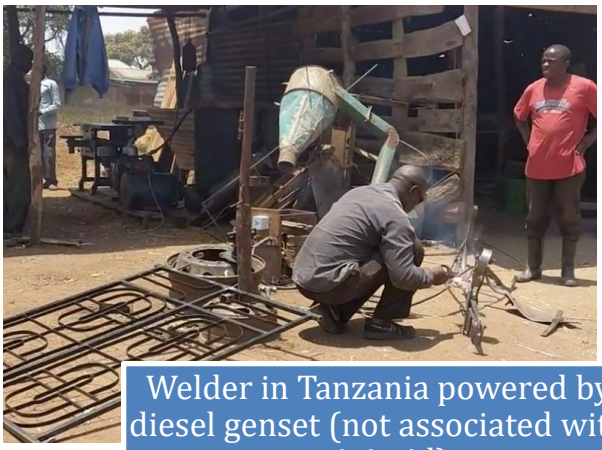

Welder in Tanzania powered by diesel genset (not associated with minigrid)

Welder testing in the CSU Energy Institute

Laboratory characterization of this hand-built stick welder revealed that the appliance *can* be supported on a minigrid or stand-alone system with the proper know-how. The biggest barrier for electrification is the fact that hand-built welding machines do not come with nameplate ratings. Each welder is slightly different, and the characteristics may vary depending on its construction (material, dimensions, etc.). Therefore, an industrially manufactured stick welder may be preferred for consistency. However, users of hand-built welders claim they are very durable, and last much longer than other welding machines.

A note on accuracy: To some extent, welder dimensions and materials may change the observed power parameters. The overall insights presented below are likely to translate to hand-built welders of different sizes, but that would require further investigation to confirm.

Recommendations for Minigrid Operators and Appliance Retailers: Hand-built welding machines can be supported by renewable energy systems. To do so most profitability, operators may consider 1) investing in trainings on welding practice and arc strength with hand-built welders for local businesses, 2) developing and communicating pricing schemes that incentivize good welding practice, 3) pairing hand-built welders with power factor correction devices, and 4) deploying smart control systems so that this load is served by batteries in a generation system, which can respond immediately to large variation in power consumption.

The performance findings here only give insight into the performance of hand-built transformer welders, and is not a comparison to industrially-manufactured welding machines.

Findings:

1. **In-Rush Current** – This appliance does not generate in-rush current since it is not motor-powered.
    a. **Proposed Resolution** – No remedial action is needed.
2. **Peak Current** – During normal operation, this appliance frequently reached a maximum value of 61 Amps, which is nearly three times the steady state average current draw of 21A. This amperage might exceed a smart meter's threshold, even if it is designed for "commercial use." Exceeding the rating of the smart meter could cause the meter to shut off. Additionally, this appliance could exceed the output limits of the system inverter, which could cause a grid-wide shut-down.
    a. **Proposed Resolution** – Check that current draw does not exceed ratings of other power system equipment before connecting. Use a hand-held multi-meter with a clamp to measure voltage and current draw of the hand-built welder during operation while connected to an alternate power source (e.g. a generator).
3. **Power Factor** – This hand-built welder has a poor power factor of about 0.66 likely due to its construction. As a result, the welder may cause a low power factor at the inverter, which might be lower than the operating threshold of the inverter. Additionally, a diesel generator trying to export power to an appliance with a low power factor may cause parts of the generator to wear out prematurely. Lastly, serving low power factor loads ultimately reduces the revenue collected per unit of electricity generated (per the above discussion on power factor).
    a. **Proposed Resolution** – Add a power factor correction (e.g., correction capacitor) device to bring the welder power factor up to a level that meets power system requirements.
4. **Total Harmonic Distortion** – the measured THD was reasonable and lower than expected for an informal machine. The measured value was between 6.5-8.8%, relatively close to the most conservative power system industry recommendation of max 5% THD.[2]
    a. **Proposed Resolution** – No resolution needed.
5. **Power Consumption Variability** – This particular welder exhibited extreme power consumption variability (Figure 3) due to its construction and the way in which operators use it. This erratic profile is a problem because diesel generators are not able to instantly respond to large power draw. As mentioned above, rotational generators need time to "spin up" before they can dispatch power. Since most hand-built welders feature similar construction and mode of operation, other hand-built welders are expected to carry a similar power consumption characteristic.
    a. **Proposed Resolution** – Battery systems have the capability to respond to instantaneous demand. To ensure reliable operation, the demand can be met by energy in the battery bank, and the diesel generators can recharge the batteries as-needed. Additionally, make sure that welder operators have proper protective equipment so he/she can properly see their work. An appliance retailer should train the welder on how to use short-arc welding methods to minimize the power variability.

[2] IEEE Std 519-1992, IEEE Recommended Practices and Requirements for Harmonic Control in Electrical Power Systems, New York, NY: IEEE.

A note on construction: Due to the simplistic construction of these welders, a significant difference compared with industrially manufactured welders is a lack of voltage control. Commercial welders often include the ability to vary the turns ratio, effectively allowing the welder to operate at varying voltages with constant current. The hand-built stick welder has a fixed turns ratio and as such is a constant voltage machine, causing current draw to be dictated by the length of the weld arc. A lack of proper welder operator equipment and training in the context of most rural industry often leads to an inconsistent weld arc length. This inconsistency results in significant variations in current over short periods of time.

Compared to an AC induction motor (provided for illustration in the third graph in Figure 3), the load profile for the informal welder is highly erratic. In the absence of the voltage control that comes with industrially manufactured welders, the load profile of a hand-built welder may be partially dictated by a user's capacity to maintain a strong weld arc (level of variability is lower for a strong short weld arc vs a weak long weld arc).

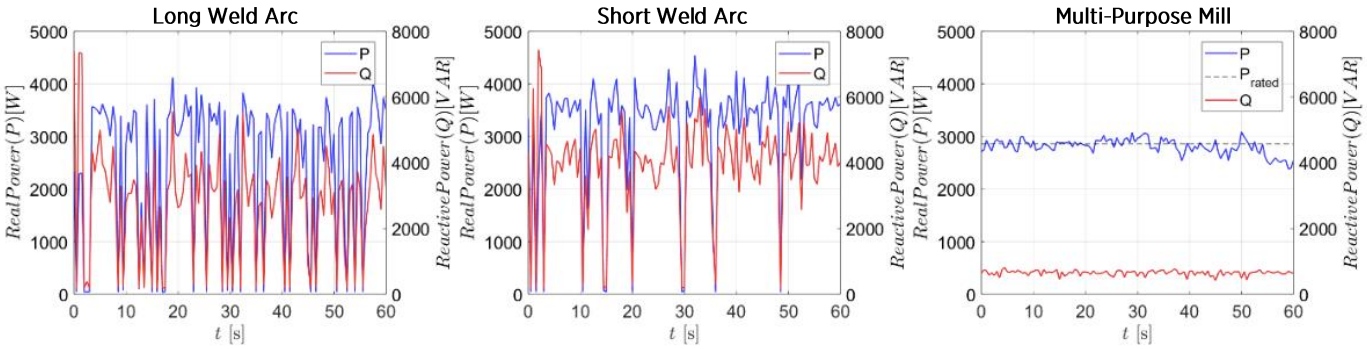

Figure 3. Welder: Power Variability over Time

4.3. Multi-Purpose Mill – A One Page Summary

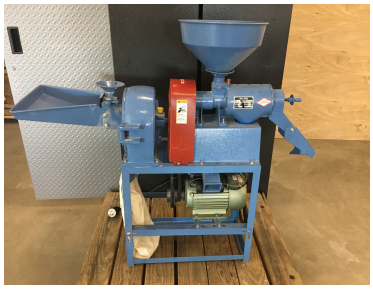

Multi-Purpose Mill

Date of test: 10/2018

Lab Name: CSU Energy Institute

Lab Location: Fort Collins, Colorado

Appliance Description

This appliance is a dual purpose electric rice huller and hammer mill acquired from a manufacturer in China. The primary purpose of the mill is to increase crop value through modes of processing. The rice huller portion removes the indigestible hull from a grain of rice and the hammer mill pulverizes grain into flour. For ease of use, an adjustable hopper allows for controlled grain input into the machine. The body of the machine is powder coated sheet metal and angle iron with die-cast components. This mill is driven by a capacitor enabled AC single phase motor coupled with a standard v-belt and pulley configuration.

Key Appliance Manufacturer Ratings

Manufacturer:	Sichuan Jingyan Lianyi Machine Factory	Rated Current (A):	13.7
Model Number:	6N40-9FQ21	Hammer Mill Rated Throughput (kg/hr)	≥300
List Price (USD):	$253	Rice Huller Rated Throughput (kg/hr)	≥150
Motor Voltage Rating (VAC):	220	Rated Speed (RPM)	2800
Motor Rating (kW/hp)	2.2/3	Electrical to Mechanical Efficiency (%):	77
		Rated Power Factor	0.95

Modes of Operation Tested (hammer mill function only)

Hammer Mill Coarse Screen

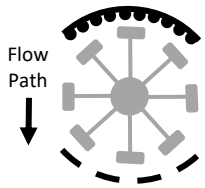

Higher throughput & Lower energy intensity

Hammer Mill Fine Screen

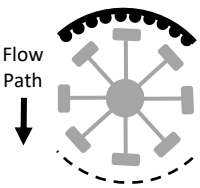

Lower throughput & Higher energy intensity

Lab Testing Parameters	Coarse	Fine
Supply current, avg. [A_{RMS}]	10.9	13.7
Steady state current, peak [A]	13.7	19.2
Transient current, peak [A]	40-60	40-60
Real power, avg [kW]	2.4	2.9
Reactive power, avg [kVAR]	0.57	0.55
Total Harmonic Distortion, supply current (%)	14.3	-
Supply power factor	0.970	0.982
Throughput (kg/hr)	324	231
Energy Intensity [Wh/kg]	7.3	12.7

Grain Size Distribution

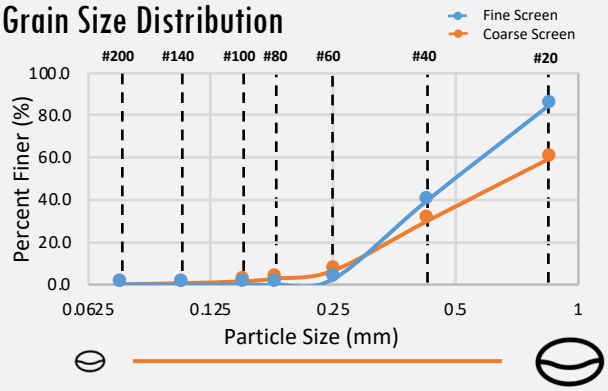

Power

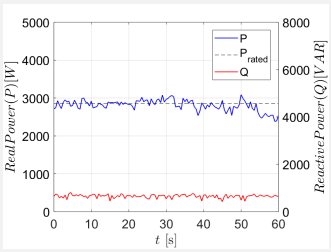

The power the mill consumed during testing conformed with the manufacturer rating and produced a consistent and predictable load profile. Inrush current of ~35A was recorded at 100 V and 50 Hz, which needs to be validated at 220V but could be mitigated with ancillary equipment.

4.4. Detailed Multi-Purpose Mill Results

Testing production and electrical characteristics at CSU

Milled maize resulting from mill testing at CSU

Laboratory characterization of the multi-purpose mill produced data for manufacturer rating comparisons and highlighted a few advantages of this electric mill over its conventional diesel counterpart. First, the efficiency and productivity of the mill far exceeded expectations, which were based on observing the performance of mills powered from 24HP diesel engines. The Lianyi maize mill tested was powered by a 2.2kW motor and has a similar milling throughput (280-300kg/hr) as a mill commonly driven by diesel engines in emerging markets. Although the quality (primarily in terms of fineness) of the milled grain needs to be further evaluated, there is compelling evidence that the large diesel engines often found in-market may be over-powered for the task at hand. As such, the engines may be operating far below their full rated load, significantly reducing efficiency.

Furthermore, this particular appliance can run two different agri-processing functions using a single electric motor in a compact form factor. Only the hammer mill operation was tested, but the appliance also has a crushing / grinding function for removing grain hulls. During in-market on field visits, several posho mill operators were observed to have a single diesel engine from which they operate two milling machines. They often need to switch the belt that connects the engine to the mill several times per day. In contrast, the milling function on the Lianyi machine is simply changed with a flip of a switch.

Recommendations for Minigrid Operators and Appliance Retailers: Smaller, electrically-powered mills may be able to effectively replace large, diesel-engine mills without sacrificing performance or quality of milled product. Electric-powered mills need to overcome the stereotype that they have a lower throughput or a poorly milled product. To overcome these challenges, minigrid operators are encouraged to connect one of these mills to an islanded minigrid or stand-alone power system and demonstrate its capability. Part of the exercise may be to ensure that the quality of the milled cereal meets customer expectations, and is at least, indistinguishable from the product milled by an incumbent diesel-powered mill. The other part of the exercise may be to validate and demonstrate the energy efficiency so that mill operators can be convinced that they can run a more profitable, reliable, and easier operation than with a diesel engine.

Findings:

1. **In-Rush Current** – Without any ancillary equipment between the power supply and appliance, the motor in the mill exhibited significant in-rush current. The in-rush current was likely 4 times the normal (or "steady state") operating current and tripped the testing equipment that was used to supply power. Due to equipment limitations, a specific value could not be identified, but was over 41Amps. Therefore, without any modifications (e.g., applying a motor-starter to mitigate the problem), this motor may cause a meter or entire minigrid to shut down.
    a. **Proposed Resolution** – A minigrid operator or appliance retailer can add a motor-starter between the power supply and the motor. Attaching a circuit breaker/smart meter equipment that can handle current up to 60Amps may be one solution, but a motor-starter will lengthen the lifetime of the motor as well as provide in-rush protection.
2. **Peak Current** – The maize milling machine exhibited peak current when the mill operator "forced" grain into the machine. Over the duration of a typical milling event (e.g., 20kgs or 4-5 minutes), a mill may draw varying amounts of current as the appliances tries to cope with varying amounts of grain being fed into the system. However, the difference between "steady state" and peak current is fairly subtle for this machine and is not a problem for a minigrid operator or appliance retailer.
    a. **Proposed Resolution** – No action needed.
3. **Power Factor** – The power factor of this machine is excellent – about 0.95. The high power factor is beneficial for a renewable energy power system.
    a. **Proposed Resolution** – No action needed.
4. **Total Harmonic Distortion** – The THD was higher than expected – almost 3x the amount considered safe for power electronics equipment. With a THD of about 14%, this could potentially ruin sensitive electronics or computer equipment on the grid over time, cause incremental damage to other motors on the grid, or interfere with power-line communication. In short, the threat of powering this device on a renewable energy system is not immediate, but rather a consideration for long-term maintenance of the system.
    a. **Proposed Resolution** – For this mill, poor motor construction may ultimately be the cause of high THD. Therefore, a higher-quality motor or additional harmonic filter or capacitor may be a necessary upgrade.
5. **Power Consumption Variability** – There was insignificant variance in power consumption over the course of each milling test.
    a. **Proposed Resolution** – No action needed.
6. **Overloading** – The mill has two "screens" which determine the size of the milled grain particles. The smaller the screen, the finer the milled flour, and the greater the peak power and energy consumption. Both the coarse and fine screens were tested, and the mill's steady state peak current was 40% higher than the motor's rating when using the fine screen. Any motor operating beyond its rated capacity can lead to high heat generation, prematurely degrading the motor.
    a. **Proposed Resolution** – Request a higher rated, larger motor from the manufacturer if the fine screen operation mode is desired. A slightly larger motor is likely to retain the compelling energy consumption profile of this machine.

A note about grain size and energy consumption: The mill was tested using two different processing screens: a coarse screen and a fine screen. Under coarse screen operation the mill produced a higher average grain diameter, correlating to a lower consumption of energy per kilogram of grain compared to fine screen operation. Compared to coarse screen operation, fine screen operation required 1.7 times more energy to process one kilogram of grain. Preferences may vary by region and by customer for grain size. Most customers may prefer fine flour for making staple meals, but in order to achieve

this product, there may be one step ahead of milling to select *only* the part of grain that yields fine flour (e.g., remove the hard tip of a whole grain, or remove the outer layer of a whole grain). This extra step would require pre-processing and, therefore, an additional appliance. The practicality of this approach in rural areas is uncertain given the behavior change and additional appliance investment required.

In order to arrive at a quantifiable result for the quality of the milled maize this machine produces, a particle size distribution test was conducted to measure the percent of grain at each particle size. An analogous in-market test that also captures grain preferences would inform the sector on grain screen size and mill performance. Figure 4 below illustrates the test and above one page summary displays the distribution of milled maize particle size for each screen. The dimensions of the openings in each of the sieves below can be found by searching "US Sieve Size" and matching up the Sieve number with the mesh dimensions.

Figure 4. Particle Size Distribution Test and Sample of Results

4.5. Solar Water Pump – A One Page Summary

Surface Solar Water Pump

Date of test: 12/2018

Lab Name: CSU Energy Institute

Lab Location: Fort Collins, Colorado

Appliance Description

This appliance is a surface reciprocating piston pump manufactured by Futurepump that is powered by a stand-alone solar panel system and brushed DC motor. The primary purpose of the pump is to boost crop productivity through irrigation. The body of the machine is powder coated sheet metal and angle iron with pieces of molded plastic and aluminum. If power is not being generated by the solar panel system, the pump can be operated manually with a screw-in handle on the flywheel. A kit of spare parts and tools is provided alongside the pump to aid in maintenance over time. The pump can operate with 2 or 3 provided solar panels and with an either small or large pulley attached to the motor, driving the flywheel.

Key Appliance Manufacturer Ratings

Manufacturer:	Futurepump	Inlet Vertical Suction Limit (m)	7
Model Number:	SF2 – 2 panel	Max total vertical lift, small pulley (m)	15
List Price (USD):	$675	Max total vertical lift, large pulley (m)	9
Motor Voltage Rating (VDC):	36	Flow rate, small (LPM)	12.5 - 29
Motor Rating (W/hp)	60/0.08	Flow rate, large (LPM)	24.5 - 38
Rated No Load Current (A):	2.5	Peak System Efficiency (%):	70%

Modes of Operation Tested (2 panels only)

*Lab Testing Parameters	Small	Large
Supply voltage [V]	11.8 – 42.5	7.7 - 39.6
Drawn current [A]	0.7 – 2.6	0.9 – 2.6
Demanded power [W]	8 - 85	8 - 87
Total Differential Head [m]	2.3 – 17	3.1 – 8.7
Flow Rate [LPM]	4.9 - 28.6	1.2 - 43.1
Flywheel speed, maximum [RPM]	375	324
Electric to Hydraulic Efficiency, maximum [%]	55.2	51.4

*Power vs Flow (P vs Q)

Small Pulley

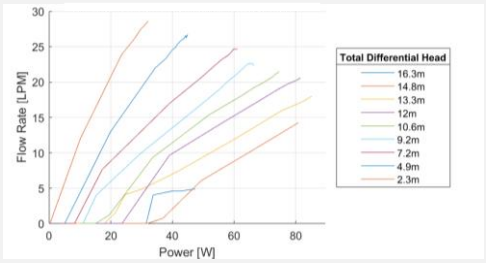

Large Pulley

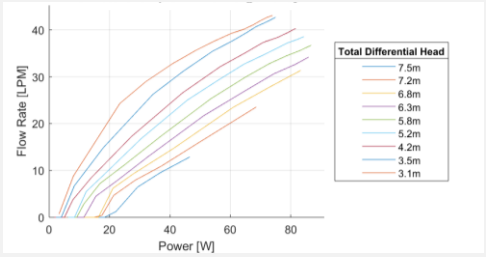

*Average Efficiency vs Head

The efficiency at each point along the head curves in the P vs Q graphs was averaged to display mean efficiency over an exhaustive range of irradiance (W/m^2). The efficiency values are preliminary and are subject to further method and data instrument validation.

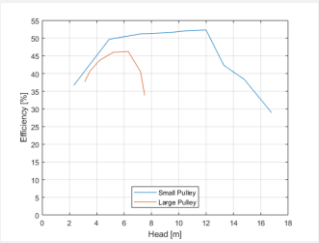

The data presented was created in a lab with a simulated photo-voltaic power supply and is subject to further validation

4.6. Detailed Solar Water Pump Results

Testing production and electro-mechanical characteristics at CSU

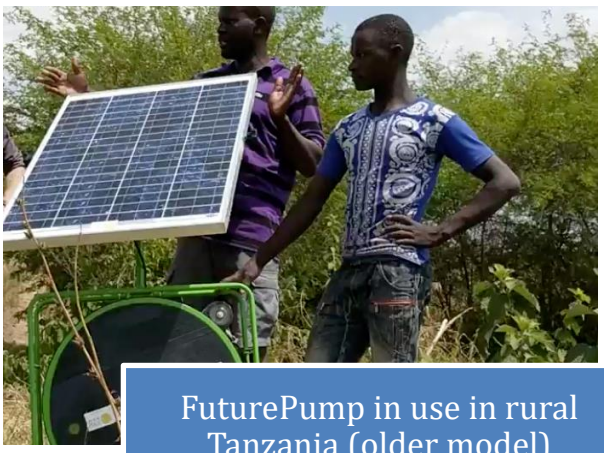

FuturePump in use in rural Tanzania (older model)

Laboratory characterization of a Futurepump surface solar water pump produced preliminary data for manufacturer rating comparisons and highlighted the complexity of testing hydraulic systems. Simulating the conditions that a pump is subject to in the field demands a highly interdependent system of sensors and guidance from the manufacturer on intended operation. Due to the complexity, pump manufacturers serving emerging markets will often rely on a bucket and stop watch to provide technical information to distributors and end-users. This solar water pump sector is still nascent and presents a need for testing institutions to collaboratively work with pump manufacturers. These relationships will lead to the generation of reliable data, informing customers as well as future product development.

The Futurepump has gone through several design iterations and adjustments to fit the needs of a farmer. There are intuitive operation settings that can be easily adjusted, the pump is mobile and light, and maintenance is straightforward. The pump comes paired with a solar panel system and controls. If the power system is stripped out and instead a minigrid powers the pump, the reduced CAPEX cost to the customer may help expand Futurepump's customer base while providing an income generating load to the minigrid. However, attaching the pump to a minigrid distribution line reduces a farmer's ability to physically move the pump around for security or to reach a new water supply.

Recommendations for Minigrid Operators and Appliance Retailers: A solar pump, similar to the Futurepump pump that was tested, can be reliably operated on a minigrid if paired with an AC to DC converter, and if electricity transmission to the pump site already exists. From a technical perspective, solar pumps are "minigrid friendly" loads, but there are potential economic factors that reduce the value proposition for the minigrid operator. Working with pump companies is recommended to determine the right sized AC to DC converter and testing the pump's functionality using a different power supply if applied to an AC minigrid. Otherwise, the appliance is built to work on a stand-alone basis, and might be operated and distributed by a minigrid developer, even if it's not physically connected. Low power surface pumps like Futurepump are best suited for areas near a minigrid with

shallow wells or abundant surface water to serve plots up to an acre in size. Deeper wells demand higher powered, larger pumps that can provide the lift required to irrigate fields.

Findings:

1. **In-Rush Current** – This appliance is powered by a 60W, 48V rated brushed DC motor. The resulting in-rush current is not high enough to be a concern.
    a. **Proposed Resolution** – No remedial action is needed.
2. **Peak Current** – During normal operation, this appliance did not surpass 4A. At an amperage this low, a Futurepump could be added into a low-energy smart meter with existing loads.
    a. **Proposed Resolution** – No resolution needed
3. **Power Factor** - If the pump is added to a minigrid and an AC to DC drive is wired in-between, there will be power factor implications. An AC to DC drive was not tested for this work, but power electronics providers will have specifications available regarding drive power factor. A brushed DC motor on its own has a power factor of 1.
    a. **Proposed Resolution** – Source an AC to DC drive with the highest power factor that fits within a defined budget.
4. **Total Harmonic Distortion** – no testing was completed to test motor THD.
5. **Power Consumption Variability** – The Futurepump is a reciprocating machine resulting in fluctuating load and flow while under operation. Compared to an impeller (centrifugal) based pump, the Futurepump's power consumption will have greater variability. At such low amperage due to the small motor size, the variability is not expected to negatively impact a minigrid.
    a. **Proposed Resolution** – No resolution needed
6. **Overloading** – The pump and motor can be overloaded if connected to an application that induces a back pressure on the pump that is higher than its rated capability. Overloading may burst pump seals and overheat the motor, reducing its serviceable life.
    a. **Proposed Resolution** – Use a clinometer and measuring tape to assess the vertical and horizontal distances that the pump has to overcome. Calculate the back pressure from the aggregated distances and compare each application to the maximum rated pressure.

A note on manufacturer rating comparison: The Futurepump is powered by standalone solar panels that provide a fluctuating voltage to the motor. In a DC motor application, voltage dictates motor speed and consequently flow rate at an associated hydraulic head. The lab testing was completed using a simulated solar supply and research grade instruments to provide the pump with the expected fluctuating voltages. Among the tests completed, flow rates and achievable head aligned well with Futurepump's reported performance, but efficiency did not. The discrepancies may be due to the test method or instrument precision and need to be validated further. Specific concerns include comparing provided power from the PV simulator to the actual PV panels for the pump, electronic pressure transducer signals to physical manometer readings, and flow rates from the electro-magnetic flow meter to a bucket-stop watch method.

5. Appendix

5.1. Stick Welder Test Methods

Test Method for Shielded Metal Arc Welders with Transformer Power Supplies

Colorado State University
Factor[e] Ventures
430 N College Ave.
Fort Collins, CO 80524
11 January 2019

Table of contents

1. Objective 1
1.1. Scope 1
1.2. Safety 1
2. Instrumentation 1
2.1. Voltage 1
2.2. Current 1
2.3. Power 1
2.4. Temperature 1
2.5. Electromagnetic noise 2
2.6. Accuracy 2
2.7. Calibration 2
3. Test Configuration 2
3.1. Description of testing components 3
3.1.1. AC power supply 3
3.1.2. Current sensor 3
3.1.3. Watt-meter 3
3.1.4. Voltage sensor 3
3.1.5. SMAW power transformer 3
3.1.6. Welding electrode 3
3.1.7. Steel plate 3
4. Preliminary Transformer Tests 4
4.1. Turns ratio 4
4.2. Winding resistance measurement 5
4.2.1. Volt-meter ammeter method 5
4.2.2. Bridge method 6
4.3. Load losses and impedance voltage 7
4.4. No-load loss 9
4.4.1. No-load loss waveform correction 10
4.5. Winding temperature rise 10
5. Welder Performance Testing 12
5.1. Welder test methodology 12
5.2. Power quality assessment 12
6. References 12

List of figures

Figure 1. Test configuration diagram. 3
Figure 2. Equivalent circuit for a practical single phase, two-winding transformer. 4
Figure 3. Schematic diagram for resistance measurement using the voltmeter-ammeter method. 6
Figure 2. Wheatstone bridge. 6
Figure 3. Kelvin bridge. 7

Figure 4. Load loss test diagram. 8
Figure 5. No-load loss test diagram. 9

1. Objective

The purpose of this document is to outline the preferred method for testing simple, foreign-built, Shielded Metal Arc Welder (SMAW) power supplies. These power supplies consist of single phase, two winding, fixed-coil, transformers.

1.1. Scope

This testing is for determining the electrical parameters and characteristics for the SMAW power supply. Unlike modern domestic SMAWs that actively regulate the output to maintain constant current, these welders use a fixed-coil transformer-type power supply that generally steps down 115V or 220V utility mains electricity to achieve lower voltage, higher current operation. The scope of this test standard is limited to the electrical performance evaluation and characterization only. Evaluating the quality of the finished welds is outside of the scope of this testing document.

1.2. Safety

All safety precautions noted in the latest edition of ANSI/ASC Z49.1-88 Safety in Welding and Cutting should be adhered to during testing. This standard does not address all potential safety hazards inherent with the operating of this equipment. The user is responsible for maintaining personnel safety during testing, and for adhering to any relevant regulatory limitations.

2. Instrumentation

It is recommended that, whenever possible, all measurements be taken using electronic instruments with analog outputs that can be read and recorded by a data logger.

2.1. Voltage

Voltage measurements should be made at or as near to the winding terminals as possible. If, for some reason, they cannot be, then the error should be evaluated and subsequent readings corrected. Tests should be conducted at the anticipated operating voltage and frequency of the welder.

2.2. Current

Current measurements can be made with in-line current sensors or current transformers if the magnitude of the measured current is too high. Hall effect sensors may also be used. Current draw by instruments, such as volt and/or wattmeters, should be subtracted to obtain the net welder current.

2.3. Power

Power measurements can be made using a dedicated wattmeter. A power analyzer or oscilloscope capable of evaluating power quality metrics, including: power factor, harmonics, and THD is also required.

2.4. Temperature

Temperature may be measured using thermocouples, thermistors, Resistance Temperature Detectors (RTDs), thermometers, or other suitable devices.

2.5. Electromagnetic noise

Electronic instruments feature higher input impedance than passive instruments, which means they draw less current, thereby reducing the need to make corrections for current drawn by the instrument. They are, however, more susceptible to electromagnetic noise.

Common noise sources include:

- Inductive or electrostatic coupling of signal leads to power circuits
- Inadequate common mode rejection
- Common impedance coupling or ground loops
- Conducted interference from power circuits

Good practices for minimizing electromagnetic noise should be adhered for all electronic instruments. These include:

- Using shielded, twisted pair wires for signal leads
- Grounding the shield at only one point
- Maintaining as much distance as is practical between signal leads and power cables
- Grounding all exposed metal parts

2.6. Accuracy

Instrument error is rated as a percentage of the full scale for the measurement instrument. For this reason, it is important to size measurement instruments appropriately such that the full scale of the instrument is close to the expected range of operating values. Instrument transformers should be avoided if possible because they can inject additional error into measured values. If instrument transformers are used, their error must not exceed ±0.3%.

Accuracy for all measurement devices must adhere to the values specified in Table 1.

Table 1. Instrument accuracy requirements.

Measurement parameter	**Accuracy**
Losses	±3.0%
Voltage	±0.5%
Current	±0.5%
Resistance	±0.5%
Temperature	±2.0°C

2.7. Calibration

All instruments shall have been calibrated within the past 12 months.

3. Test Configuration

The recommended welder test configuration is shown in the diagram in Figure 1, below.

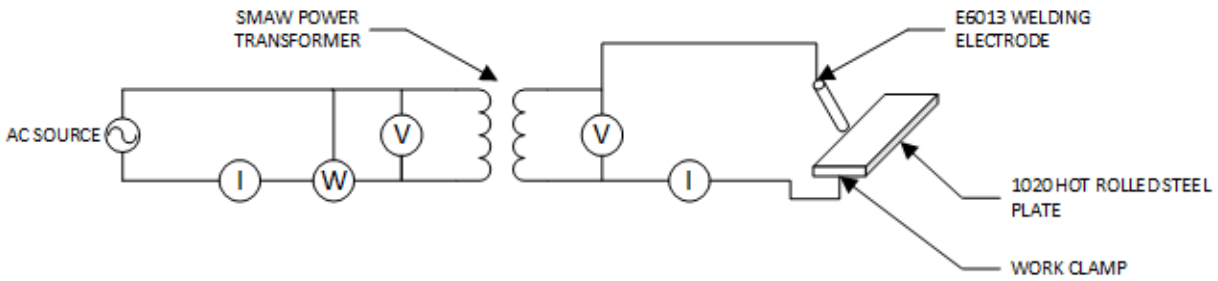

Figure 1. Test configuration diagram.

3.1. Description of testing components

This section describes the various aspects of the testing setup shown in Figure 1.

3.1.1. AC power supply

An AC power supply capable of supplying the full load current of the welder at the rated voltage and frequency shall be provided. (Note: if the welder does not have a rated voltage or frequency, the anticipated operating voltage and frequency should be used.) The voltage waveform should be as close to purely sinusoidal as possible; voltage waveform deviation should not exceed 10%. The frequency should be maintained within ±0.5% of the required testing value.

3.1.2. Current sensor

Both the input and output current shall be monitored using an in-line current meter, current transformer, or Hall effect current sensor meeting the requirements in section 2.

3.1.3. Watt-meter

A watt-meter or power analyzer capable of monitoring real power (W), reactive power (VAR), apparent power (VA), and power factor (PF) meeting the requirements in section 2.

3.1.4. Voltage sensor

The voltage on both the input and output coils of the welding power supply shall be monitored either directly or by means of a voltage divider, or an AC voltage transducer, meeting the requirements in section 2.

3.1.5. SMAW power transformer

The SMAW power supply under test. This is typically a single-phase, two winding, step-down, fixed-coil transformer.

3.1.6. Welding electrode

A standard welding electrode rod, such as the E6013, should be used for all tests. The E6013 welding electrode is acknowledged as being suitable for sheet metal, and is typically used for training.

3.1.7. Steel plate

A standard steel plate with good weldability characteristics should be used, such as 1020 hot rolled steel.

4. Preliminary Transformer Tests

As the welding power supply is a transformer, an initial electrical characterization may be made by subjecting it to typical test methods for dry type electrical transformers. A practical equivalent circuit representation for a single phase, two-winding transformer is presented in

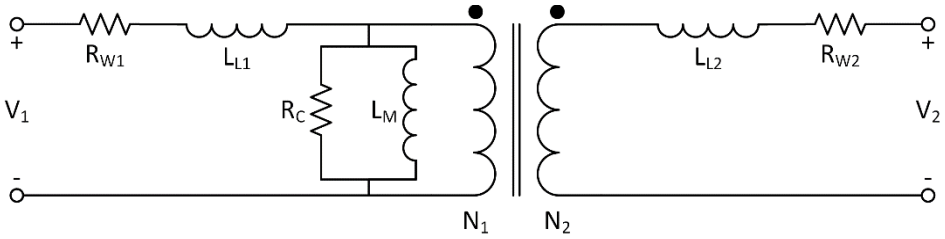

Figure 2. Equivalent circuit for a practical single phase, two-winding transformer.

The key features of this model can be found using the tests in this section. The parameters include:

- Turns ratio (N_1:N_2) – the ratio of the number of turns on each winding of the transformer. This relationship dictates the voltage and current relationships found in the transformer. Found in 4.1.
- Winding resistance (R_W) – the electrical resistance of the winding. This value contributes to load losses in the transformer that increase with the square of the operating current (I^2R losses). This is found in 4.2.
- Leakage inductance (L_L) – this is a self-reactance in the transformer winding contributes to voltage drop, and hence loss, in the transformer windings. This is found in 4.3.
- Core loss (R_C) – some real power is lost in the transformer core, which can be represented by a core loss resistor in parallel with the magnetic core. This is found in 4.4.
- Magnetizing inductance (L_M) – a certain amount of reactive current is required to maintain the flux in the transformer core, which can be represented as an additional inductor in parallel with the magnetic core. The current drawn by the core loss and magnetizing inductance are sometimes referred to collectively as *excitation current.* This is found in 4.4.

4.1. Turns ratio

The turns ratio is the number of turns on the high voltage (input) winding to the number of turns on the low voltage (output) winding (N_1:N_2). The turns ratio should be determined using two voltmeters, one on each winding. A variable AC source should be applied to the high voltage terminal, and measurements from both voltmeters should be read simultaneously.

A total of four test points should be taken at 80%, 90%, 100%, and 110% of rated voltage. The turns ratio is calculated as the ratio of the high voltage to low voltage, and measured by the voltmeters. The results should all be within 1% of each other – if not, the results are considered invalid, and the test should be conducted again with different voltmeters.

Next, the voltmeters should be swapped between the high and low voltage windings and repeated to compensate for instrument errors, and the average value of the two sets of readings should be taken as the final result.

4.2. Winding resistance measurement

The electrical resistance of the transformer windings (R_W) should be established in order to estimate conduction (I^2R) loss in the welder, as well as determining temperature rise in the windings. Resistance measurements should be taken under "cold" conditions when the welder has sat idle in a draft-free area for at least 24 hours with neither voltage nor current applied. Internal temperature sensors should measure within 2°C of ambient, and ambient temperature should not have changed by more than 3°C in the past three hours prior to obtaining measurements.

All resistance measurements should be corrected to a standard reference temperature of 25°C. Temperature correction should be calculated using EQ. 1:

$$R_s = \frac{R_t(t_s + k)}{(t_t + k)} \qquad \text{EQ. 1}$$

Where:

R_s= Resistance of winding measured at specified reference temperature t_s (Ω)
R_t = Resistance of winding at measured temperature t_t (Ω)
t_s = Specified reference temperature (25°C)
t_t = Measured temperature (°C)
k = 234.5 for copper
225 for aluminum
229 if both copper and aluminum windings are used in the same transformer

As a result of the effects of magnetic core saturation, it may take some time for the measurement readings to reach stable, steady-state values. Measurement time intervals of 5-10s are recommended, and longer readings may be required. The required time for the cold resistance measurements to reach steady state should be noted, and the same time should be observed when taking hot resistance measurements.

In order to maintain consistent core magnetization, the same relative polarity should be maintained during all resistance measurements. Changing the measurement polarity can change the time constant and result in erroneous readings. Polarity should be maintained by always applying the same measurement lead to the same transformer winding terminal.

There are two allowable methods for measuring resistance: the voltmeter-ammeter method and the bridge method. The voltmeter-ammeter method is most common, but the bridge method may be used when higher accuracy is required, or if the transformer winding dictates that the measuring current must be less than 1 A.

4.2.1. Volt-meter ammeter method

In this method, a DC voltage source is connected to one of the windings of the transformer while the other winding is an open circuit. This DC source can be a

switching power supply, battery, filtered rectifier, or other suitable supply, but should be relatively ripple-free. The resulting current is measured, along with the voltage across the winding, and the resistance is calculated according to Ohm's law. The current should not exceed 15% of the rated current to prevent temperature rise in the windings, which will skew the results. If the measured current is < 1A, the bridge method in section 4.2.2 should be used.

It is recommended that the voltage and current measurements be recorded and time-stamped using a data acquisition system to make it easier to document the time required for the values to reach steady state equilibrium. An optional resistor may be added in series with the winding to reduce the time required for the current to reach steady-state. If used, this resistor should have an impedance much larger (at least an order of magnitude greater) than the winding resistance. The DC voltage source will need to be increased in order to compensate for voltage drop across this resistor.

A diagram showing the test circuit for the voltmeter-ammeter method is shown in Figure 3.

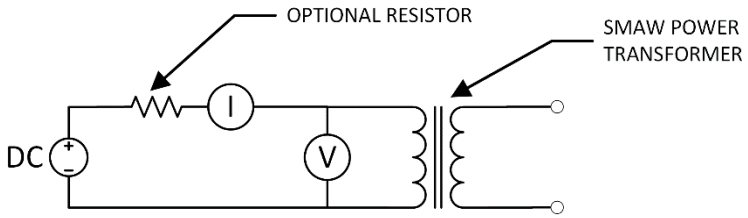

Figure 3. Schematic diagram for resistance measurement using the voltmeter-ammeter method.

4.2.2. Bridge method

The bridge method is the preferred method for measuring low resistances with high accuracy, without the high equipment cost of a precision resistance meter or impedance analyzer. The Wheatstone bridge circuit, shown in Figure 4, is typically used for high precision measurements of resistance ≥ 1Ω.

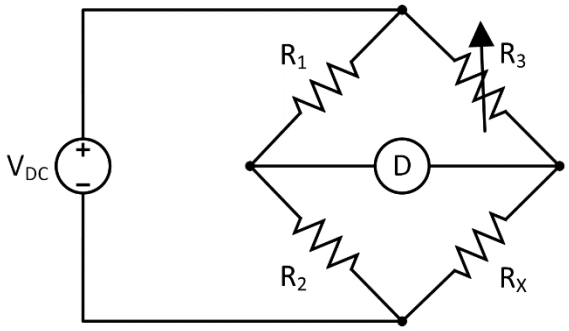

Figure 4. Wheatstone bridge.

Two known resistors, R_1 and R_2, are connected to the unknown winding resistance R_X, along with an adjustable resistor R_3. A detector (either current or voltage) is connected between the two nodes as shown. When the circuit is balanced, there will be no voltage nor current flow through the detector. When this occurs, the unknown resistance R_X can be calculated by EQ. 2.

$$R_X = \frac{R_2 R_3}{R_1} \qquad \text{EQ. 2}$$

For resistances < 1Ω the lead wire resistances should be compensated for; the Kelvin bridge, shown in Figure 5 is therefore recommended.

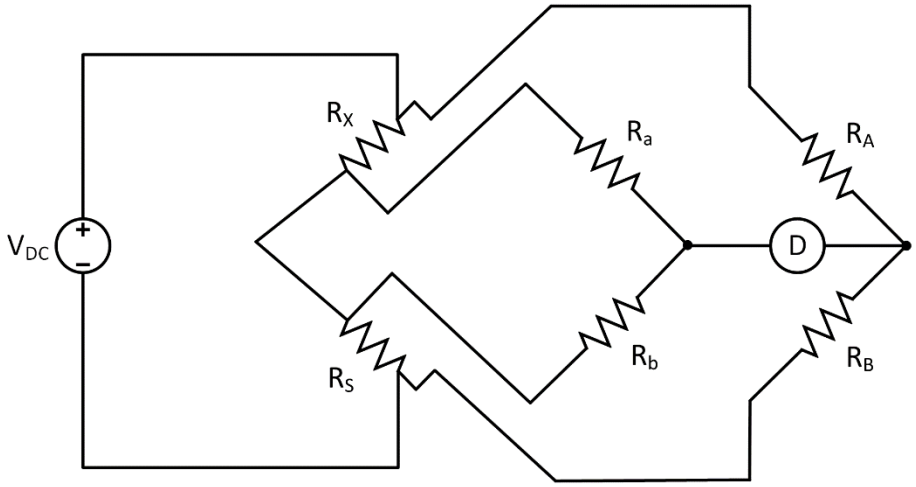

Figure 5. Kelvin bridge.

In this case, the unknown resistance R_X can be calculated by EQ. 3:

$$R_X = R_S \frac{R_A}{R_B} + \left[\frac{R_b R_y}{R_a + R_b + R_y}\right]\left[\frac{R_A}{R_A} - \frac{R_a}{R_b}\right] \qquad \text{EQ. 3}$$

Where R_y is the resistance of all the associated wires and leads (yoke). For this reason, yoke resistance should be minimized as much as possible. Assuming R_y is negligible and R_A/R_B exactly equals R_a/R_b, EQ. 3 can be simplified and rewritten as EQ. 4:

$$R_X = R_S \frac{R_A}{R_B} \qquad \text{EQ. 4}$$

4.3. Load losses and impedance voltage

Transformer load losses consist primarily of I^2R losses from heat and eddy current losses in the windings. These are found using a short-circuit test. A diagram for this test is shown in Figure 6.

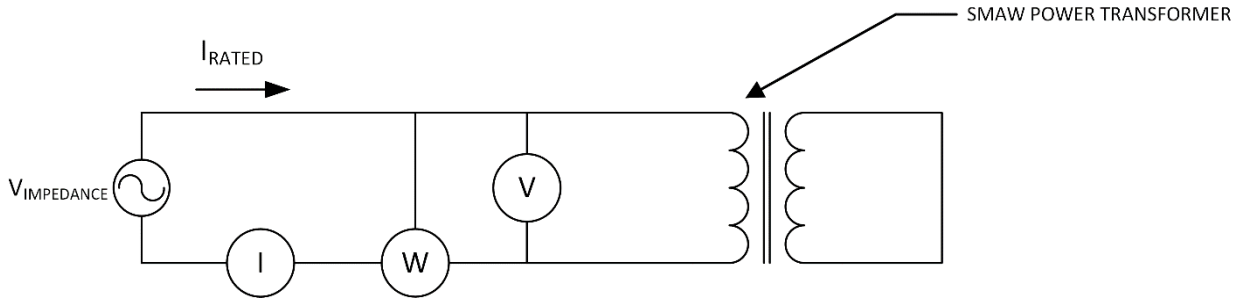

Figure 6. Load loss test diagram.

In the short-circuit test, one set of windings is directly connected to form a short circuit. A variable voltage AC power supply is connected to the other set of windings, and the voltage is slowly increased until rated current flows through the winding. For the purposes of this test, either set of windings can be shorted. However, due to the high values of current that are typically found in the low voltage winding of a welding power transformer, it may be more practical to apply voltage to the high voltage winding and short the low voltage winding, as this requires much less current from the power supply. The conductor used to short-circuit the winding must have a cross sectional area equal to or greater than the winding.

The voltage required to circulate rated current through one of the two transformer windings is referred to as the impedance voltage. Once rated current has been established in the winding, the corresponding voltage as measured by the voltmeter in parallel with the winding should be recorded.

Load-losses, particularly eddy current losses, are proportional to frequency, therefore the frequency of the AC power source used for the load-loss test shall be within ±0.5% of rated frequency. The winding resistance is proportional to temperature. Winding temperature shall be established at the beginning and end of the test, and the winding temperature shall not exceed 5ºC. Winding temperature should be determined by measuring the DC resistance of the winding, using the methods in 4.2.

Assuming that $|L_M|>>|L_L|$, the equivalent impedance for the transformer under short-circuit conditions (Z_{SC}) can then be determined according to EQ. 5:

$$Z_{SC} = \frac{V_{IMPEDANCE}}{I_{RATED}} = (R_{W1} + R_{W2}) + j\omega(L_{L1} + L_{L1}) \qquad \text{EQ. 5}$$

The real portion of Z_{EQ} should match the winding resistances found in 4.2, when corrected for temperature. Assuming that $L_{L1} \cong L_{L2}$, the winding inductances can be calculated from the imaginary portion of Z_{SC} according to EQ. 6:

$$L_{L1} = L_{L2} = \frac{1}{2\omega} Im\{Z_{SC}\} \qquad \text{EQ. 6}$$

4.4. No-load loss

No load losses refer to the power consumed by the transformer to maintain excitation when no load is applied. These include: core loss from hysteresis and eddy-currents, and conductor I^2R losses arising from the excitation current. No load losses are typically assessed using an open circuit test. In open circuit, core losses tend to predominate, and are affected by the magnitude, frequency, and waveform shape of the applied voltage. For this reason, it is necessary to assess no-load loss at rated voltage and frequency, with a minimum of voltage waveform distortion.

The standard method employed for determining no-load losses is shown in Figure 7. One winding is energized at rated voltage and frequency using a sinusoidal voltage source, while the other is left in open circuit. Either the high-voltage or low-voltage winding can be energized for the purposes of this test. Two voltmeters in parallel should be used, one measuring true Root-Mean-Squared (RMS) and one measuring the average. (Average measurement is to ensure the ac voltage source doesn't have a dc bias.) An ammeter and wattmeter should also be connected as shown.

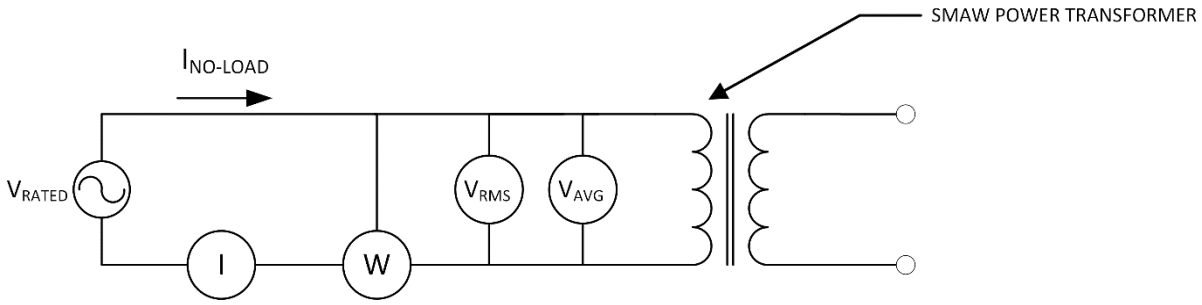

Figure 7. No-load loss test diagram.

The AC voltage source must be adjusted such that the *average* reading voltmeter shows the rated voltage. Frequency must not deviate more than ±0.5% during the course of testing, or the results shall be considered invalid. Simultaneous readings of all voltage, current, and power values shall be collected.

The instrument power consumption should be established by disconnecting the transformer and recording the value reported by the wattmeter. The instrument loss should be subtracted from the measured no-load loss.

The open circuit equivalent impedance (Z_{OC}) can then be calculated as shown in EQ. 7:

$$Z_{OC} = \frac{V_{RATED}}{I_{NO-LOAD}} \qquad \text{EQ. 7}$$

From this, the core loss and magnetizing inductance of the transformer can be calculated using the real and imaginary portions of Z_{OC}, respectively, as shown in EQ. 8 and EQ. 9:

$$R_C = Re\{Z_{OC}\} - R_{Wn} \quad \text{EQ. 8}$$

$$L_M = \frac{1}{\omega} Im\{Z_{OC}\} - L_{Ln} \quad \text{EQ. 9}$$

Where n=1 or 2 depending on which winding had the applied voltage.

4.4.1. No-load loss waveform correction

As mentioned previously, no-load losses are sensitive to distortions in waveform, and deviations from a pure sine wave voltage source can skew the results. Therefore, the no-load losses should be corrected for waveform distortion as shown in EQ. 10.

$$P_c(T_m) = \frac{P_m}{P_1 + kP_2} \quad \text{EQ. 10}$$

Where:

T_m = Core temperature at the time of test (°C)

$P_c(T_m)$ = No-load losses, corrected for waveform, at temperature T_m (W)

P_m = Measured no-load losses at temperature T_m

P_1 = Per-unit hysteresis loss (pu)

P_2 = Per-unit eddy-current loss (pu)

$k = \left(\frac{E_r}{E_a}\right)^2$

Where:

E_r = Test voltage measured by the RMS voltmeter

E_a = Test voltage measured by average-voltage voltmeter

If actual values for hysteresis and eddy-current losses are unknown, they can each be assigned a value of 0.5pu.

If a correction factor of more than 5% is required, the test voltage waveform shall be deemed too distorted to achieve valid test results, and an improved voltage source must be obtained for the test.

4.5. Winding temperature rise

In order to determine the ultimate temperature rise in the windings, the welding transformer should be run at rated load, in an area free from drafts, under normal conditions and normal means of cooling. The transformer should be loaded using a resistive load or load bank sufficient to run at rated current, with rated frequency and voltage. The ultimate temperature rise is considered to be the final temperature of the windings above ambient once the temperature has become constant. Temperature rise shall be considered constant when the measured temperature does not vary by more than 2°C during a period of three consecutive hours.

After temperature has stabilized, the voltage and current should be removed. Average winding temperature (T_w) shall be determined by measuring the winding resistance as specified in 4.2, using EQ. 11. Measurements should be taken as quickly as possible.

$$T_w = \frac{R}{R_o}(k + T_o) - k \qquad \text{EQ. 11}$$

Where

T_w = Average winding temperature (°C)
R_o = Cold winding resistance determined in 4.2 (**Ω**)
T_o = Cold resistance temperature (25°C)
R = Measured hot winding resistance
k = 234.5 for copper
225 for aluminum
229 if both copper and aluminum windings are used in the same transformer

The total winding temperature rise is then the difference between the winding temperature (T_w) and ambient temperature. Typically, ambient temperature is rated at 30°C. If the ambient temperature was something other than 30°C, the temperature rise should be corrected according to EQ. 12.

$$T_{c1} = T_r \left[\frac{T_r + T_k + T_{ra}}{T_r + T_k + T_a}\right]^n \qquad \text{EQ. 12}$$

Where:

T_{c1} = Average winding temperature rise corrected for ambient temperature (°C)
T_r = Measured average winding temperature rise (°C)
T_a = Measured ambient temperature at the end of the test (°C)
T_{ra} = Rated ambient temperature (typically 30°C)
n = 0.7 for sealed units, 0.8 for ventilated units, and 1.0 for forced-air-cooled units
k = 234.5 for copper
225 for aluminum
229 if both copper and aluminum windings are used in the same transformer

If the test was conducted at an altitude greater than 1,000m (3,281’), the temperature rise must be corrected using EQ. 13.

$$T_{c2} = T_{c1}\left\{1 + F\left[\frac{(A - 1{,}000)}{1{,}000}\right]\right\} \qquad \text{EQ. 13}$$

Where:

T_{c2} = The altitude-corrected average winding temperature rise (°C)
T_{c1} = The temperature-corrected average winding temperature rise as calculated by EQ. 12. (°C)
A = Altitude (m)
F = Empirical factor, defined as 0.005 for dry-type, self-cooled transformers

5. Welder Performance Testing

Welder performance testing involves running the welder during normal operations, while monitoring the input and output voltage and current. The arc current for a SMAW is inversely proportional to the arc length, so a number of different arc lengths should be used.

5.1. Welder test methodology

The welder performance test will consist of using a 1/8" diameter E6013 welding electrode rod to put a bead on a metal plate of 1020 hot rolled steel. The weld line length for each bead-on-plate weld should be approximately 6" (150mm).

Two different arc lengths will be evaluated:

- Short – indistinguishable distance above the material
- Long – an arc length equal to the electrode diameter [approximately 1/8" (3.2mm)]

5.2. Power quality assessment

For each test weld, the following electrical parameters should be recorded:

- Input voltage
- Input frequency
- Average input current
- Peak input current
- Input power factor
- Input current harmonics (even and odd up to 15th harmonic)
- Input current THD
- Output voltage
- Output current

6. References

[1] L. Jeffus, *Welding and Metal Fabrication*, Clifton Park, NY: Cengage Learning, 2012.
[2] *IEEE Standard for General Requirements for Dry-Type Distribution and Power Transformers*, IEEE Standard C57.12.01, 2015.
[3] *IEEE Standard Test Code for Dry-Type Distribution and Power Transformers*, IEEE Standard C57.12.91, 2011.
[4] *IEEE Standard for Single-Phase Induction Motors*, IEEE Standard 114, 2010.
[5] J.D. Glover, M.S. Sarma, and T.J. Overbye, *Power System Analysis and Design*, Toronto, ON: Thomas Learning, 2008.
[6] *Standard for AWS Certified Welders*, American Welding Society Standard AWS QC7, 1993.
[7] *Specification for the Qualification of Welder Test Facilities*, American Welding Society Standard AWS B5.4, 2005.

[8] *Standard for Accreditation of Test Facilities for AWS Certified Welder Program*, American Welding Society Standard AWS QC4, 1989.

5.2. Stick Welder Test Report

Shielded Metal Arc Welder (SMAW) Test Report

A study to evaluate the performance of a hand-built stick welder

Colorado State University
Factor[e] Ventures
430 N College Ave.
Fort Collins, CO 80524
11 January 2019

Table of contents

1 Overview 1
2 Description of SMAW 1
3 Test and Measurement Equipment Description 1
3.1 Voltage 1
3.2 Current 1
3.3 Power 1
3.4 Impedance 2
3.5 Temperature 2
4 Testing Description and Results 2
4.1 Transformer characterization tests 2
4.1.1 Turns ratio 3
4.1.2 Winding resistance and leakage inductance 3
4.1.3 Core resistance and magnetizing inductance 8
4.1.4 Practical equivalent circuit 13
4.2 Steady-state efficiency 13
4.3 Temperature Rise Testing 15
4.4 Welding Performance Testing 20
5 References 26
Appendix A: Data file description 27

List of figures

Fig. 1 Equivalent circuit for a practical single phase, two-winding transformer. 2
Fig. 2. Short circuit test schematic. 4
Fig. 3. Impedance analyzer results of the primary winding with the secondary winding in short circuit. 5
Fig. 4. Impedance analyzer results of the secondary winding with the primary winding in short circuit. 6
Fig. 5. Voltage and current waveforms for short-circuit test. 7
Fig. 6. Current FFT amplitude spectrum for short-circuit test. 8
Fig. 7. Impedance analyzer results for the primary winding with the secondary winding in open circuit. 9
Fig. 8. Open circuit test schematic. 9
Fig. 9. No-load voltage and current waveforms. 10
Fig. 10. No-load current amplitude spectrum. 10
Fig. 11. Magnitude of no-load fundamental and third harmonic current vs. voltage. 11
Fig. 12. Open circuit resistance and inductance vs. excitation. 12
Fig. 13. Percentage of primary current third harmonic vs. magnitude of fundamental. 12
Fig. 14. Transformer practical equivalent circuit, linear region. 13
Fig. 15. Transformer practical equivalent circuit at 220V, 50Hz. 13
Fig. 16. Steady state efficiency vs. load current. 14
Fig. 17. Experimental setup for temperature rise test. 15
Fig. 18. Discoloration of insulation due to excessive temperature rise. 17
Fig. 19. Primary winding temperature vs. time, rising. 17
Fig. 20. Primary winding temperature vs. time, falling. 18
Fig. 21. Simulated temperature rise at 30% duty cycle for eight hour shift. 19
Fig. 22. Simulated temperature rise at 25% duty cycle for eight hour shift. 20
Fig. 23. Photo of active welding testing. 21
Fig. 24. Real and reactive power for short arc test. 22
Fig. 25. Primary winding voltage and current waveforms for short arc test. 23
Fig. 26. Bead on plate welds created by short arc. 23
Fig. 27. Real and reactive power for long arc test. 24
Fig. 28. Primary winding voltage and current waveforms during long arc test 24
Fig. 29. Bead on plate welds created by long arc. 25
Fig. 30. Thermal image of SMAW immediately after welding. 25

1 Overview

This report will describe the tests conducted to evaluate and characterize a Shielded Metal Arc Welder (SMAW) obtained from Kigali, Rwanda. Welders in this region are typically hand-built, rather than procured commercially. Consequently, they do not feature manufacturer's data sheets or specifications. The purpose of this testing was to obtain basic electrical characteristics, determine equivalent circuit parameters, and provide performance benchmarks.

2 Description of SMAW

The SMAW that was obtained from Kigali is typical of devices used in sub-Saharan Africa. It is a hand-built, step-down transformer. The core consists of thin steel plates pressed together with two wood blocks at the top and bottom. The windings are insulated using cellulose, most likely electrical kraft paper or crepe paper, which are commonly used materials for transformer winding insulation. The primary winding is copper conductor with a diameter of approximately 2.1mm, roughly equivalent to a 12AWG wire. The secondary winding was aluminum conductor, approximately 9.3mm in diameter (2/0AWG).

The SMAW transformer was shipped in a wooden crate with no protective enclosure, packing, or dunnage, which caused some of the insulation to be abraded away due to friction contact with the inner surface of the crate.

The SMAW transformer shipped as an open core, with no enclosure or housing, which is how they are commonly used in the field. For safety and ease of connection, a polycarbonate enclosure was built to house the transformer, with built-in, locking electrical connections and a DIN-rail mounted fuse block for the primary winding. Voltage sense leads and Current Transformers (CTs) were also added for measurement instrumentation purposes.

3 Test and Measurement Equipment Description

This section describes the test and measurement equipment used for capturing the various data parameters during testing

3.1 Voltage

A Keysight N2791A High voltage differential probe was used for obtaining measurements on the primary (high voltage) winding of the transformer. This probe has a rated accuracy of ±2.0% and an offset of ±7.5mV. The voltage probe has a BNC output and was connected to a Keysight MSOX3012T mixed signal oscilloscope.

3.2 Current

Current measurements on the primary (high voltage side) were taken using a Pico TA018 60A current probe. When set to 100mV/A, the probe has a rated accuracy of ±2.0%, ±5mA over the range of 10mA-10A. When using the 10mV/A range the probe's accuracy is ±2.0%, ±30mA when measuring between 100mA-40A. The current probe signal was recorded using the same Keysight MSOX3012T oscilloscope as the voltage probe in 3.1.

3.3 Power

A Bitronics M572 meter was used for recording voltage, current, real power, and reactive power. The Bitronics has two channels, with channel 1 connected to the primary side of the transformer and channel 2 connected to the secondary. Because of the relatively low

voltage values, voltage sense leads were connected directly to the primary and secondary windings. Primary current measurements were recorded using Rish CT 12G460 100:5A CTs and the secondary currents were recorded using Rish CT 12G462 200A:5A CTs.

3.4 Impedance

Resistive and inductive impedance measurements were conducted using a Keysight E4990A impedance analyzer.

3.5 Temperature

Temperature values were measured using a Tacklife IT-T05 infrared thermometer with rated accuracy of ±2.0°C when measuring ≤100°C.

4 Testing Description and Results

Two different types of testing were conducted. The first represented tests conducted on dry-type transformers, using IEEE Standard C57.12.91, 2011 as a guideline for developing and conducting tests.

These tests consisted of:

- Turns ratio test
- Open circuit test
- Short circuit test
- Temperature rise test

In addition, two series of welding tests were conducted.

4.1 Transformer characterization tests

The SMAW is a step down transformer designed to take line voltage, typically 220V 50Hz in Rwanda, and transform that to low voltage, high current power suitable for welding. As such, it can be characterized using the standard equivalent circuit for a practical, single phase, two-winding transformer, as shown in Fig. 1.

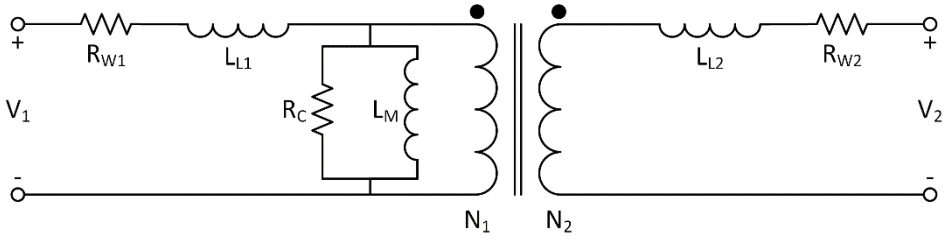

Fig. 1 Equivalent circuit for a practical single phase, two-winding transformer.

The key features of this model can be found using the tests in this section. The parameters include:

- Turns ratio (N_1:N_2) – the ratio of the number of turns on each winding of the transformer. This relationship dictates the voltage and current relationships found in the transformer.

- Winding resistance (R_W) – the electrical resistance of the winding. This value contributes to load losses in the transformer that increase with the square of the operating current (I^2R losses).
- Leakage inductance (L_L) – this is a self-reactance in the transformer winding contributes to voltage drop, and hence loss, in the transformer windings.
- Core loss (R_C) – some real power is lost in the transformer core, which can be represented by a core loss resistor in parallel with the magnetic core.
- Magnetizing inductance (L_M) – a certain amount of reactive current is required to maintain the flux in the transformer core, which can be represented as an additional inductor in parallel with the magnetic core. The current drawn by the core loss and magnetizing inductance are sometimes referred to collectively as *excitation current.*

Transformer characterization tests were conducted at 50Hz, unless noted otherwise. A Schneider Conext XW+ 5548 inverter was used to provide a relatively distortion-free 50Hz voltage source. The voltage output was adjusted using a 0-250V, 5kVA autotransformer.

4.1.1 Turns ratio

The turns ratio of the transformer was determined by taking simultaneous waveform measurements of the primary winding voltage (V_P) and the secondary winding voltage (V_S) using the Bitronics M572 meter. A total of four primary voltages near rated voltage (220V) were chosen, with steps of approximately 10%. The measured waveforms were processed using Matlab, which computed the Fast Fourier Transform (FFT) to obtain the amplitude of the fundamental (50Hz) voltage component. The RMS value of the fundamental was determined by dividing the amplitude by √2; the primary and corresponding secondary RMS voltages are given in Table I.

Table I. Primary and secondary winding voltages and turns ratio

$V_{P,RMS}$	$V_{S,RMS}$	N_1:N_2
182.90	43.31	4.22
201.95	47.69	4.23
222.90	52.37	4.26
242.92	56.66	4.29

The results indicate that the turns ratio for the transformer is approximately 4.25, although the results show more variability than would be expected.

4.1.2 Winding resistance and leakage inductance

Winding resistance and leakage inductance were assessed using a Keysight E4990A impedance analyzer, and by applying voltage to the primary winding with the secondary winding in short-circuit and measuring the resulting current. The secondary winding was shorted using a 1.73m (68”) piece of 2/0AWG welding cable, as shown in the schematic in Fig. 2. Short circuit test schematic.. The nominal resistance of 2/0AWG wire is 0.2557mΩ/m, yielding an overall short circuit impedance of approximately 0.4417mΩ.

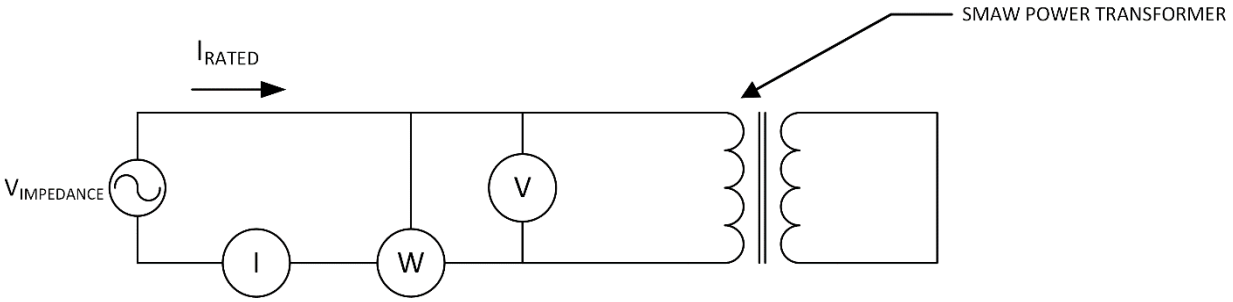

Fig. 2. Short circuit test schematic.

The results of the impedance analyzer for the primary winding are shown in Fig. 3. In order to obtain an accurate result, the impedance sweep range was confined to a narrow, low frequency region of 20Hz-100Hz. This was to avoid non-linear effects that occur at higher frequencies, such as saturation and resonance, which could skew the results. The oscillator amplitude was set to $500mV_{RMS}$. The transformer was analyzed using an equivalent circuit consisting of an inductance and resistance in series, corresponding to the winding resistance and leakage inductance, with a shunt capacitance which represents the capacitance formed between adjacent windings of the transformer. At low frequencies, this capacitance is mostly negligible, as the results indicate.

These measurements were taken with the transformer equal to ambient temperature, roughly 29.2°C. The results indicate that R_W is approximately 1.22Ω and L_L is approximately 13.5 mH. Resistive measurements should be normalized to a standard test temperature of 20°C. Therefore, the corrected measurements were determined to be:

$$R_{W1} = 1.18\Omega$$
$$L_{L1} = 13.52\text{mH}$$

The secondary was evaluated in a similar manner using the impedance analyzer. These results, shown in Fig. 4, were determined to be as follows when corrected to 20°C:

$$R_{W2} = 0.113\Omega$$
$$L_{L2} = 755\mu\text{H}$$

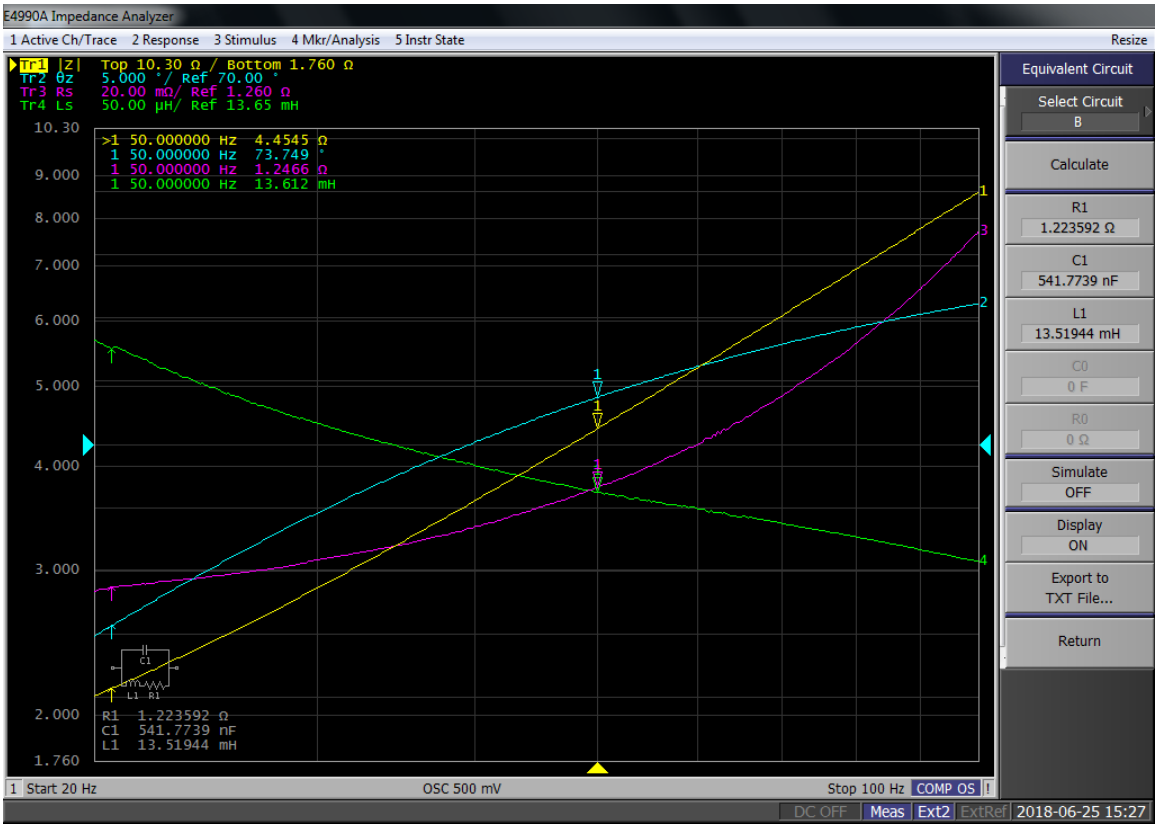

Fig. 3. Impedance analyzer results of the primary winding with the secondary winding in short circuit.

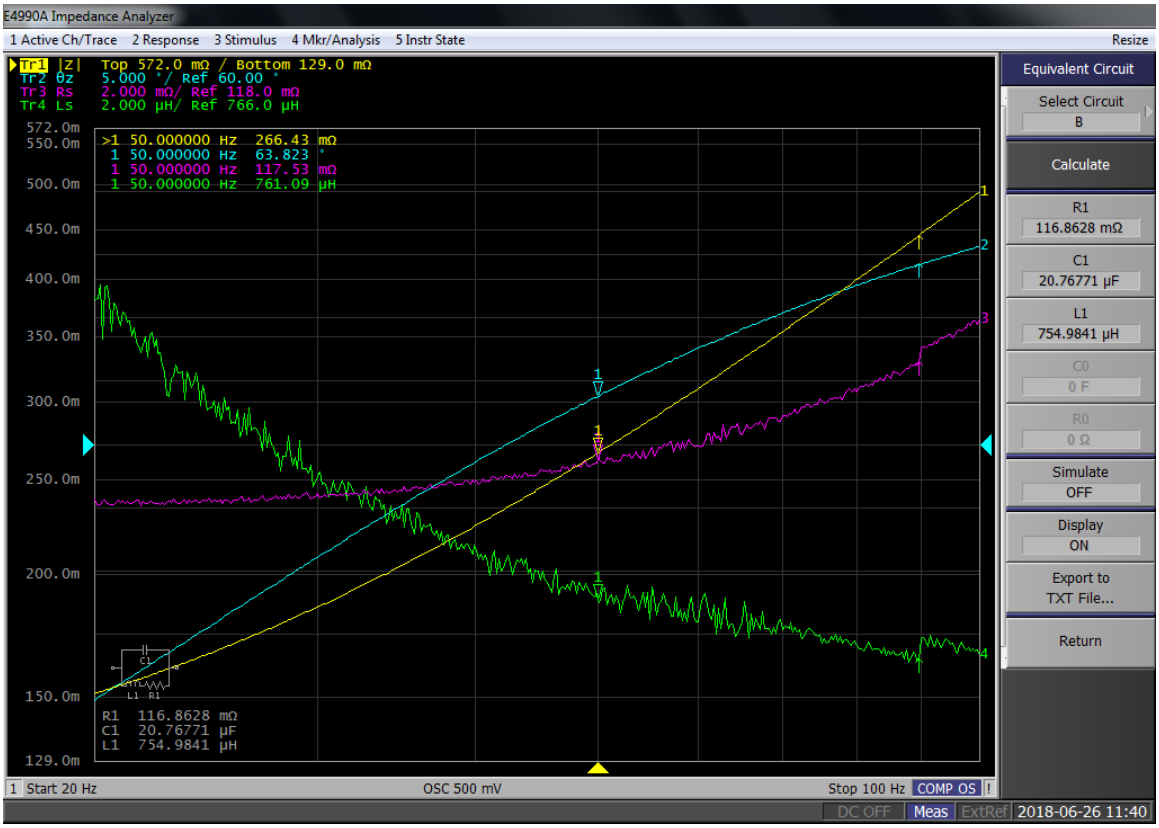

Fig. 4. Impedance analyzer results of the secondary winding with the primary winding in short circuit.

Next, the values obtained using the impedance analyzer were verified using the short-circuit impedance test. The short-circuit impedance test involves applying voltage to the primary winding of the transformer with the secondary winding still in short circuit. Sufficient voltage must be applied such that rated current flows in the windings; this is referred to as the *impedance voltage*. The winding resistance and leakage inductance can then be determined from real and reactive portions of the short circuit impedance using EQ. 1.

$$Z_{SC} = \frac{V_{IMPEDANCE}}{I_{RATED}} = (R_{W1} + R_{W2}) + j\omega(L_{L1} + L_{L1}) \qquad \text{EQ. 1}$$

The short circuit test was conducted using the Schneider Conext 5548 inverter to provide a 50Hz voltage source, with the 5kVA autotransformer used to adjust the voltage to deliver the short circuit current. No manufacturer's data sheet was available for this device, thus there was no *rated current*. However, the average RMS current in the primary winding during active welding operations was observed to be approximately 25A, so this value was chosen as the nominal current for performing the short circuit test. The impedance voltage required to circulate 25A in the primary winding was found to be approximately $117V_{RMS}$. The surface temperature of the windings at the time of the test was approximately 31.7°C.

$$Z_{SC} = 4.69\angle(73.6^{o}) \qquad \text{EQ. 2}$$

$$R_{W1} + R_{W2} = |Z_{SC}|\cos(\angle Z_{SC}) = 1.327\Omega$$

When corrected for temperature, the equivalent resistance at 20°C is approximately 1.267Ω.

Likewise, the leakage inductance can be found by:

$$L_{L1} + L_{L2} = \frac{|Z_{SC}|\sin(\angle Z_{SC})}{\omega} = 14.32\text{mH} \qquad \text{EQ. 3}$$

When comparing these values to the values found using the impedance analyzer, the winding resistance found by the short circuit method was within 2% of the sum of R_{W1} and R_{W2} as found by the impedance analyzer. Likewise, the leakage inductance found by the short circuit test was within 0.3% of the sum of the leakage inductances found using the impedance analyzer. Therefore, we can have confidence in the results of these tests as they correlate strongly with one another.

The voltage and current waveforms that were measured in the primary winding during the short-circuit test are plotted in Fig. 5. The amplitude spectrum, as determined by the Fast Fourier Transform (FFT) of the primary current is plotted in Fig. 6. These show that voltage and current distortion were fairly low during this test – Total Harmonic Distortion (THD) was calculated to be 3.4% for the voltage waveform and 1.2% for the current waveform.

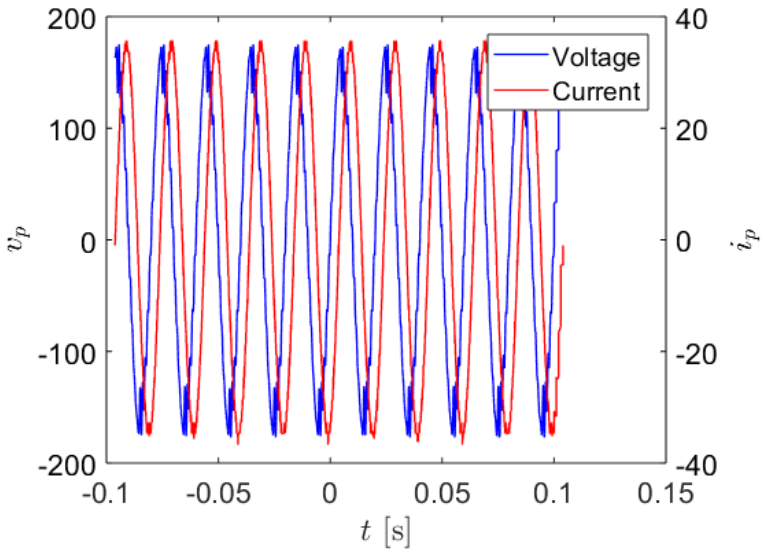

Fig. 5. Voltage and current waveforms for short-circuit test.

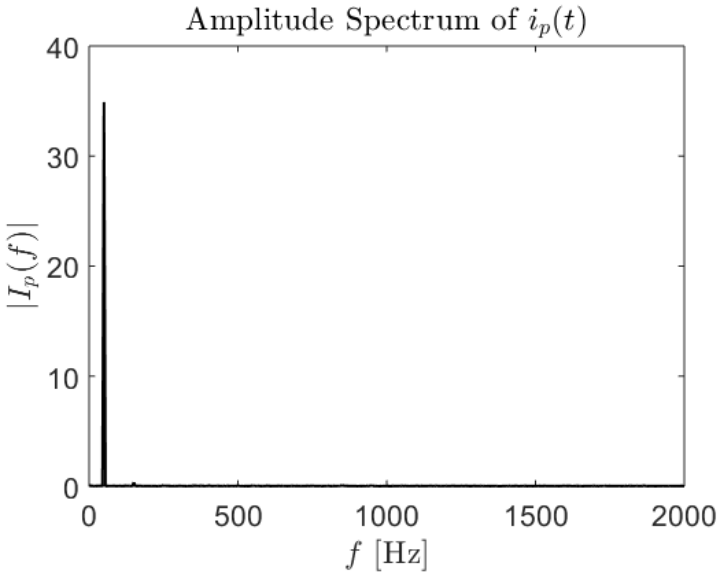

Fig. 6. Current FFT amplitude spectrum for short-circuit test.

4.1.3 Core resistance and magnetizing inductance

Core resistance (R_C) and magnetizing inductance (L_M) collectively account for the majority of 'no-load losses' experienced by transformers. The current drawn at no load is often referred the *excitation current* and is responsible for developing the flux in the transformer core. The parameters RC and LM were analyzed using the Keysight E4990A impedance analyzer. Excitation current was determined under expected field operating conditions – i.e., 220V, 50Hz.

The E4990A impedance analyzer was connected to the primary winding of the transformer. The oscillator was set to current controlled output as this tends to yield more stable outputs when evaluating transformers and other highly inductive loads. The maximum oscillator output of 20mA was used to increase the signal-to-noise ratio of the measured impedance. A narrow frequency range (20Hz-100Hz) was chosen in order to remain in the linear region of the transformer and avoid saturation or resonant effects. Because the results were observed to vary slightly from one sweep to the next, an averaging function was used which averaged 16 consecutive sweeps to obtain the most accurate results. These are shown in the screen capture in Fig. 7. Unlike the short circuit tests, these results tended to demonstrate more instability, and were much more sensitive to frequency and oscillator level. The parameters can be most closely determined as:

$$R_C \approx 1{,}010.5\Omega$$
$$L_M \approx 965.5\text{mH}$$

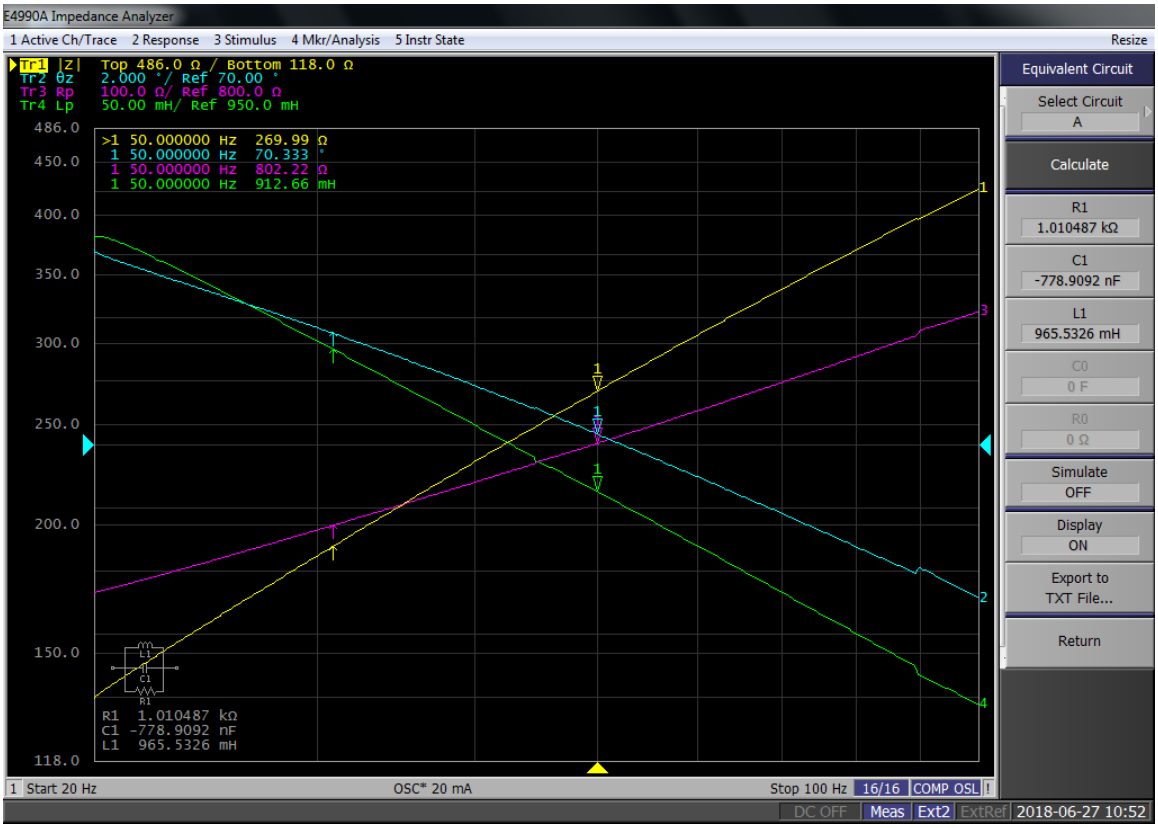

Fig. 7. Impedance analyzer results for the primary winding with the secondary winding in open circuit.

Next, no-load (excitation) current was determined by applying 200V, 50Hz to the primary winding with the secondary winding in open circuit, as shown in Fig. 8.

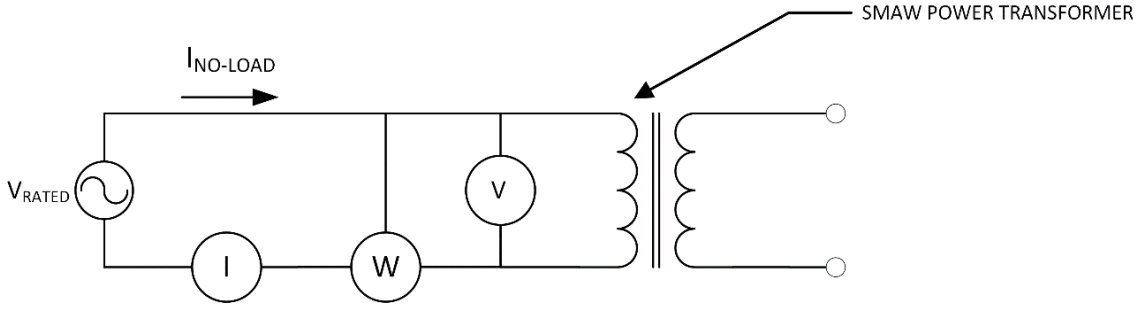

Fig. 8. Open circuit test schematic.

The resulting voltage and current waveforms are shown in Fig. 9. These results show that the no-load current was significantly distorted. The amplitude spectrum as determined by the FFT, plotted in Fig. 10, indicates significant third and fifth harmonic content. Current THD was determined to be 59.4%. This increased harmonic content in the current waveform had an increase on voltage THD, raising it to 5.4%, whereas voltage THD during the short-circuit test was only 3.4%.

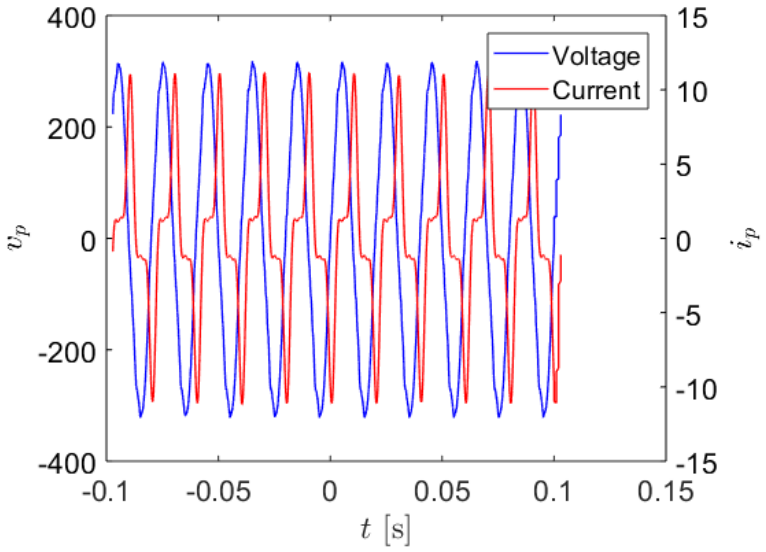

Fig. 9. No-load voltage and current waveforms.

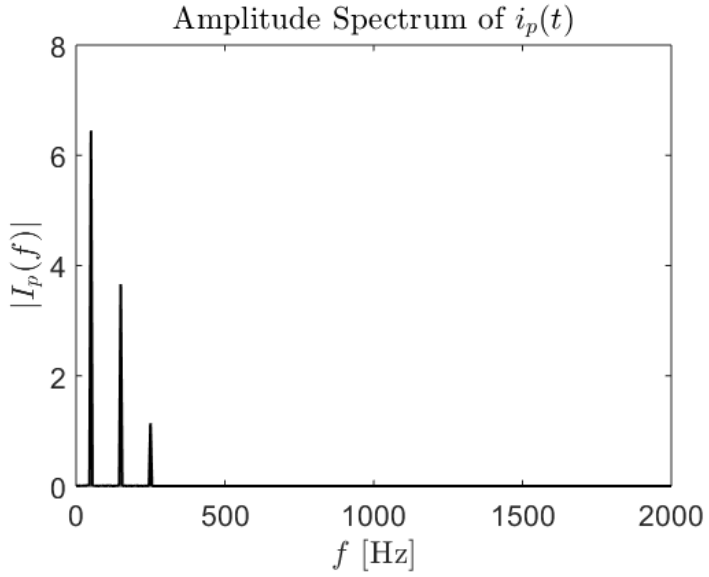

Fig. 10. No-load current amplitude spectrum.

Based on the measured voltage and current, the equivalent impedance values for R_C and L_M were found to be:

$$R_C \approx 691.0\Omega$$
$$L_M \approx 153.5\text{mH}$$

Note that these are significantly different from the impedance measurement results. The impact of saturation was found to dramatically change the equivalent impedance. To further investigate the impacts of saturation, the magnitude the fundamental and third harmonic of the no-load current was determined under a wide range of voltage conditions, varying from $25V_{RMS}$ to $240V_{RMS}$. The results, plotted in Fig. 11, show an approximately exponential relationship between voltage and current, as opposed to the

linear relationship that is typically governed according to Ohm's Law. The third harmonic also shows evidence of an exponential rise in response to increasing excitation voltage.

The characteristic impedance was also observed to vary significantly in response to different excitation voltage. As Fig. 12 shows, R_C increased slightly from approximately 1kΩ to a peak of 1.13kΩ at $100V_{RMS}$; above $100V_{RMS}$ R_C decreased at a rate of about 4.1Ω/V. In contrast, L_M was observed to increase by approximately 14mH/V up to a peak value of 2.3H at roughly $50V_{RMS}$, before exhibiting a non-linear decrease above $50V_{RMS}$.

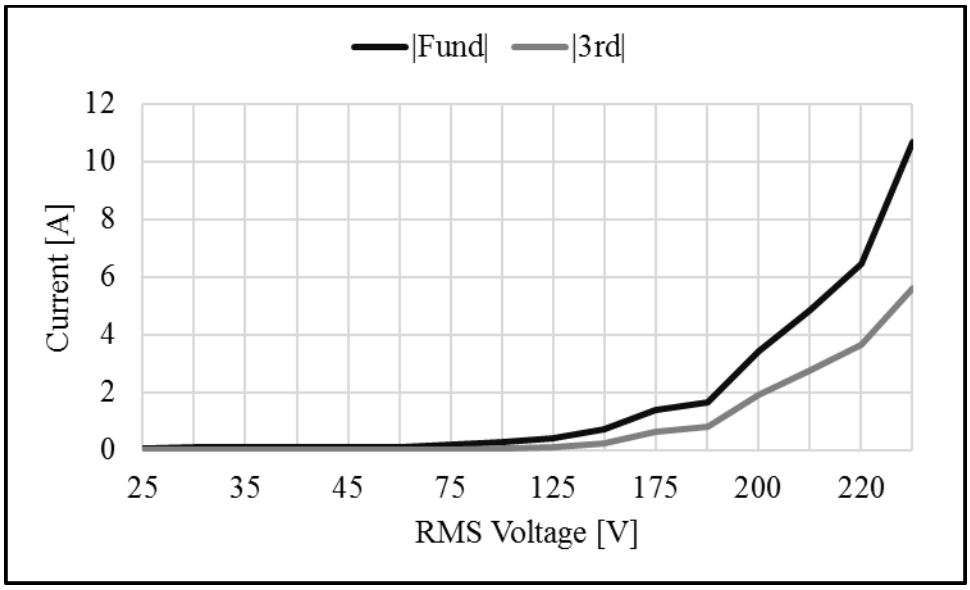

Fig. 11. Magnitude of no-load fundamental and third harmonic current vs. voltage.

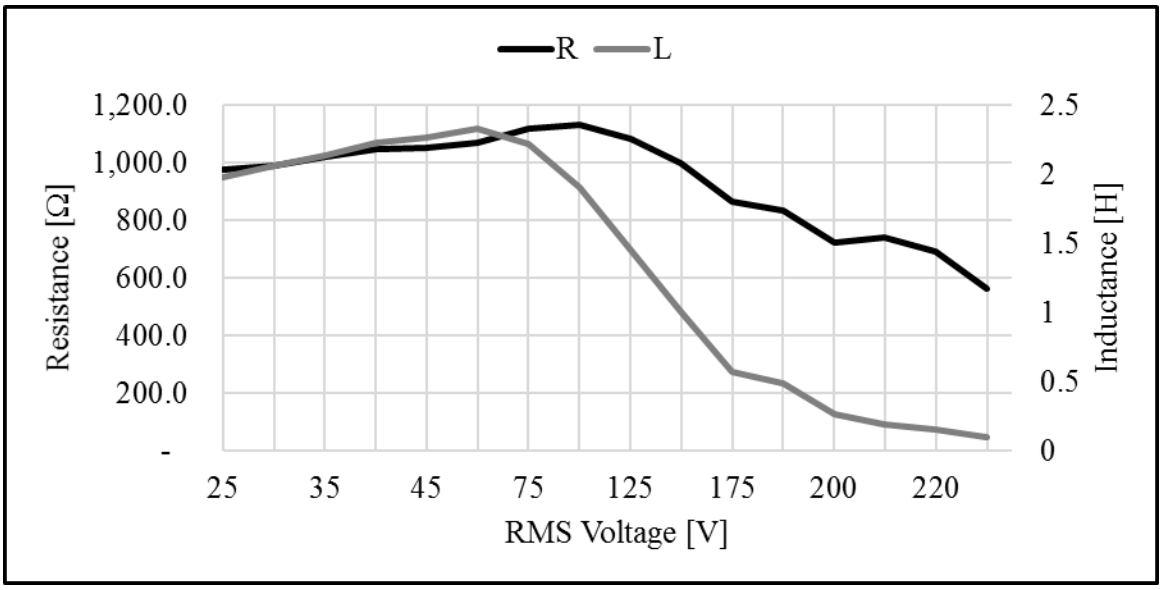

Fig. 12. Open circuit resistance and inductance vs. excitation.

The presence of harmonic content, particularly the third harmonic, was used as a proxy to determine the degree to which the transformer was saturated. Fig. 11 plots the percentage of third harmonic measured in the primary winding current versus the magnitude of the fundamental current. This plots shows that significant third harmonic was present, even at relatively low current magnitudes. Therefore, in order to accurately determine the linear parameters for the equivalent circuit, the analysis must be performed at low current amplitudes.

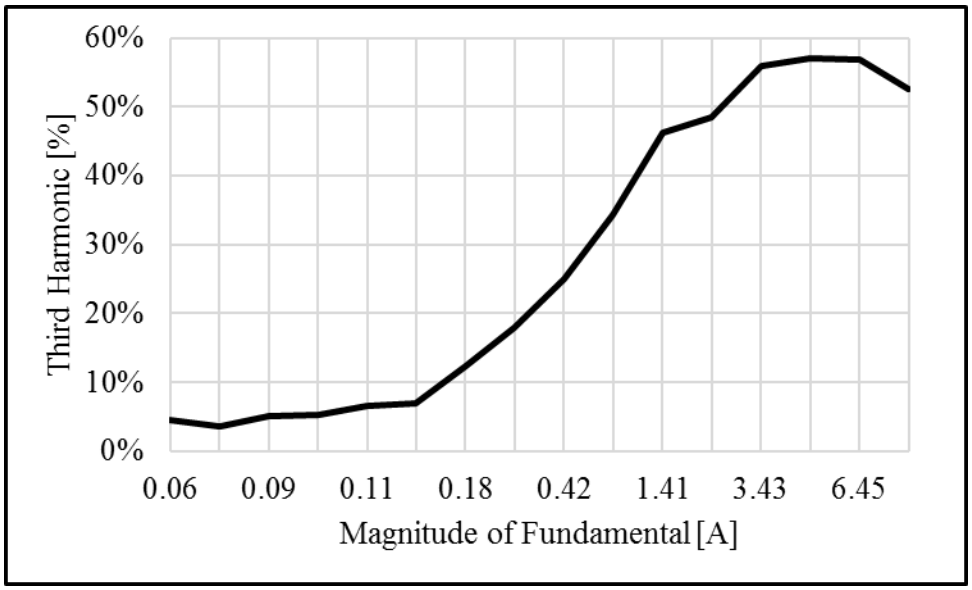

Fig. 13. Percentage of primary current third harmonic vs. magnitude of fundamental.

At rated voltage and frequency, the no-load (excitation current) was found to be:

$$I_{NO\text{-}LOAD} = 6.45 \angle 86^{o}A$$

The corresponding no-load real and reactive losses of the transformer, at rated voltage and frequency, could then be determined as:

$$P_{NO\text{-}LOAD} = 69.63W$$
$$Q_{NO\text{-}LOAD} = 997.7VAR$$

4.1.4 Practical equivalent circuit

Using the parameters found in 4.1.2 and 4.1.3, the practical equivalent circuit for the transformer operating in its linear region can be drawn as show in Fig. 14. The magnetization branch uses the values obtained from the impedance analyzer. These results are believed to reflect the most accurate parameters for the transformer operating in its linear region as the oscillator level was set to 20mA, and the impedance analyzer is capable of much higher precision and resolution at low current amplitudes compared to the current probe used for higher current measurements.

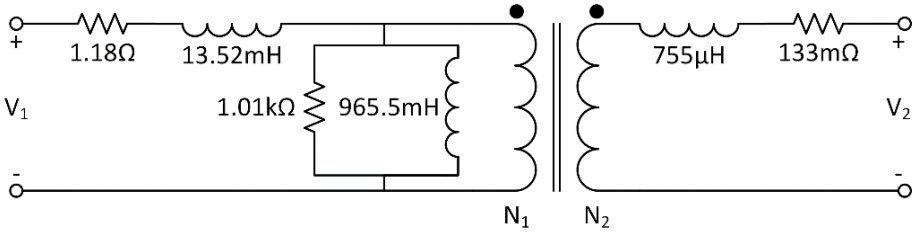

Fig. 14. Transformer practical equivalent circuit, linear region.

At rated voltage and frequency, the transformer core is saturated, which affects the equivalent impedance of the magnetization branch. Fig. 15 shows the practical equivalent circuit with R_C and L_M as determined at $220V_{RMS}$, 50Hz.

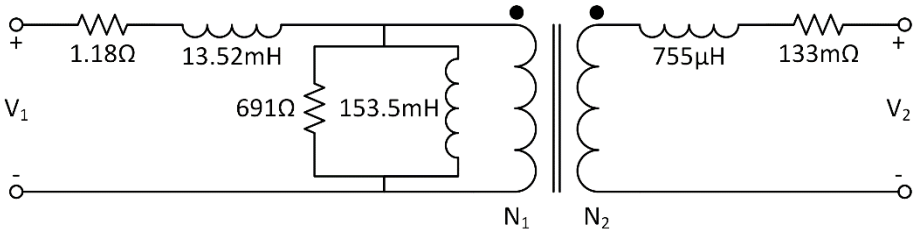

Fig. 15. Transformer practical equivalent circuit at 220V, 50Hz.

4.2 Steady-state efficiency

Steady state efficiency was evaluated by running the transformer at rated voltage and frequency using the Schneider Conext 5548 inverter as a 50Hz voltage source with the autotransformer adjusted to provide $220V_{RMS}$ to the primary winding. The secondary winding was connected to a programmable electronic load bank. Unfortunately, the load bank was limited to $36A_{RMS}$, which was not sufficient to drive the welding transformer to the high secondary currents observed during active welding. These were typically observed

to be approximately $25A_{RMS}$ for the primary winding and $105A_{RMS}$ for the secondary winding.

The RMS load current was varied in 5A intervals from 5-$35A_{RMS}$. The results, plotted in Fig. 16, demonstrate that efficiency steadily increases with load current, from a low value of 73.4% at 5A to a high value of 90.2% at 35A. This increase in efficiency as loading increases aligns with expectations, as no-load losses are typically fixed for a given voltage and frequency. At low loads, the no-load losses tend to dominate, reducing overall efficiency. However, with increasing load, the I^2R load losses from the winding resistances tend to dominate, and the no-load loss is less significant. Efficiency was essentially flat between 30-35A.

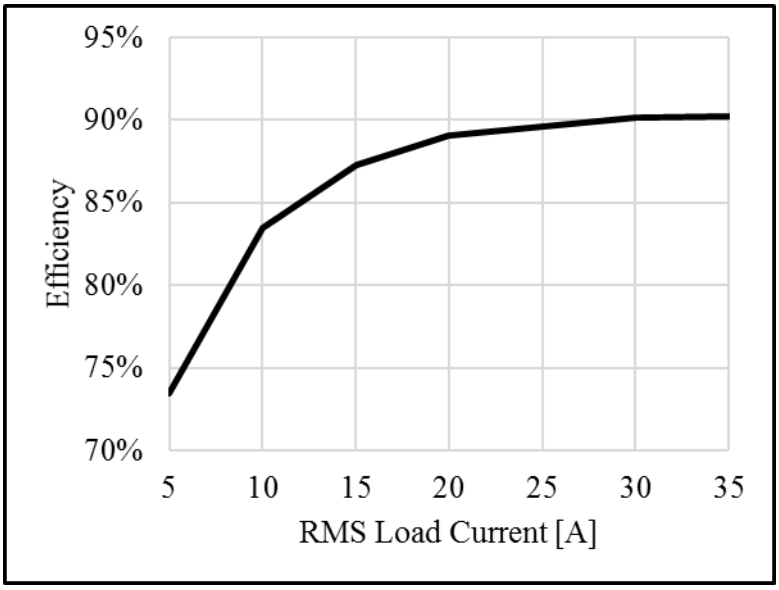

Fig. 16. Steady state efficiency vs. load current.

Using the measured losses, core (no-load) loss found in 4.1.3 and the winding resistance found in 4.1.2, the stray losses can be found. These are given in Table II.

Table II. Loss summary.

	Core loss [W]	Load loss [W]	Stray loss [W]	Total loss [W]
5A	69.63	22.54	2.23	92.17
10A	69.63	36.10	8.07	105.7
15A	69.63	59.45	22.15	129.1
20A	69.63	92.06	42.81	161.7
25A	69.63	133.8	64.60	203.4
30A	69.63	184.4	99.02	254.0
35A	69.63	250.3	140.9	319.9

4.3 Temperature Rise Testing

Most commercially available welders come have a manufacturer specified *duty cycle*, typically normalized to a 10 minute period. The duty cycle dictates the amount of time that the welder can be operated in a given 10 minute period in order to prevent overheating. For example, a welder with a 50% duty cycle may only be operated for five minutes out of every ten; it must be allowed to cool during the other five.

The SMAW that was received from Kigali did not have a rated duty cycle, so it was subjected to a temperature rise test to quantify the temperature rise and fall characterization test in order to develop one. The test configuration resembled that of the short circuit test; the secondary winding was short-circuited with a short length of 2/0AWG conductor, and the primary winding was connected to the Schneider Conext 5548 inverter operating at 50Hz. The autotransformer was adjusted until the current circulating in the primary winding was roughly equal to the average primary current that was observed during active welding (about $25A_{RMS}$). The experimental setup is shown in Fig. 17.

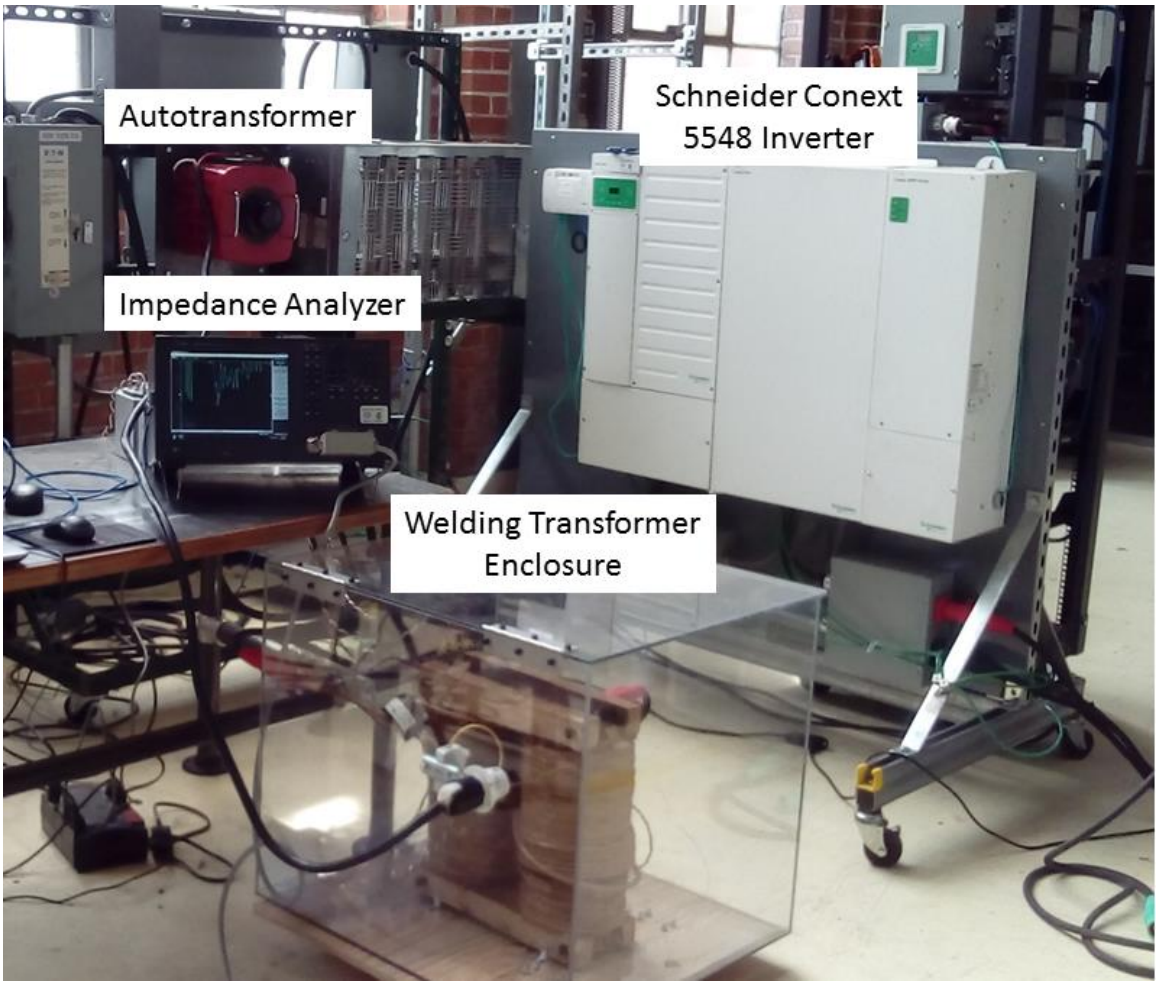

Fig. 17. Experimental setup for temperature rise test.

Temperature rise was measured by observing the change in the primary winding resistance over time. Resistance increases with temperature, so the temperature rise of the winding could be calculated using EQ. 4.

$$T_w = \frac{R}{R_o}(k + T_o) - k \qquad \text{EQ. 4}$$

Where:

T_w = Average winding temperature (^{o}C)
R_o = Initial winding resistance (Ω)
T_o = Initial winding temperature (^{o}C)
R = Measured hot winding resistance
k = 229 for transformers with a mix of aluminum and copper

The temperature rise test was conducted after the welding transformer had sat idle for a period of several hours, such that the internal winding temperature could be assumed to be equal to the surface temperature. The surface temperature was established using the Tacklife IT-T05 infrared thermometer, and the corresponding initial winding resistance was determined using the Keysight E4990A impedance analyzer using the same procedure as in 4.1.2. Full current ($25A_{RMS}$) was applied to the primary winding in three minute intervals. In between each three minute interval, the transformer was de-energized, and the winding resistance was determined using the impedance analyzer. This led to the transformer being de-energized for approximately 30s while the readings were being taken; during this period, the winding temperature may have decreased by 0.5-0.8^{o}C.

Although in the field these welding transformers are operated in free air, it was deemed unsafe to conduct the temperature rise test in this manner. For this reason, the testing was performed with the welder inside the polycarbonate enclosure with the lid closed. It must be acknowledged that operating the transformer inside the enclosure will greatly increase the overall temperature rise compared to operating in free air. These results can therefore be taken as conservative or "worst case" values.

Electrical cellulose insulation (such as kraft paper or crepe paper) is typically rated for 90^{o}C (formerly IEC thermal class Y) or 105^{o}C (formerly IEC class A). The insulation class for this transformer was unknown. The first temperature rise test was conducted until the winding temperature was determined to be approximately 105.1^{o}C. At this temperature, significant discoloration of the insulation was observed, indicating that the insulation was experiencing thermal damage. It was therefore determined that this insulation is only suitable for a maximum temperature of 90^{o}C. Fig. 18 shows a photo of the discoloration; note that the exposed conductor was the result of insulation abrasion during shipping, and not the temperature rise test.

Fig. 18. Discoloration of insulation due to excessive temperature rise.

The temperature rise can be observed in Fig. 19 which plots the primary winding temperature vs. time.

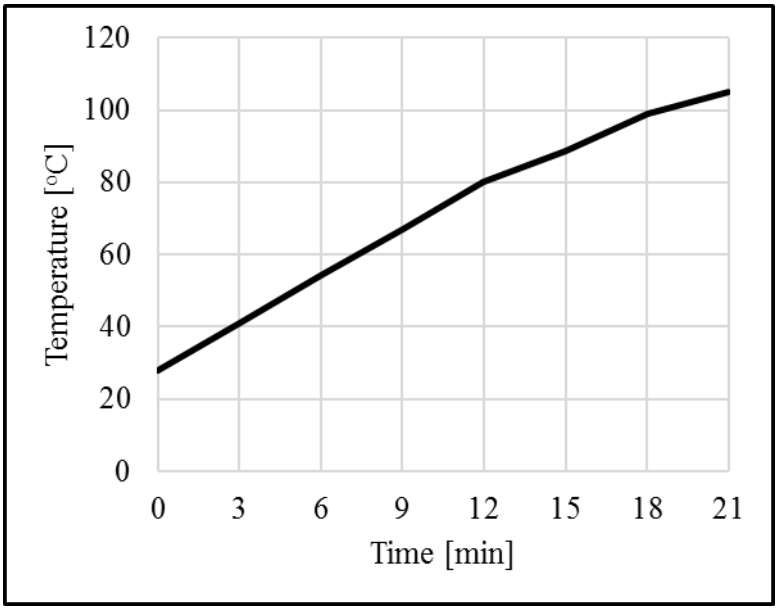

Fig. 19. Primary winding temperature vs. time, rising.

The temperature rise as a function of time can be closely approximated by the quadratic equation EQ. 5.

$$T_{Rise}(t) = -0.0621t^2 + 5.31t + 16.6 \quad \text{EQ. 5}$$

Next, the transformer was de-energized, and resistance measurements were taken in five minute intervals to plot the temperature fall, starting at 90°C. These results are plotted in Fig. 20.

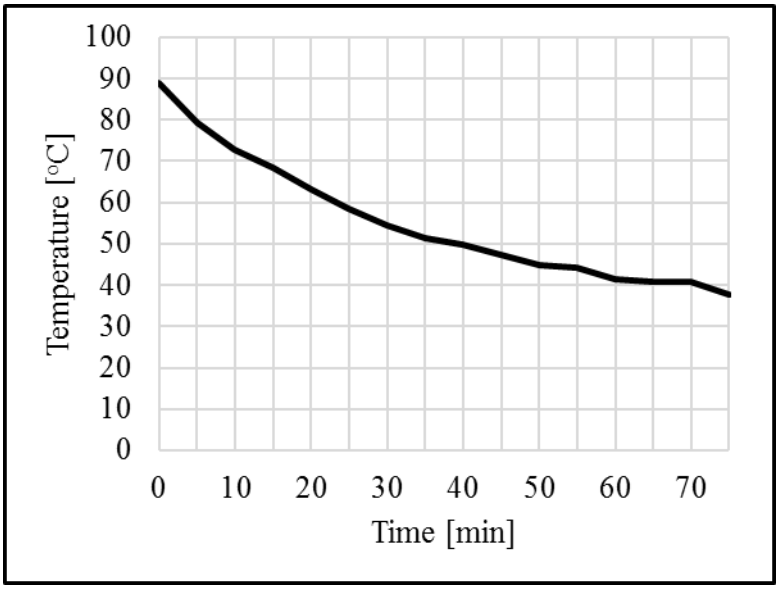

Fig. 20. Primary winding temperature vs. time, falling.

Temperature fall as a function of time can be approximated by the cubic equation EQ. 6.

$$T_{Rise}(t) = -1.11 * 10^{-4}t^3 + 2.48 * 10^{-2}t^2 - 2.11t + 107 \quad \text{EQ. 6}$$

Using these equations, the temperature rise and fall for different duty cycles was simulated, assuming a fixed constant duty cycle for an eight hour shift. The simulations began with an ambient temperature of 25°C. The results for a 30% duty cycle are plotted in Fig. 21.

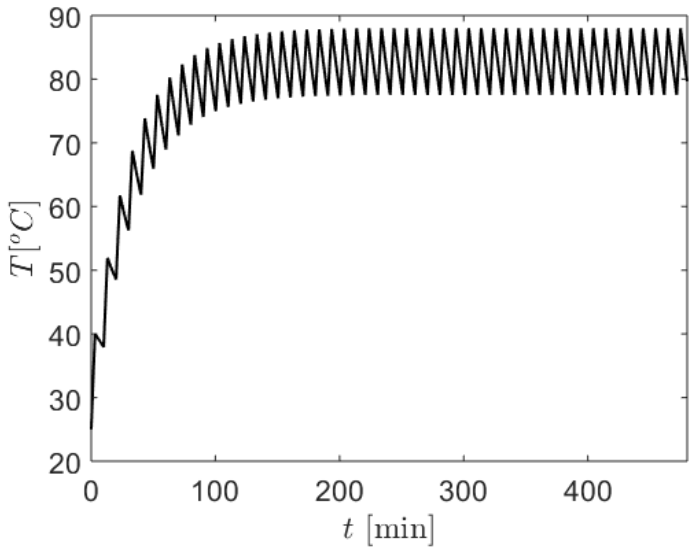

Fig. 21. Simulated temperature rise at 30% duty cycle for eight hour shift.

These results show that, for the first three hours of use, the temperature rise will exceed the temperature fall, leading to an overall increase in winding temperature. After this, the temperature rise and fall will cancel each other out during each 10 minute period, and the winding temperature will remain within 77-88ºC over the course of each period for the duration of the shift. Note that the upper end of this range, 88ºC, is very close the maximum allowable temperature of 90ºC. Therefore, if prolonged use of the welder in an enclosed area is anticipated, a 25% duty cycle should be maintained.

The results for a 25% duty cycle are plotted in Fig. 22 and show a peak winding temperature of 79.2ºC.

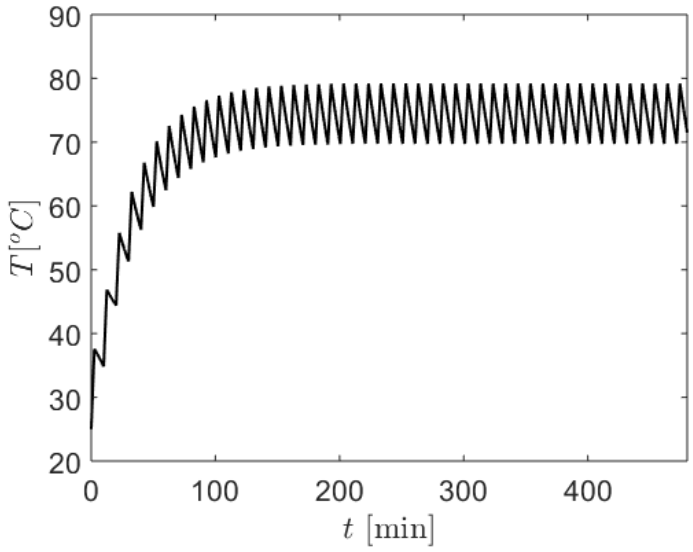

Fig. 22. Simulated temperature rise at 25% duty cycle for eight hour shift.

4.4 Welding Performance Testing

Two rounds of active welding were performed using the SMAW. The first was done for the purposes of determining baseline expected values for peak and average current, active and reactive power, and power factor. In the second round of testing, voltage and current waveforms were collected on both the primary and secondary windings, and a variety of steady-state average power metrics were recorded.

The SMAW was set up in the welding shop connected to a 50A, 208V, 60Hz outlet. Welder testing was conducted at 60Hz, rather than 50Hz, due to the impracticality of installing a 50Hz source in the welding shop. Welding was conducted using E6013 welding rods as these are suitable for low current, sheet metal welding. Steel plate and steel angle stock that was available on hand was used. The E6013 rods were used to weld beads onto the steel plate. In each test, the arc length was maintained until the welding rod was completely expended. A photo of the welder testing is included in Fig. 23.

People performing welding work in Africa often lack basic protective equipment, including appropriate welding face shields. As a result, the arc lengths tend to be longer, as the welder cannot see the tip of the electrode. For this reason, welding testing was performed with two arc lengths: a short arc, where the tip of the welding electrode was barely above the steel plate, and a longer arc, where the tip of the welding electrode was maintained at approximately 1/8” above the steel plate.

Two sets of measurements were taken using a Bitronics M572 power meter. Steady state, average values were recorded at a rate of two samples per second for a variety of power and power quality metrics. Waveform data was also captured for primary and secondary voltage and current at a rate of 128 samples per cycle (7.68kS/s). The results for these two tests are summarized in Table III.

Fig. 23. Photo of active welding testing.

Table III. Welding performance test results

	Short arc 1	Short arc 2	Long arc 1	Long arc 2
Primary current, avg. [A_{RMS}]	24.51	23.65	17.31	18.69
Primary current, peak [A]	61.20	64.49	59.91	60.34
Secondary current, avg. [A_{RMS}]	99.35	95.56	68.23	74.64
Secondary current, peak [A]	192.8	224.6	219.2	173.2
Primary real power, avg. [W]	3,199	3,066	2,389	2,597
Primary real power, peak [W]	4,542	4,319	4,167	4,127
Secondary real power, avg. [W]	2,268	2,189	1,818	1,955
Secondary real power, peak [W]	2,895	2,954	2,884	2,800
Primary reactive power, avg. [VAR]	3,917	3,671	2,557	2,732
Primary reactive power, peak [VAR]	7,443	7,458	7,417	7,414
Secondary reactive power, avg. [VAR]	359.3	427.7	410.2	435.3
Secondary reactive power, peak [VAR]	1,164	1,148	1,150	1,524
Primary current THD [%]	12.6	4.9	2.3	10.7
Primary power factor, avg.	0.63	0.64	0.68	0.69

Energy [Wh]	56.42	60.46	62.72	66.72
Weld length [cm]	15.24	15.56	22.23	26.04
Throughput [Wh/cm]	3.702	3.888	2.822	2.563
Efficiency	70.9%	71.4%	76.1%	75.3%

For the short arc tests, primary current was between 23.5-25A_{RMS}, average, with peaks in the 55-60A range. Average input power around 3.1kW, 0.64 PF lagging. However, as Fig. 24 shows, real and reactive power varied significantly during the course of welding, with brief surges up to 4.5kW, as well as periods where the arc extinguished and power fell to near zero, before rising again. Current distortion was much lower during active welding compared to open circuit current, which had significant third and fifth harmonic content. An example of the voltage and current waveforms is plotted in Fig. 25. Fig. 26 shows the welds created using the short arcs. The welds created were approximately 15.5cm (approximately 6") and consumed 56-60Wh, or around 3.8Wh/cm of welding. Welder efficiency, taken as the ratio of measured output power to input power, was approximately 71%.

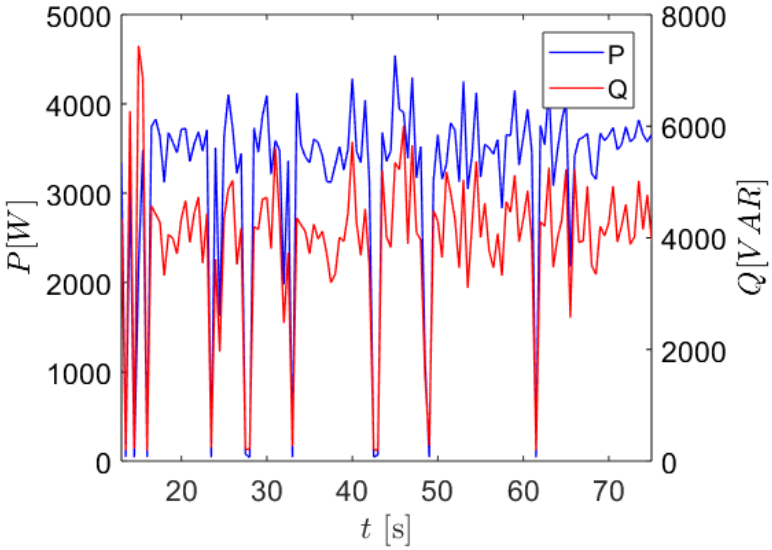

Fig. 24. Real and reactive power for short arc test.

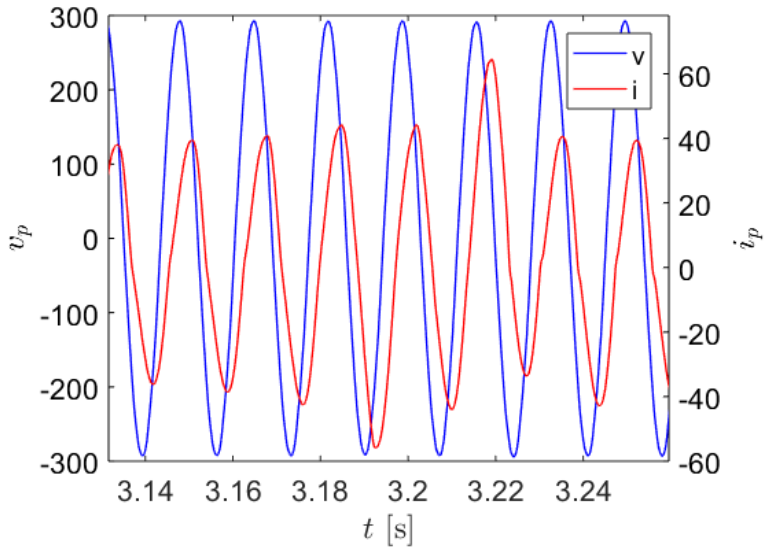

Fig. 25. Primary winding voltage and current waveforms for short arc test.

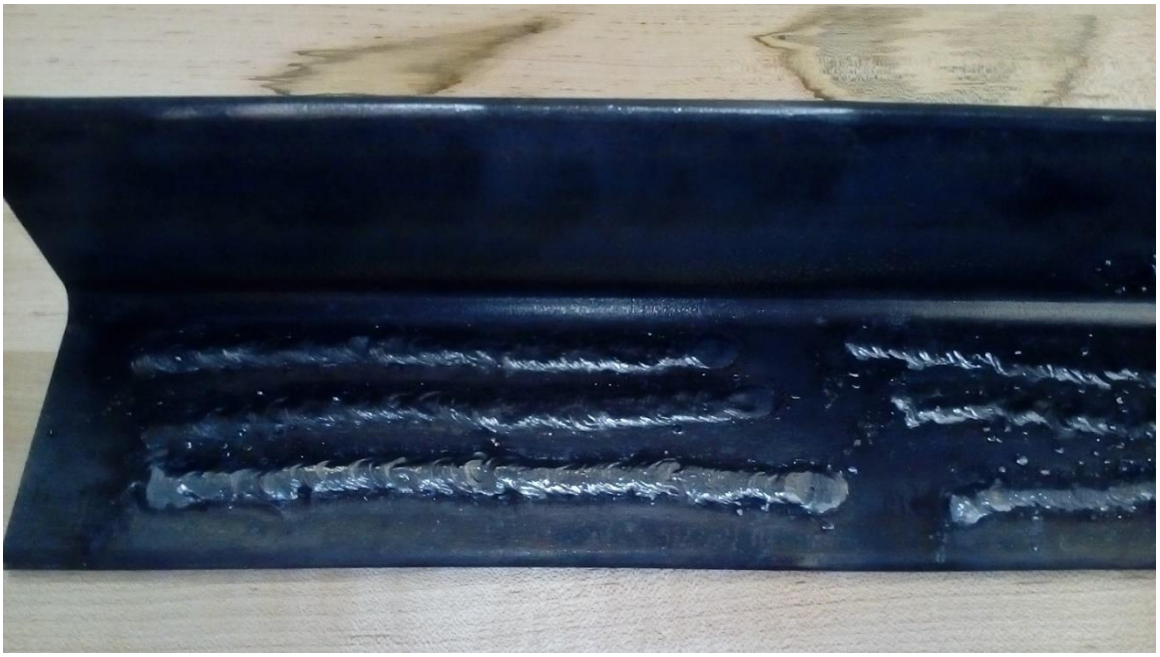

Fig. 26. Bead on plate welds created by short arc.

Longer arcs consumed less power overall, about 2.5kW at 0.68PF, lagging; peaks over 4kW were observed. Maintaining a consistent arc was more difficult, and more extinguishing events can be observed in the real and reactive power results plotted in
Fig. 27. Primary and secondary currents were about 25% lower than the short arc test; primary voltage and current waveforms can be seen in Fig. 28. Welding efficiency was higher, about 75%, and longer welds could be performed – about 22-26cm. Overall, the throughput when using a longer arc was much greater, about 2.7Wh/cm compared to 3.8Wh/cm when using a short arc. However, the longer arc produced a lower quality weld.

It was less uniform and had a “choppy” appearance, and there was more slag deposited on the steel.

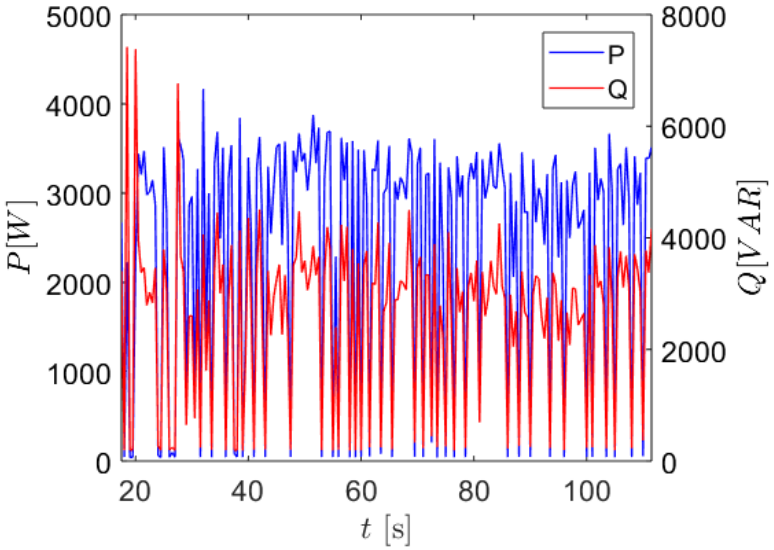

Fig. 27. Real and reactive power for long arc test.

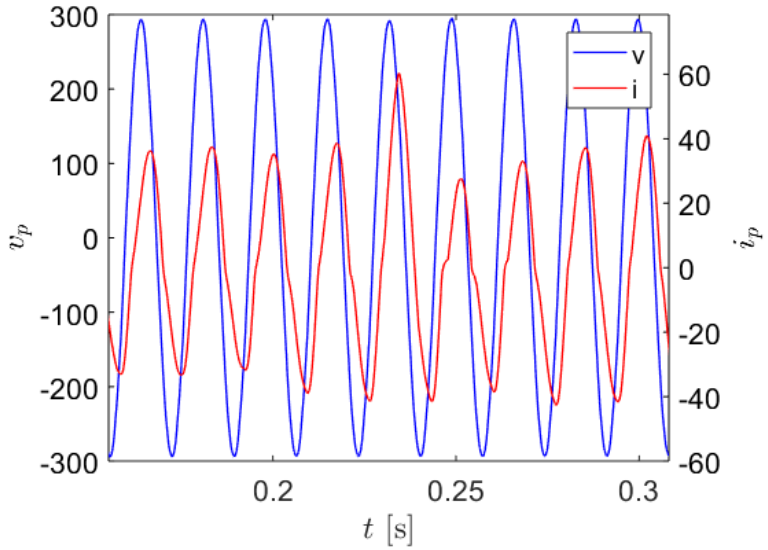

Fig. 28. Primary winding voltage and current waveforms during long arc test.

Fig. 29. Bead on plate welds created by long arc.

Temperature rise was similar to what was observed during the temperature rise test, approximately 4^{o}C/min. A thermal image taken after welding is shown in Fig. 30.

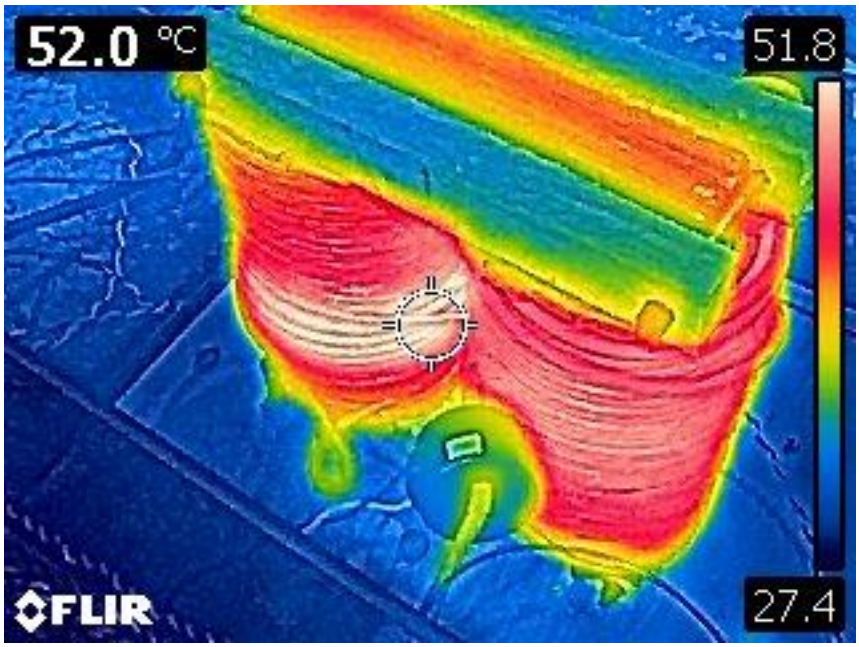

Fig. 30. Thermal image of SMAW immediately after welding.

5 References

[1] *IEEE Standard for General Requirements for Dry-Type Distribution and Power Transformers*, IEEE Standard C57.12.01, 2015.

[2] J.D. Glover, M.S. Sarma, and T.J. Overbye, *Power System Analysis and Design*, Toronto, ON: Thomas Learning, 2008.

[3] *Impedance Measurement Handbook: A guide to measurement technology and techniques*, Keysight Technologies Application Note, 6th ed., 2016.

[4] *Electrical insulation – Thermal evaluation and designation*, IEC Standard 60085, 2007.

Appendix A: Data file description

The complete data results that were captured during testing can be found in "Stick Welder Test Data_CSU2018.xls". This workbook combines the data results for all testing, with one sheet per test. Data for 20 tests total are included. These are:

- Short Arc Steady State 1 – Steady state data values while welding using a short welding arc
- Short Arc Steady State 2 – Steady state data values while welding using a short welding arc
- Short Arc Waveform 1 – High frequency waveform capture of input voltage and current while welding using a short welding arc
- Short Arc Waveform 2 – High frequency waveform capture of input voltage and current while welding using a short welding arc
- Long Arc Steady State 1 – Steady state data values while welding using a long welding arc
- Long Arc Steady State 2 – Steady state data values while welding using a long welding arc
- Long Arc Waveform 1 – High frequency waveform capture of input voltage and current while welding using a long welding arc
- Long Arc Waveform 2 – High frequency waveform capture of input voltage and current while welding using a long welding arc

The data columns for the steady state data are as follows:

- Column A – Elapsed time in seconds. Each test starts from time t=0
- Column B – RMS line to neutral voltage for primary winding, line 1
- Column C – RMS line to neutral voltage for primary winding, line 2
- Column D – RMS line to line voltage for primary winding
- Column E – RMS current for primary winding, line 1
- Column F – RMS current for primary winding, line 2
- Column G – Active power for primary winding
- Column H – Reactive power for primary winding
- Column I – Apparent power for primary winding
- Column J – Power Factor for primary winding
- Column K – Frequency of input voltage to primary winding
- Column L – Total Harmonic Distortion (THD) for primary winding voltage
- Column M – Total Harmonic Distortion (THD) for primary winding current
- Column N – RMS line to neutral voltage for secondary winding, line 1
- Column O – RMS line to neutral voltage for secondary winding, line 2
- Column P – RMS line to line voltage for secondary winding
- Column Q – RMS current for secondary winding, line 1
- Column R – RMS current for secondary winding, line 2
- Column S – Active power for secondary winding
- Column T – Reactive power for secondary winding
- Column U – Apparent power for secondary winding
- Column V – Power Factor for secondary winding
- Column W – Total Harmonic Distortion (THD) for secondary winding voltage
- Column X – Total Harmonic Distortion (THD) for secondary winding current

The data columns for the waveform data are as follows:

- Column A – Elapsed time in seconds. Each test starts from time t=0
- Column B – Instantaneous line to neutral voltage for primary winding, line 1
- Column C – Instantaneous line to neutral voltage for primary winding, line 2

- Column D – Instantaneous line to line voltage for primary winding
- Column E – Instantaneous line to neutral voltage for secondary winding, line 1
- Column F – Instantaneous line to neutral voltage for secondary winding, line 2
- Column G – Instantaneous line to line voltage for secondary winding
- Column H – Instantaneous current for primary winding, line 1
- Column I – Instantaneous current for primary winding, line 2
- Column J – Instantaneous current for secondary winding, line 1
- Column K – Instantaneous current for secondary winding, line 2

5.3. Multi-Purpose Mill Test Methods

Test Method for Grain Mills Driven by Electric Motors

Colorado State University
Factor[e] Ventures
430 N College Ave.
Fort Collins, CO 80524
11 January 2019

Table of contents

1. Objective 1
1.1. Scope 1
2. Instrumentation 1
2.1. Voltage 1
2.2. Current 1
2.3. Power 1
2.4. Speed 1
2.5. Torque 1
2.6. Temperature 2
2.7. Weight 2
2.8. Moisture content 2
2.9. Audible noise 2
2.10. Electromagnetic noise 2
2.11. Accuracy 2
2.12. Calibration 3
3. Test Configuration 3
3.1. Description of testing components 4
3.1.1. Input hopper 4
3.1.2. Decibel meter 4
3.1.3. Output catchment 4
3.1.4. Current sensor 4
3.1.5. Voltage sensor 5
3.1.6. DC power supply 5
3.1.7. AC power supply 5
4. Motor Tests 5
4.1. Winding resistance measurement 5
4.1.1. Precision resistance meter or impedance analyzer 6
4.1.2. Bridge method 6
4.1.3. Voltage Drop Method 7
4.2. Winding temperature rise 8
4.3. Efficiency 8
5. DC Motor Tests 9
5.1. Winding inductance measurement 9
5.1.1. Shunt and compound-wound machines 9
5.1.2. Series excited machines 9
5.2. Magnetic saturation 10
5.2.1. Separately driven 10
5.2.2. Self-driven 10
5.3. Voltage vs. rotational speed 10
5.4. Speed regulation 10

5.5. Efficiency 11
5.5.1. Machine loading 11
5.5.2. Segregated loss method 12
5.6. Torque-current characterization curve 12
6. AC Induction Motor Tests 13
6.1. Locked-rotor tests 13
6.1.1. Locked rotor current and torque 14
6.2. No-load test 15
6.2.1. Separately driven 15
6.2.2. Self-driven 15
6.3. Efficiency 15
6.3.1. Machine loading 16
6.4. Power Factor 17
6.5. Speed-torque and Speed-current Characteristic 17
6.5.1. Measured output 18
6.5.2. Acceleration 19
6.5.3. Input 19
6.5.4. Direct measurement 20
7. Mill Performance Testing 20
7.1. Feedstock preparation 20
7.2. Variable voltage DC systems 20
7.3. Mill test and evaluation criteria 21
7.3.1. Crushing efficiency 21
7.3.2. Throughput 21
7.3.3. Energy intensity 21
7.3.4. Average load, peak load and load factor 22
7.3.5. Tip speed and centrifugal force (hammer mills only) 22
7.3.6. Clogging 23
7.3.7. Motor winding temperature 23
7.3.8. Audible noise 23
7.3.9. Grain evaluation 23
8. References 23

List of figures

Figure 1. Test configuration diagram. 4
Figure 2. Wheatstone bridge. 6
Figure 3. Kelvin bridge. 7
Figure 4. Voltage drop method 8
Figure 5. Pump-back test system diagram. 12
Figure 6. Equivalent circuit for an induction motor (single-cage rotor model). 13
Figure 7. Induction motor locked-rotor equivalent circuit 14
Figure 8. Diagram for motor-generator slip test. 16
Figure 9. Representative speed vs. torque characteristic curve for a single-phase induction motor. 18

List of tables

Table 1. Instrument accuracy requirements. 3
Table 2. Instrument calibration intervals. 3

1. Objective

The purpose of this document is to outline the preferred method for testing agricultural grain mills driven by brushed or brushless Direct Current (DC) motors, or by AC induction motors.

1.1. Scope

This testing is for determining the electrical parameters and characteristics, overall efficiency, and general performance characteristics for the grain mill under test. Photos of the output are recommended, but a comprehensive, objective quality assessment of the crushed grain and/or flour output is outside the scope of this document. Methods for determining segregated motor losses are not addressed as part of this methodology. These and other miscellaneous motor tests are covered by the standards IEEE 113 for DC motors, and IEEE 112 and IEEE 114 for poly-phase and single-phase induction motors, respectively.

2. Instrumentation

It is recommended that all measurements be taken using electronic instruments with analog outputs that can be read and recorded by a data logger.

2.1. Voltage

Voltage measurements should be made at or as near to the terminals as possible. If, for some reason, they cannot be, then the error should be evaluated and subsequent readings corrected. Tests should be conducted at rated voltage for the motor.

2.2. Current

Current measurements can be made with in-line current sensors or current transformers if the magnitude of the measured current is too high. Hall effect sensors may also be used. For appliances with DC motors, DC compatible current sensors must be used. Current draw by instruments, such as volt and/or watt-meters, should be subtracted to obtain the net motor current.

2.3. Power

Power measurements can be made using a dedicated watt-meter. For DC motors, power can be calculated by taking the product of Voltage (as measured in 2.1) and current (as measured in 2.2).

2.4. Speed

Motor and mill speed measurements can be made using tachometers, frequency-responsive devices, or magnetic pickups. Stroboscopes are discouraged due to uncertainty in precision and limited accuracy.

2.5. Torque

Torque measurements may be made using transmission dynamometers, torsion dynamometers, strain gauge type torque measuring devices, calibrated motors, or other methods of acceptable accuracy.

If a dynamometer is being used, its rating should not exceed three times the rating of the mill motor, and the rated torque of the dynamometer should not be greater than four times the maximum rated motor torque. Additionally, the dynamometer should be sensitive to a change in torque less than or equal to 0.1% of the rated motor torque.

2.6. Temperature

Temperature may be measured using electric or mercury thermometers, or by using thermocouples or Resistance Temperature Detectors (RTDs).

2.7. Weight

Accurate scales, either electrical or mechanical, should be used for determining the weight of the unprocessed grain input and processed output.

2.8. Moisture content

Moisture content of the grain should be assessed prior to beginning testing. A resistive or capacitive moisture meter is recommended. Moisture probes should only be used for bulk grain, where the insertion depth is greater than 0.5m.

2.9. Audible noise

A decibel meter should be installed to monitor audible noise levels generated by the mill during testing.

2.10. Electromagnetic noise

Electronic instruments feature higher input impedance than passive instruments, which means they draw less current, thereby reducing the need to make corrections for current drawn by the instrument. They are, however, more susceptible to electromagnetic noise.

Common noise sources include:

- Inductive or electrostatic coupling of signal leads to power circuits
- Inadequate common mode rejection
- Common impedance coupling or ground loops
- Conducted interference from power circuits

Good practices for minimizing electromagnetic noise should be adhered for all electronic instruments. These include:

- Using shielded, twisted pair wires for signal leads
- Grounding the shield at only one point
- Maintaining as much distance as is practical between signal leads and power cables
- Grounding all exposed metal parts

2.11. Accuracy

Instrument error is rated as a percentage of the full scale for the measurement instrument. For this reason, it is important to size measurement instruments appropriately such that the full scale of the instrument is close to the expected range of operating values. Instrument transformers should be avoided if possible because they can inject additional error into measured values. If instrument transformers are used, their error must not exceed ±0.3%.

Accuracy for all measurement devices must adhere to the values specified in Table 1.

Table 1. Instrument accuracy requirements.

Measured Value	Accuracy of the instrument as a percentage of the values
Voltage	±0.2%
Current	±0.2%
Power	±0.2%
Frequency	±0.05%
Resistance	±0.2%
Torque	±0.7%
Motor speed	±0.3% or 1.0 rpm, whichever is less

2.12. Calibration

The recommended calibration intervals found in Table 2 should be followed for all instruments and measurement equipment, unless they differ from manufacturer's recommendations, in which case the manufacturer's recommended calibration interval shall be used.

Table 2. Instrument calibration intervals.

Instrument type	Calibration interval
Electrical parameters	
Voltage	12 months
Current	12 months
Power	12 months
Frequency	12 months
Resistance	12 months
Mechanical torque	
Dynamometer with scale	6 years
Dynamometer with load scale	6 months
Torque bar	1 year
Calibrated motor	Not required
Strain gauges	6 months
Rotational speed	
Tachometers	3 years
Eddy current drag	10 years
Electronic (gear teeth)	Not required
Temperature	
Electric	Electric
Mercury	Mercury

3. Test Configuration

An example diagram showing a hammer mill is shown in Figure 1.

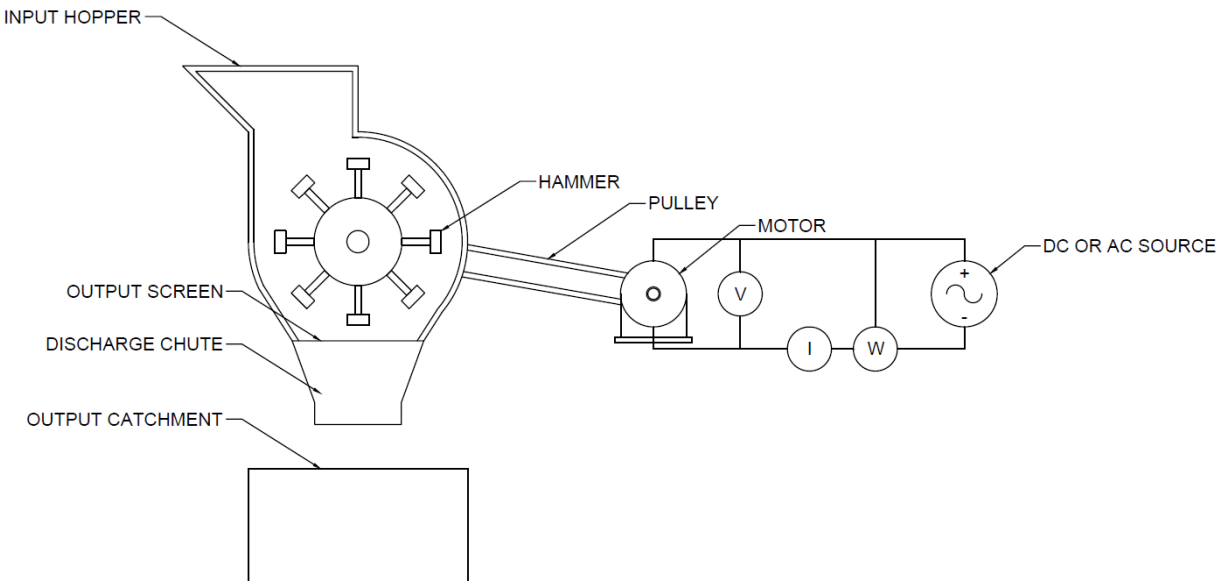

Figure 1. Test configuration diagram.

3.1. Description of testing components

This section describes the various aspects of the testing setup shown in Figure 1.

3.1.1. Input hopper

The grain level in the input hopper should be continuously fed during operation to maintain a constant level of grain flow during the test. At no point should the machine be allowed to run empty (no-load) during testing. If a hopper is used other than what is provided as part of the mill under test, care should be taken such that the hopper allows for smooth mass flow, rather than restricted 'funnel-flow'. Funnel flow is characterized by stagnant areas that form around the periphery of the hopper and are undesirable for testing.

3.1.2. Decibel meter

A decibel meter should be installed approximately one meter from the mill under test. Audible noise levels should be recorded under no-load conditions and while the mill is operating normally.

3.1.3. Output catchment

A suitable catchment vessel should be provided to capture and hold all output from the test such that the mill is able to run continuously for the entire length of the test

3.1.4. Current sensor

An in-line, Hall effect, or current transformer-type current sensor meeting the requirements in section 2 shall be used to monitor the AC or DC input current to the mill motor.

3.1.5. Voltage sensor

The input voltage to the mill motor shall be monitored either directly or by means of a voltage divider, or an AC or DC voltage transducer, meeting the requirements in section 2.

3.1.6. DC power supply

For mills with DC motors, the DC power supply shall be capable of supplying rated voltage and power to the mill motor, and must be essentially ripple free. To be considered ripple free, the peak-to-peak value of the AC current component shall be less than 6%, or the RMS value less than 2%, of the rated current of the test motor under all test conditions.

3.1.7. AC power supply

An AC power supply capable of supplying the full load current of the mill motor at the rated voltage and frequency shall be provided. The voltage waveform should be as close to purely sinusoidal as possible; voltage waveform deviation should not exceed 10%. The frequency should be maintained within ±0.5% of the required testing value. When evaluating motor efficiency, the rated frequency must be within ±0.5% of the required test value.

4. Motor Tests

This section outlines test procedures for electrically characterizing the motor used to drive the mill. This section outlines test procedures that are applicable to both DC and AC motor types. Tests methodologies that are specific to DC motors are detailed in 5. If the motor uses an AC induction motor, the procedures in 6 should be followed.

4.1. Winding resistance measurement

The electrical resistance of the motor windings should be established in order to estimate conduction (I^2R) loss in the machine, as well as determining temperature rise in the windings. The resistance measurement should be determined using a high precision milliohm meter, impedance analyzer, or via a Wheatstone bridge. Resistance measurements should be taken under "cold" conditions when the motor has sat idle for sufficient time such that the winding temperature is equal to ambient air temperature. All resistance measurements should be corrected to a standard reference temperature of 25°C. Temperature correction should be calculated using EQ. 1:

$$R_s = \frac{R_t(t_s + k)}{(t_t + k)} \qquad \text{EQ. 1}$$

Where:

R_s= Resistance of winding measured at specified reference temperature t_s (Ω)
R_t = Resistance of winding at measured temperature t_t (Ω)
t_s = Specified reference temperature (25°C)
t_t = Measured temperature (°C)
k = 234.5 for copper
224.8 for aluminum

Resistance measurements may be made using a sufficiently accurate, calibrated precision resistance meter or impedance analyzer, or by the bridge method. The voltage drop method is an acceptable alternate method.

4.1.1. Precision resistance meter or impedance analyzer

A digital precision milli-ohm or micro-ohm meter or impedance analyzer with a resolution of ≤ 0.1mΩ and an accuracy of ±0.2% may be used for resistance measurements. Four wire resistance measurements should be made to compensate for lead resistance. Resistance measurements should be made as close to the motor terminal windings as possible, with an ambient temperature at or near 25°C.

4.1.2. Bridge method

The bridge method is the preferred method for measuring low resistances with high accuracy, without the high equipment cost of a precision resistance meter or impedance analyzer. The Wheatstone bridge circuit, shown in Figure 2, is typically used for high precision measurements of resistance ≥ 1Ω.

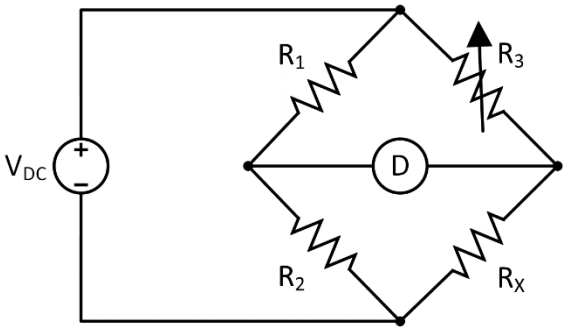

Figure 2. Wheatstone bridge.

Two known resistors, R_1 and R_2, are connected to the unknown winding resistance R_X, along with an adjustable resistor R_3. A detector (either current or voltage) is connected between the two nodes as shown. When the circuit is balanced, there will be no voltage nor current flow through the detector. When this occurs, the unknown resistance R_X can be calculated by EQ. 2.

$$R_X = \frac{R_2 R_3}{R_1} \qquad \text{EQ. 2}$$

For resistances < 1Ω the lead wire resistances should be compensated for; the Kelvin bridge, shown in Figure 3 is therefore recommended.

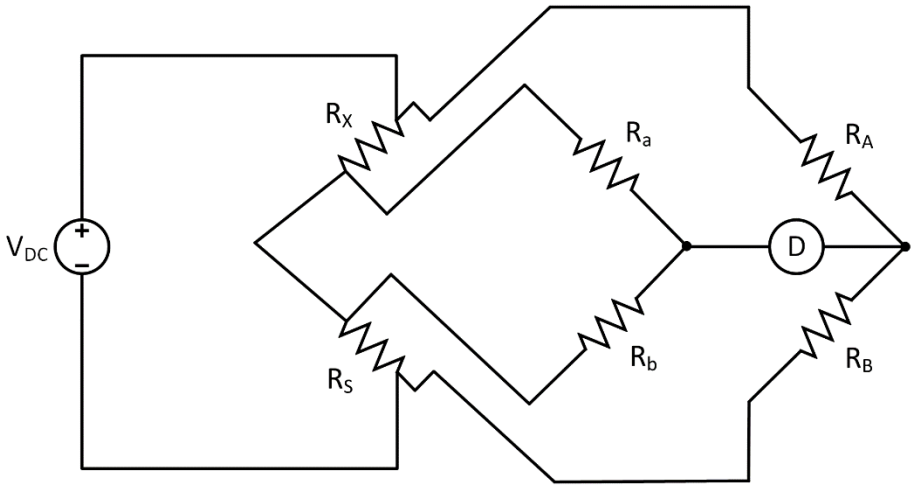

Figure 3. Kelvin bridge.

In this case, the unknown resistance R_X can be calculated by EQ. 3:

$$R_X = R_S \frac{R_A}{R_B} + \left[\frac{R_b R_y}{R_a + R_b + R_y}\right]\left[\frac{R_A}{R_A} - \frac{R_a}{R_b}\right] \qquad \text{EQ. 3}$$

Where R_y is the resistance of all the associated wires and leads (yoke). For this reason, yoke resistance should be minimized as much as possible. Assuming R_y is negligible and R_A/R_B exactly equals R_a/R_b, EQ. 3 can be simplified and rewritten as EQ. 4:

$$R_X = R_S \frac{R_A}{R_B} \qquad \text{EQ. 4}$$

4.1.3. Voltage Drop Method

This method may be alternatively be used if a precision resistance meter or bridge resistance measurement device is unavailable. The results, however, will not be as accurate relative to the aforementioned methods. In this method, a DC voltage source is connected to the motor windings. This DC source can be a switching power supply, battery, filtered rectifier, or other suitable supply, but should be relatively ripple-free. The resulting current is measured, along with the voltage across the winding, and the resistance is calculated according to Ohm's law. The current should not exceed 15% of the rated current to prevent temperature rise in the windings, which will skew the results. An optional resistor may be added in series with the winding to reduce the current flow. A diagram of the circuit for the voltage drop method is shown in Figure 4.

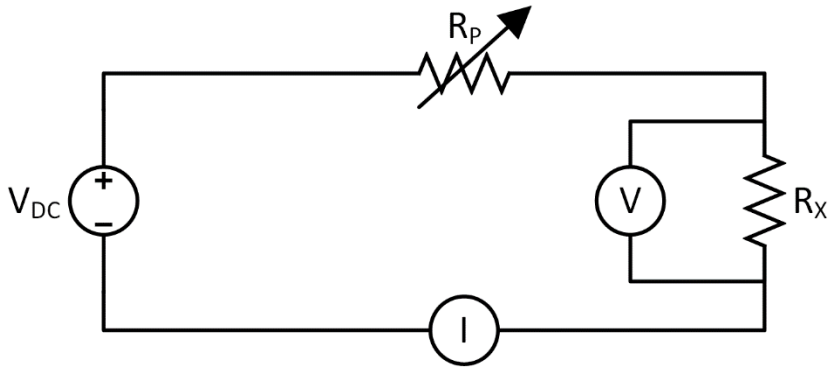

Figure 4. Voltage drop method

4.2. Winding temperature rise

In order to determine the temperature rise in the machine windings, the motor under test should be run with all covers in place, in a test environment with sufficient space for heat dissipation and no drafts. The machine should be run at rated voltage and load until winding temperature has stabilized. Readings should be taken at least once every 30 minutes, and are said to have stabilized when they do not vary more than 2% for three consecutive readings spaced at least 30 minutes apart.

Winding surface temperature is typically much lower than the internal temperature; therefore, the most reliable method of measuring temperature rise is by accurately measuring the winding resistance. Winding resistance measurements should be taken using any of the methods described in section 4.1. Measurements should be made quickly to avoid stopping the motor for a prolonged period of time, such that winding temperature is maintained. For machines ≤ 50kW readings should be taken within 60s.

4.3. Efficiency

Efficiency refers to the ratio of output power to input power. In the case of the mill motor, it represents the percentage of electrical power that is translated to mechanical power to the mill. Efficiency may be calculated by directly measuring input and output power, and taking the ratio of them (as shown in EQ. 5), or by separately determining the individual sources of loss (as shown in EQ. 6).

$$Efficiency\ [\%] = \left[\frac{P_{OUT}}{P_{IN}}\right] * 100\% \qquad \text{EQ. 5}$$

$$Efficiency\ [\%] = \left[\frac{P_{IN} - P_{LOSS}}{P_{IN}}\right] * 100\% \qquad \text{EQ. 6}$$

Efficiency data should be determined at rated voltage and speed. Measurements should be taken after the motor has been running at rated load for sufficient time to allow the winding temperature to stabilize. See 4.2 for how to determine winding temperature rise and how temperature stabilized is determined.

Motor efficiency shall be determined at six points ranging between 25-150% of rated load. Specifically, these points shall be approximately: 25%, 50%, 75%, 100%, 125%,

and 150% of rated load. Machine loading should begin with the highest loading, and points taken in descending order. Winding temperature shall be within 10% the hottest measured temperature rise as found in 4.2.

The specific parameters to be recorded at each load point differ between DC and AC motor types. Specific methods for accomplishing the machine loading also vary based on the type of motor being tested. DC motor efficiency test procedures are defined in 5.5 while those for AC motors can be found in 6.3.

5. DC Motor Tests

This section describes tests and test procedures that are unique to mills with brushed or brushless DC motors.

5.1. Winding inductance measurement

The winding inductance may be determined directly through the use of an impedance analyzer, or analytically. If determined analytically, the methodology used varies based on the specific construction of the machine under test.

5.1.1. Shunt and compound-wound machines

For these types of machines, the unsaturated inductance can be found by applying single phase 50 Hz or 60 Hz AC to the armature circuit terminals of the motor. The shunt-field winding should be short-circuited to prevent high voltages from developing within the windings. The armature should be locked in place during testing to prevent motion.

Three values of current, equally spaced, should be applied, with the largest not to exceed 20% of the current rating of the motor. An oscilloscope is required to measure the phase angle between the corresponding voltage and current waveforms. The inductance can be calculated by EQ. 7:

$$L = \frac{V sin\theta}{\omega I} \qquad \text{EQ. 7}$$

Where

L = Inductance (H)
V = Voltage (V)
I = Current (A)
θ = Phase angle between the voltage and current (^{o})
ω = Frequency times 2π (rad/s)

5.1.2. Series excited machines

For series excited machines, the armature circuit inductance varies widely with frequency, and with the magnitude of the DC and AC current components. Therefore, inductance values for frequencies other than the test frequency cannot be determined analytically using the method described in 5.1.1. For these machines, an impedance analyzer is recommended for characterizing the inductance over a broader frequency range.

5.2. Magnetic saturation

The no-load magnetic saturation curve for the mill motor refers to the nonlinear relationship between the terminal voltage of the armature and the field current at rated speed. The motor may be separately driven or self-driven during this test.

Data points should be taken at regularly spaced intervals from zero field current up to 125% of rated voltage, with three of the readings taken as near as possible to 90%, 100%, and 110% rated voltage. Field current, armature voltage, and machine speed readings should be recorded during the duration of the test.

In order to avoid hysteresis effects skewing the results, measurements should be taken on separate ascending and descending curves. While on the ascending curve, the armature terminal voltage should only increase from one point to the next. If the voltage exceeds the intended test point while on an ascending curve, the field current must be reduced to zero and the armature terminal voltage should be increased to the test point. Similarly, while on the descending curve, the voltage should only be decreased; it should never be taken below the intended test point and then increased. If necessary, the field current must be increased to the maximum value and the armature terminal voltage decreased to the intended test point.

5.2.1. Separately driven

For separately driven tests, the machine should be driven at rated speed by any suitable source. Field current should be supplied from a separate source to stabilize the armature terminal voltage.

5.2.2. Self-driven

In cases where an acceptable separate drive is available, a no-load saturation curve may be approximated by driving the uncoupled mill motor using a ripple-free DC power source capable of operating between 25%-125% of the rated motor voltage. In this case, some field current will be required to maintain the machine speed, so the results will not be as exact as those obtained by the separately driven method mentioned in 5.2.1.

5.3. Voltage vs. rotational speed

For DC motors, the rotational speed is directly proportional to the input voltage. A no-load voltage vs. RPM curve should be created using an adjustable, ripple-free DC power supply. The lower boundary for the curve should be the voltage that most closely corresponds to 50% of the rated speed, and increased to 125% of rated voltage.

5.4. Speed regulation

Speed regulation refers to the effects of machine loading on the rotational speed of the motor. The test should be conducted after the motor has been running continuously at rated load for sufficient time such that the winding temperature has stabilized. The machine loading should be varied several times from full load to no load and back, and the machine speed should be recorded. Speed regulation can then be calculated by EQ. 8.

$$Speed\ regulation\ [\%] = \left[\frac{\omega_{no\ load} - \omega_{full\ load}}{\omega_{full\ load}}\right] * 100\% \qquad \text{EQ. 8}$$

Where ω is the rotational speed of the machine.

5.5. Efficiency

Efficiency characterization shall be determined at six load points as defined in 4.2. At each load point the following values shall be recorded:

1. Voltage input to power supply
2. Voltage input to armature circuit
3. Current input to armature circuit
4. AC component of armature circuit current
5. Power input to armature current
6. AC component of power input to armature circuit
7. Voltage input to shunt-field circuit
8. Current input to shunt-field circuit
9. Power input to shunt-field circuit
10. Speed
11. Torque
12. Armature temperature or resistance
13. Field-coil temperature or resistance
14. Ambient temperature

Machine loading can be accomplished via a brake, dynamometer, through the pumpback method.

5.5.1. Machine loading

Machine loading can be accomplished in a number of different ways. The first method is to use a brake and pulley to provide loading to the motor. The motor can also be loaded using a dynamometer and torque meter. In this case, the mechanical power can be calculated from EQ. 9:

$$P_{mech} = \tau * \omega \qquad \text{EQ. 9}$$

Where τ is the measured torque in Newton-meters (Nm) and ω is the rotational speed in radians per second (rad/s).

If a dynamometer is used, it must be rated to less than or equal to three times the power rating of the machine being tested, and it must be sensitive to a torque that is at least 0.1% of the rated torque of the machine under test.

A third option is to use the Pump-back method, which requires two duplicate machines. The two machines can be coupled together and electrically connected as shown in Figure 5.

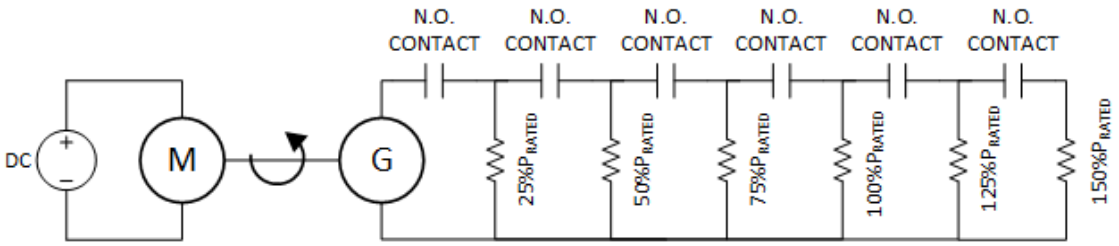

Figure 5. Pump-back test system diagram.

In this configuration, one machine is operated as a generator while the other acts as a motor. The main power produced by the generator is pumped back into the system via the motor, and the DC power supply only supplies the system losses. An optional booster generator can be used to stabilize the system voltages.
In the diagram in Figure 5, six power resistors are shown to represent the six load steps at which measurements will be taken. The normally open (N.O.) contacts can be manually or remotely operated during testing.

5.5.2. Segregated loss method

For large machines where direct calculation of machine efficiency may not be possible, efficiency can be determined by measuring each source of loss individually. These sources of loss include:

- Armature I^2R loss
- Series connected winding I^2R
- Brush contact
- Stray load
- Shunt field I^2R
- Rheostat
- Exciter
- Rotational core
- Brush friction
- Friction and windage
- Ventilating

The methods for testing and measuring each loss source is beyond the scope of this document, and can be found in IEEE-113.

5.6. Torque-current characterization curve

The torque-current characterization is the relationship between the field current drawn by a DC motor at a particular mechanical load (torque). The machine can be loaded in any of the methods described in 5.5.1. Data points should be gathered at the six load points used to evaluate machine efficiency. If it is anticipated that this motor might run on DC power source with a variable voltage output, such as a solar photovoltaic array, these curves should be generated for each voltage value that will be used for mill testing (see 7.2 for a description of how to determine these voltages).

6. AC Induction Motor Tests

This section describes the tests used to characterize an AC induction motor for mills. A common equivalent circuit model for an induction motor is shown below in Figure 6.

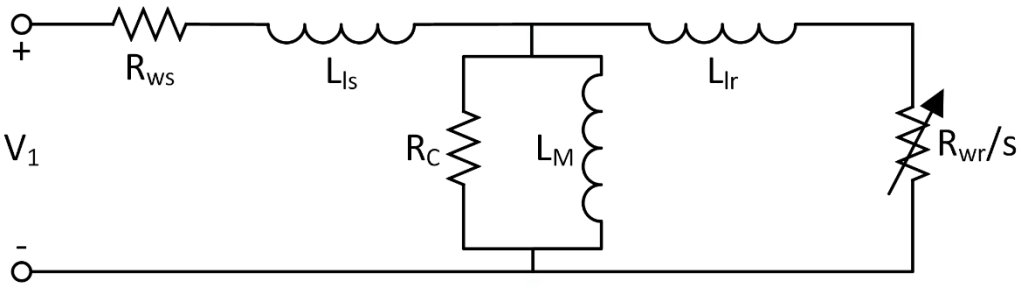

Figure 6. Equivalent circuit for an induction motor (single-cage rotor model).

The equivalent circuit shown in Figure 6 is a single-cage rotor model, which is sufficient for predicting the motor characteristics in the normal operational range. If low speed and/or motor starting characteristics are of particular interest, a double-cage model should be used (see [4]).

The key parameters of this model are:

- Stator winding resistance (R_{ws}) – the electrical resistance of the stator winding. This value contributes to load losses in the motor that increase with the square of the operating current (I^2R losses). This is found in 0.
- Stator and rotor winding leakage inductance (L_{ls} and L_{lr}) – this is a self-reactance in the stator and rotor windings that contributes to voltage drop, and hence loss, in the motor windings. These are found in 6.1.
- Core loss resistance (R_C) – some real power is lost in the motor core, which can be represented by a shunt core loss resistor. Core losses tend to be insensitive to motor loading, and can be assumed to be essentially constant regardless of motor load. This is found in 6.1.1.
- Magnetizing inductance (L_M) - a certain amount of reactive current is required to maintain the motor excitation, which can be represented as an additional shunt inductor. This is found in 6.1.1.
- Slip (s) – this is the difference between synchronous speed and measured rotational speed of the motor. It is typically as a per unit value relative to synchronous speed, as shown in EQ. 10.

$$s = \frac{n_{synchronous} - n_{measured}}{n_{synchronous}} \qquad \text{EQ. 10}$$

- Rotor winding resistance (R_{wr}) - the electrical resistance of the rotor winding, which is inversely proportional to slip. This value contributes to load losses in the motor that increase with the square of the operating current (I^2R losses). This is found in 6.1.

6.1. Locked-rotor tests

Running the motor with the rotor locked allows winding resistance and reactance values to be determined. The rotor should be locked to prevent rotation, using any available

means, such as a brake, dynamometer, or torque table. During locked rotor, the magnetizing branch can be neglected, and slip is one per unit (s=1pu), such that the equivalent circuit can be drawn as shown in Figure 7.

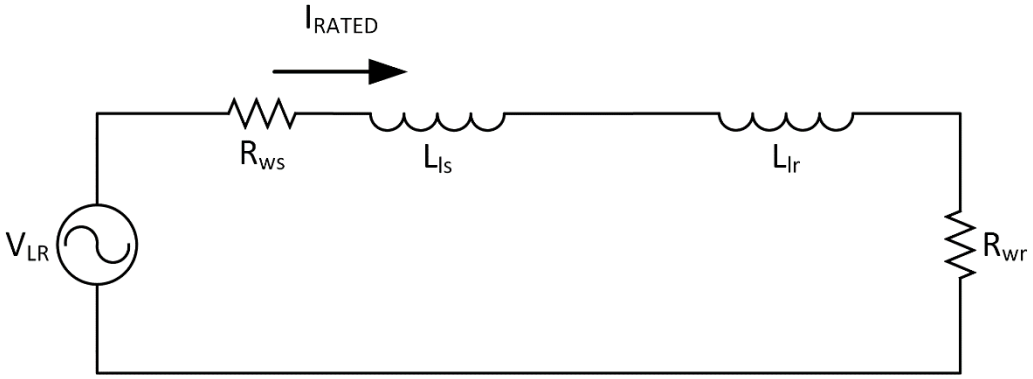

Figure 7. Induction motor locked-rotor equivalent circuit.

A variable AC voltage source with rated frequency is required. The applied voltage should start at zero, and should be slowly increased until rated current is measured. The voltage at which rated current is achieved should be noted and recorded as the locked-rotor voltage (V_{LR}). The equivalent impedance (Z_{LR}) can then be determined from EQ. 11.

$$Z_{LR} = \frac{V_{LR}}{I_{RATED}} \qquad \text{EQ. 11}$$

Using this, along with the stator winding resistance found in 0, the rotor winding resistance can be calculated using the real part of Z_{LR} as shown in EQ. 12.

$$R_{wr} = Re\{Z_{LR}\} - R_{ws} \qquad \text{EQ. 12}$$

Assuming L_{ls} is equal to L_{lr}, these can be found by from the imaginary part of Z_{LR} using EQ. 13.

$$L_{ls} = L_{lr} = \frac{1}{2\omega} Im\{Z_{LR}\} \qquad \text{EQ. 13}$$

6.1.1. Locked rotor current and torque

The locked rotor current [also referred to as Locked Rotor Amps (LRA)] should be determined at rated frequency and within ±5% of rated voltage. Note that this test is potentially destructive, so all readings must be made as quickly as possible. All readings must be taken within 5s of applying voltage.

The locked rotor torque will vary as a function of angular position of the rotor with respect to the stator. For this reason, determining the locked rotor torque requires making several measurements, with the rotor adjusted approximately 1/8 turn between each reading. The results should then be plotted as a torque versus angular position plot. The locked rotor torque is defined as the minimum torque developed at rest in any angular position of the rotor.

6.2. No-load test

Running the unloaded motor allows the no-load losses to be determined. No load losses are the sum of stator resistive loss, rotor resistive loss, core loss, and friction and windage losses. No load testing can also be used to find R_C and L_M parameters. There are two different ways to conduct no-load testing: the separately driven method uses a separate DC machine to rotate the motor under test at rated speed, while the self-driven runs the motor runs the motor unloaded at rated frequency and voltage. Core loss is sensitive to frequency, so frequency must be maintained within ±0.5% of rated during this test.

6.2.1. Separately driven

The most accurate method for determining no-load losses is to use a separate DC machine to drive the induction motor to synchronous speed, such that slip equals zero. At zero slip ($s=0$), the rotor winding resistance R_{wr}/s term will be infinite, meaning the rotor branch can be treated as an open circuit. An AC voltage source is used to supply rated voltage and frequency. The no-load impedance (Z_{NL}) can then be calculated by from the measured no-load current (I_{NL}) as shown in EQ. 14.

$$Z_{NL} = \frac{V_{RATED}}{I_{NL}} \quad \text{EQ. 14}$$

From here, the core resistance and magnetizing inductance can be found from the real and imaginary components, respectively, of the no-load resistance, as shown in EQ. 15 and EQ. 16.

$$R_C = Re\{Z_{NL}\} - R_{ws} \quad \text{EQ. 15}$$

$$L_M = \frac{1}{\omega} Im\{Z_{NL}\} - L_{ls} \quad \text{EQ. 16}$$

Where R_{ws} is the stator winding resistance, as found in 0 and L_{ls} is the stator leakage reactance as found in 6.1.

6.2.2. Self-driven

If a separate DC motor that is sufficient to drive the induction motor to synchronous speed is unavailable, no-load losses can be approximated by the power consumed by the unloaded motor when driven at rated voltage and frequency. Note that because slip is non-zero during this test, rotor resistance and leakage reactance will affect the results, such that the results, notably the core resistance, will be less accurate than the separately driven method.

The measured no-load current (I_{NL}) can be used to find R_C and L_M using the same equations that were used for the separately driven method (EQ. 14, EQ. 15 and EQ. 16).

6.3. Efficiency

Induction motor efficiency shall be determined in accordance with the requirements in 4.3. At each of the six points the following parameters shall be recorded.

1. Electrical input power (real and reactive)
2. Input voltage
3. Input current
4. Input frequency
5. Slip
6. Output torque
7. Ambient temperature
8. Stator winding temperature and/or stator winding resistance

For item 8 the winding resistance shall be corrected to a standard temperature of 25°C.

6.3.1. Machine loading

Machine loading can be accomplished in a number of different ways. The first method is to use a brake and pulley to provide loading to the motor. The motor can also be loaded using a dynamometer and torque meter. In this case, the mechanical power can be calculated from EQ. 17.

$$P_{mech} = \tau * \omega \quad \text{EQ. 17}$$

Where τ is the measured torque in Newton-meters (Nm) and ω is the rotational speed in radians per second (rad/s).

If a dynamometer is used, it must be rated to less than or equal to three times the power rating of the machine being tested, and it must be sensitive to a torque that is at least 0.1% of the rated torque of the machine under test.

If a suitable source of mechanical load is not available, another method for loading the motor using the motor-generator slip method can be used. This method requires two identical machines. The machines are coupled together as shown in Figure 8.

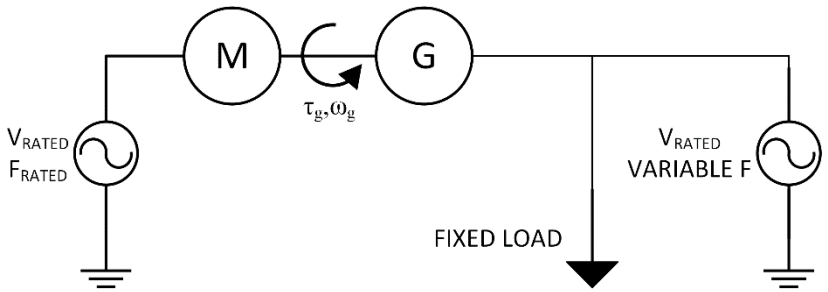

Figure 8. Diagram for motor-generator slip test.

An AC power source at rated frequency and voltage should drive one machine acting as the motor. This is coupled an identical machine that will act like a generator. Torque and speed should be calculated at the point where the machine shafts are coupled together for determined mechanical power according to EQ. 17.

The stator of the machine acting as a generator should be connected to a variable frequency AC source, such as a Variable Frequency Drive (VFD), operating at

rated voltage, which will supply the necessary excitation current. A fixed load will be connected on parallel with both the generator machine and the variable frequency AC source. By adjusting the frequency of the variable frequency AC supply, the relative slip between the generator and the AC source can be controlled. The power output of the generator can thus be controlled using the slip.

The advantage to this method is that high power resistive loads and VFDs are readily available and can generally be procured for a much lower cost than a dynamometer. The other advantage is that dynamometers must be rated within 1.5-3 times the motor under test; therefore testing multiple motor sizes may require multiple dynamometers. This method, in contrast, can be easily adapted to different motor sizes. A torque meter sensitive to a change in torque of ≤ 0.1% of the rated motor torque and tachometer or other speed measurement instrument meeting the accuracy requirements in 2.11 are required.

Care should be taken to avoid reverse power flow into the variable frequency AC source if it is not rated for reverse power flow.

6.4. Power Factor

Power Factor (PF) is the ratio of real power to total apparent power.

$$PF = \frac{P}{VI} = \frac{P}{\sqrt{P^2 + Q^2}} \qquad \text{EQ. 18}$$

PF should be recorded at no load, and at the six load test points used for efficiency measurements. These points should be used to generate a PF versus loading curve.

6.5. Speed-torque and Speed-current Characteristic

The speed-torque characteristic of a motor refers to the torque delivered to a load as a function of motor speed. When plotted as a curve, key motor parameters can be identified. A representative characteristic speed-torque curve is shown in Figure 9.

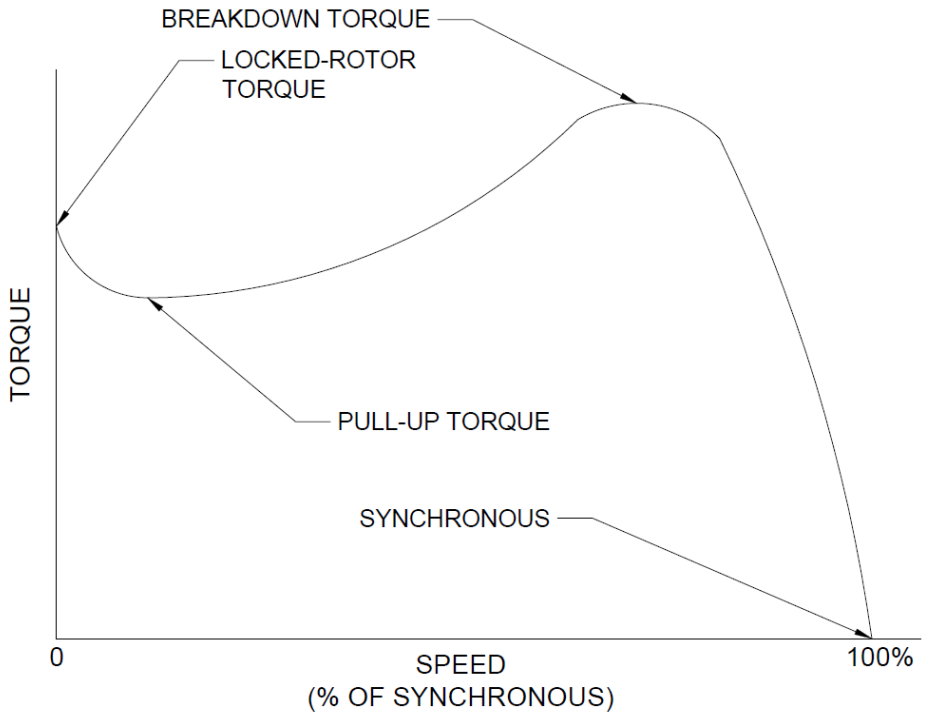

Figure 9. Representative speed vs. torque characteristic curve for a single-phase induction motor.

The key parameters of the curve include:

- Locked rotor torque – the minimum torque produced by a motor at zero speed (see 6.1.1)
- Pull-up torque – the local minimum of the curve between the locked-rotor torque and breakdown torque
- Breakdown torque – the maximum torque delivered by the motor as it accelerates from rest to synchronous speed (note that this is typically much greater than rated torque)
- Synchronous – at synchronous speed, slip and torque are both zero. In practice, the motor will always be slightly below synchronous speed, unless it is separately driven by an external source.

Similar curves can be derived for the speed-current relationship. These are often plotted together, with a common speed scale on the x-axis.

Four methods of obtaining the speed-torque and speed-torque characteristics are outlined in IEEE-114. In all methods, the motor should be driven at rated voltage and frequency.

6.5.1. Measured output

The motor is loaded via a dynamometer or any other method as defined in 6.3.1. For maximum accuracy, the friction and windage losses of the load must be known and the results must be compensated to account for them.

At least ten, equally spaced points shall be measured at speeds ranging from roughly 1/3 of the synchronous speed up to the maximum speed of the motor. At each point the input voltage and current, and output torque shall be recorded. Data shall be recorded while the motor is at steady state, such that acceleration or deceleration effects do not influence the results. The y-intercept of the curve should be the locked-rotor torque found in 6.1.1.

The corrected torque, when accounting for the load friction and windage losses, can be calculated by EQ. 19.

$$\tau_c = \frac{k(P_o - P_l)}{n} \qquad \text{EQ. 19}$$

Where:

τ_c = Torque, corrected for load losses (Nm)
k = Constant based on units of measure
P_o = Measured output power (W)
P_l = Friction and windage losses of the load (W)
n = Motor speed (rpm)

6.5.2. Acceleration

This method requires the rotational moment of inertia to be known for all rotating parts, either through calculation or via measurement. The motor is accelerated from rest to its maximum speed approaching synchronous. As the motor accelerates, simultaneous readings of input current and motor speed must be taken at regular, fixed time intervals. Torque can be calculated at each recorded speed value using EQ. 20.

$$\tau = \frac{aJ}{k} \qquad \text{EQ. 20}$$

Where:

τ = Torque (Nm)
k = $109.7 \cdot 10^{-4}$ for the units shown
a = Acceleration (rpm/s)
J = Rotational moment of inertia (kg·m^2)

6.5.3. Input

This method calculates torque by subtracting losses from the measured input power. At least ten, equally spaced points shall be measured at speeds ranging from roughly 1/3 of the synchronous speed up to the maximum speed of the motor. At each point the input voltage, current, and power shall be recorded and plotted against speed. The y-intercept of the curve should be the locked-rotor torque found in 6.1.1.

$$\tau = \frac{k}{n}(P_i - P_l) - \tau_{fw} \qquad \text{EQ. 21}$$

Where:

τ = Torque (Nm)
k = Constant based on units of measure
n = Motor speed (rpm/s)
P_i = Input power (W)
P_l = Stator resistive loss (I^2R_{ws}, W)
τ_{fw} = Friction and windage torque at speed n (Nm)

The friction and windage torque (τ_{fw}) is defined as the torque required to rotate the de-energized motor to the specified speed n.

6.5.4. Direct measurement

The direct measurement method uses continuous data acquisition to record input current and output torque over the full range of motor speeds. Data should be recorded and plotted at chosen speeds to determine the key torque characteristics, such as the pull-up and breakdown torque. The motor should be given sufficient time to settle at each speed point such that steady state values can be obtained.

7. Mill Performance Testing

Mill performance testing should be conducted using the setup configuration shown in the diagram in Figure 1. The test should be conducted in an environment relatively free from noise and dust.

7.1. Feedstock preparation

All testing should be conducted with an identical clean, dry feedstock. Examples include: whole corn, whole oats, or whole wheat kernels. Grains mixed with molasses should not be used. Grains should be as whole as possible, with a minimum of pre-processing.

Moisture content should be kept as consistent as possible between tests. Representative samples should be measured with a resistive or capacitive moisture meter meeting the requirements in section 2 prior to testing. Ideal grain moisture content should be between 12-15%. Excessive moisture content can increase the degree of clogging during testing, and may reduce crushing efficiency. Drying may be required to meet the required ideal range.

7.2. Variable voltage DC systems

If the DC voltage source to the mill motor is variable, such as a solar photovoltaic array, then a range of representative DC voltages should also applied. The lower boundary should be the voltage that was found to correspond to a motor speed of 50% of the rated, no-load speed, as determined by the voltage vs. speed curve defined by 5.3. The upper voltage should be either the rated voltage of the mill motor, or the maximum anticipated input voltage from the DC source, whichever is greater. Due to the inverse relationship between photovoltaic voltage and temperature, the maximum power voltage (V_{mp}) should be calculated for the minimum anticipated ambient operating temperature (T_{min}) using EQ. 22:

$$V_{mp@T_{min}} = V_{mp@STC}[1 + \beta_V(25^oC - T_{min})] \quad \text{EQ. 22}$$

Where:

$V_{mp@Tmin}$ = Maximum power voltage at minimum temperature (V)
$V_{mp@STC}$ = Maximum power at standard test conditions (STC) [1,000 W/m^2 and 25^{o}C], according to the manufacturer's datasheet (V)
β_v = Temperature coefficient of the module voltage according to the manufacturer's datasheet (V/^{o}C)
T_{min} = Is the minimum operating temperature as determined by NEC 690.7 (^{o}C)

Six voltages, approximately equally spaced, between the maximum and minimum voltages should be applied.

7.3. Mill test and evaluation criteria

Milling tests are to be conducted to evaluate machine efficiency and performance, and to electrically characterize the machine loading of the milling process.

7.3.1. Crushing efficiency

Crushing efficiency is the ratio of total grain mass collected at the output of the mill compared to the mass of the grain that entered the hopper. Crushing efficiency (η_c) is calculated by EQ. 23:

$$\eta_c = \frac{m_{out}}{m_{in}} \quad \text{EQ. 23}$$

Where:

m_{out} = Mass of milled grain in output catchment vessel (kg)
m_{in} = Mass of whole grain that entered hopper during test (kg)

Crushing efficiency is primarily influenced by moisture content; greater moisture content will cause grain to adhere to the milling surfaces, preventing it from exiting the mill into the output catchment. Larger particles that fail to pass through the output grate or sieve will also reduce crushing efficiency.

7.3.2. Throughput

Throughput is a measure of the total grain mass that was processed by the mill per unit time (kg/hour). Throughput should be measured after the mill has been running at rated load for sufficient time such that the motor temperature has stabilized. Temperature is said to be stabilized when measurements do not vary more than 2% for three consecutive readings spaced at least 30 minutes apart. The motor can be loaded with an alternate method, such as a dynamometer or other mechanical load, to accelerate winding temperature rise before being connected to the mill.

Once this condition has been met, the machine should be run at a period of 30 minutes continuously to determine average throughput. Care must be taken to ensure that the hopper is always maintained at least 25% full at all times.

7.3.3. Energy intensity

Energy intensity is the ratio of the total grain mass output of the mill to the total electrical energy (kWh) consumed by the mill motor. Energy intensity should be determined after the mill has been running under load for sufficient time such that

the motor temperature has stabilized. To determine a representative, average energy intensity, the mill should be run continuously for a period of 30 minutes.

Note: energy intensity and throughput can be evaluated concurrently during the same test.

7.3.4. Average load, peak load and load factor

The instantaneous electrical power consumed by the motor should be recorded for the entire duration of the Throughput and Energy intensity tests described in sections 7.3.2 and 7.3.3. The average and peak load (in W) should be recorded, along with load factor.

Load factor is a measure of electrical utilization, and is defined as the ratio of the average load over peak load. It is defined in EQ. 24:

$$LF = \frac{E}{P_{peak} * t} \quad \text{EQ. 24}$$

Where:

LF = Load factor
E = Total energy consumed by the motor over the course of the test (Wh)
P_{peak} = Peak instantaneous power observed during test (W)
t = Total test duration (hours)

7.3.5. Tip speed and centrifugal force (hammer mills only)

For hammer mills, tip speed refers to the velocity of the tip of the hammers, and is a critical factor in evaluating the performance of hammer mills. For other mill types, such as roller mills, tip speed does not apply.

Tip speed can be calculated by multiplying the total hammer length by the rotational velocity of the mill rotor as shown in EQ. 25:

$$v = l\omega \quad \text{EQ. 25}$$

Where:

v = Tip speed (m/s)
l = Hammer length (m)
ω = Rotational speed (rad/s)

From this, and the mass of the rotor/hammer mechanism (m), the centrifugal force (F_c) of the hammers can be determined by EQ. 26:

$$F_c = \frac{mv^2}{l} = m\omega^2 l \quad \text{EQ. 26}$$

7.3.6. Clogging

Clogging occurs when the sieve screen holes become blocked, reducing the efficiency and capacity of the mill. If output becomes noticeably reduced due to clogging during the course of testing, the test should be momentarily halted, and the sieve cleared as quickly as possible so that testing can resume. Material removed without the sieve in place should be collected and stored separately from the milled output, and should not be counted as output for the purposes of calculating crushing efficiency, throughput, or energy intensity. At the discretion of the tester, this material may be placed back into the hopper and run through a second time. Clogging events, and the duration of the pause in testing to remedy the clog, should be recorded.

7.3.7. Motor winding temperature

Motor winding temperature should be measured and recorded according to the methods specified in 4.2 at the beginning and end of each test.

7.3.8. Audible noise

A decibel meter meeting the requirements in section 2 should be used to evaluate the audible noise produced by the mill during testing. The decibel meter should be placed in an open, unobstructed area approximately 0.5m from the mill and 1.5m above ground level. Measurements should be taken and recorded under three conditions:

1. Baseline – taken to establish the normal, background noise level of the environment prior to beginning testing.
2. No-load – taken with the mill running with no grain in the hopper
3. Running – taken while the mill is actively processing grain

At least three recordings should be taken during each condition and averaged together.

7.3.9. Grain evaluation

The milled grain output should be put through a series of seven standard soil test sieves with standard sieve designations of: 0.85, 0.425, 0.25, 0.18, 0.15, 0.106, and 0.075mm. The approximate weight of the grain which is entrapped within each sieve should be recorded.

A qualitative analysis of the processed grain output from the mills is outside the scope of this test method. The quality of milled grains can be hard to objectively define, and may be subject to regional variation and crop characteristics. Therefore, it is recommended that test reports contain clear, close-up, high quality, color photographs of a representative sample of the mill output.

8. References

[1] *IEEE Guide: Test Procedures for Direct-Current Machines*, IEEE Standard 113, 1985.
[2] *IEEE Standard Test Procedure for Single-Phase Induction Motors*, IEEE Standard 114, 2010.
[3] *IEEE Standard Test Code for Resistance Measurement*, IEEE Standard 118, 1978.

[4] M.H. Haque. “Determination of NEMA Design Induction Motor Parameters From Manufacturer Data,” *IEEE Trans. on Energy Conversion*, vol. 23, no. 4, pp. 997-1004, Dec. 2008.
[5] S. Jurkovic. “Induction Motor Parameters Extraction,” Available online: http://web.mit.edu/kirtley/binlustuff/literature/electric%20machine/motor-parameters.pdf. Accessed May 5, 2018.
[6] G. Mehos and D. Morgan. *Hopper Design Principles.* Chemical Engineering Online. Jan. 2016. Online: http://www.chemengonline.com/hopper-design-principles/
[7] O. Adekomaya and O.D. Samual. “Design and Development of a Petrol-powered Hammer mill for rural Nigerian Farmers”. *Journal of Energy Technologies and Policy*, vol. 4, no. 4, pp. 65-74, Jan. 2014.
[8] D. Armitage, T. Wontner-Smith, and R. Wilkin. *Grain Moisture – guidelines for measurement*. HGCA publications. London, England. 2008.
[9] G.C. Mrema, et. al., *Rural structures in the tropics: design and development*. Food and Agriculture organization of the United Nations. Rome, Italy. 2011.
[10] K. Koch, *Hammermills and Rollermills*, Kansas State University, May 2002. Online: https://www.bookstore.ksre.ksu.edu/pubs/mf2048.pdf
[11] D.L. King, J.A. Kratochvil, and W.E. Boyson. “Temperature Coefficients for PV Modules and Arrays: Measurement Methods, Difficulties, and Results,” presented at the 26th IEEE Photovoltaic Specialists Conf., Anaheim, USA, 1997.
[12] *Standard Specification for Wire Closth and Sieves for Testing Purposes*, ASTM Standard E11, 2004.

5.4. Multi-purpose Mill Test Report

Grain Mill Test Report

A study to evaluate the performance of the Sichuan Jingyan Lianyi multi-purpose mill

Colorado State University
Factor[e] Ventures
430 N College Ave.
Fort Collins, CO 80524
11 January 2019

Table of contents

1 Overview 1
2 Description of Grain Mill 1
3 Test and Measurement Equipment Description 2
3.1 Voltage 2
3.2 Current 2
3.3 Power 2
3.4 Impedance 2
3.5 Torque 2
3.6 Motor Speed 3
3.7 Grain Moisture 3
3.8 Audible Noise 3
3.9 Temperature 3
3.10 Weight 3
3.11 Data Acquisition (DAQ) 3
4 Motor Description and Testing 3
4.1 No Load Test 5
4.2 Block Rotor Test 6
4.3 Free Acceleration Test 7
4.4 Efficiency 9
5 Mill Testing Description and Results 9
5.1 Grain Sieve Testing 14
5.2 Other Testing 16
6 Results Discussion and Conclusion 17
7 References 18
Appendix A: Mill Datasheet 20
Appendix B: Mill Motor Datasheet 22
Appendix C: Data file description 24

List of figures

Fig. 1. Photo showing mill with motor, pulley, and belt assembly. 1
Fig. 2. Photo of mill showing three pole, double throw switch. 2
Fig. 3. Capacitor start, capacitor run induction motor diagram. 4
Fig. 4. Induction motor equivalent circuit (auxiliary winding omitted). 5
Fig. 5. Motor test setup. 6
Fig. 6. Current and motor speed during free acceleration with $100V_{RMS}$ applied. 8
Fig. 7. Experimental setup. 10
Fig. 8. Real and reactive power vs. time for Run 3. 12
Fig. 9. Real and reactive power vs. time for Run 5. 12
Fig. 10. Input voltage and current waveforms for the mill motor. 13
Fig. 11. FFT amplitude spectrum for mill motor current. 14
Fig. 12. Particle size distribution results for sieve testing. 15
Fig. 13. Photo of sieve testing setup. 16

1 Overview

This report will describe the tests conducted to evaluate and characterize a 6N40-9FC23 combination crusher/rice mill machine obtained from Sichuan Wanma Machinery Co. This type of Chinese-produced electric mill is an interesting alternative to the diesel-run mills that are commonly found in emerging markets. The purpose of this testing was to obtain basic electrical characteristics and provide performance benchmarks.

2 Description of Grain Mill

The Sichuan Jingyan Lianyi 6N40-9FC23 combination crusher/mill (henceforth referred to as the *grain mill*) was obtained from Sichuan Jiangyan Lianyi Machinery Co in China. The milling end is a hammer-mill, typically used for crushing maize, with two available screens: a coarse (1.2mm) mesh and a fine (0.8mm) mesh. The crusher end is designed to remove the hulls from rice. Both the crusher and rice mill ends of the grain mill are belt-driven from a single motor.

The motor may be purchased with the mill, or supplied separately. The motor that was provided by the manufacturer was an YL90L-2 2.2kW (3HP), capacitor-start capacitor-run, single phase induction motor rated for 220V, 50Hz service. A pulley was affixed to the motor with slots for both belts. The pulley was designed such that in forward rotation (counter-clockwise) both belts were driven, while in reverse rotation (clockwise) only the rice mill belt was driven. A three pole, double throw switch connected to the mill allowed the mill motor to be driven in either direction, with an off position in the center between forward and reverse.

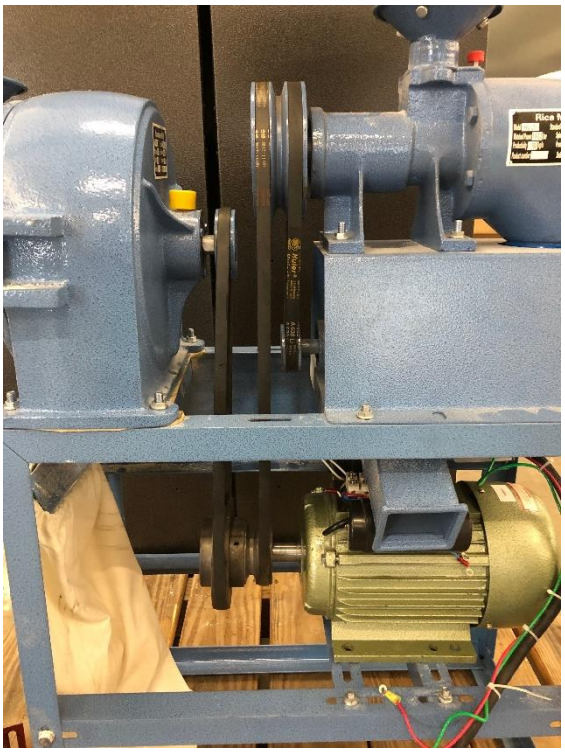

Fig. 1. Photo showing mill with motor, pulley, and belt assembly.

Fig. 2. Photo of mill showing three pole, double throw switch.

The rated throughput of the grain mill is ≥300kg/hr for the milling side and ≥150kg/hr on the crushing side. The outer dimensions of the mill are approximately 700x540x350mm and the net weight (excluding the motor) is approximately 65kg.

3 Test and Measurement Equipment Description

This section describes the test and measurement equipment used for capturing the various data parameters during testing

3.1 Voltage

Voltage measurements were obtained using a LEM LV 25-P voltage transducer. The transducer is rated for 10-500V AC or DC with a rated accuracy of ±0.8%.

3.2 Current

Current measurements were recorded using a CR Magnetics CR5410-50 hall effect current transducer rated for up to 50A AC or DC. Rated accuracy of this device is ±1.0%.

3.3 Power

Real and reactive power values were calculated using the measured voltage waveforms obtained using the voltage transducer in 3.1 and the current waveforms using the current transducer described in 3.2.

3.4 Impedance

Resistive and inductive impedance measurements were conducted using a Keysight E4990A impedance analyzer.

3.5 Torque

Torque measurements were obtained using a Futek TRS605 FSH02056 rotary torque sensor with encoder. This sensor is rated for 20 Netwon-meters (Nm) and includes a rotary encoder that can be used to obtain rotor position and speed. Rated accuracy of this device is ±0.2%.

There was insufficient space to install the torque sensor between the motor and pulley on the grain mill, therefore torque measurements could only be obtained when the motor was run separately on a motor test stand, and not as an integral part of the grain mill.

3.6 Motor Speed

In addition to the rotary encoder, a Monarch Instruments ROS-P optical LED sensor was used to obtain motor speed while the motor was connected to the grain mill. The ROS-P pulses once per revolution and can thus be used to obtain the rotational period (hence rotational speed) of the grain mill motor. Because no mechanical connection is required, the sensor could be installed on the mill for obtaining motor speed measurements during mill testing.

3.7 Grain Moisture

Grain moisture levels were taken using a General DSMM600 soil moisture meter.

3.8 Audible Noise

Audible noise levels were captured using an Exetech 407730 sound level meter.

3.9 Temperature

Temperature values were measured using a Tacklife IT-T05 infrared thermometer with rated accuracy of $\pm 2.0^{o}$C when measuring $\leq 100^{o}$C.

3.10 Weight

Weight measurements were recorded using an Ohaus SD35 digital scale with a capacity of 35kg and 0.02kg resolution.

3.11 Data Acquisition (DAQ)

Real time measurements of voltage, current, and motor speed were recorded using a National Instruments LabView application. The analog inputs were read using an NI 9201 C series analog input module at a fixed sample frequency of 32 samples per cycle (1.6 kHz). Digital inputs were sampled using an NI 9381 multifunction I/O C series module at a rate of 100 kHz. The high frequency sampling was handled using the on-board FPGA that is integrated into the NI cRIO 9064 chassis. A real-time program aggregated the data in 0.5 second increments, computed the average and RMS for all signals, and communicated these via a network stream over TCP/IP. Finally, a host program was used to collect the data from the network stream and save to an NI TDMS file.

As a point of verification and data validation, a Bitronics M571 power meter was also connected and simultaneous measurements were obtained, also in 0.5 s increments.

4 Motor Description and Testing

The prime mover for the grain mill was a YL90L-2, single phase, two pole, 2.2kW capacitor start, capacitor-run motor. Although the customer had the option of providing a motor, this particular motor was what was provided by the manufacturer. A summary of several pertinent parameters is given in Table I.

Table I. Motor parameters

Model	YL90L-2
Rated power	2.2kW (3 HP)
Rated voltage	110/220V
Rated Current	27.4/13.7A
Rated Frequency	50/60Hz
Poles	2
Speed	2,820 RPM @ 50Hz, 3,380 @ 60Hz
Run Capacitor	45μF
Start Capacitor	250μF

The motor start capacitor was required in order to start the motor from stall. Once the motor had reached approximately 75% of synchronous speed, a centrifugal switch opened which disconnected this capacitor. If used, the optional run capacitor remained in the circuit after the switch opened. A winding diagram showing the main and auxiliary windings, start and run capacitors, and centrifugal switch is shown in Fig. 3.

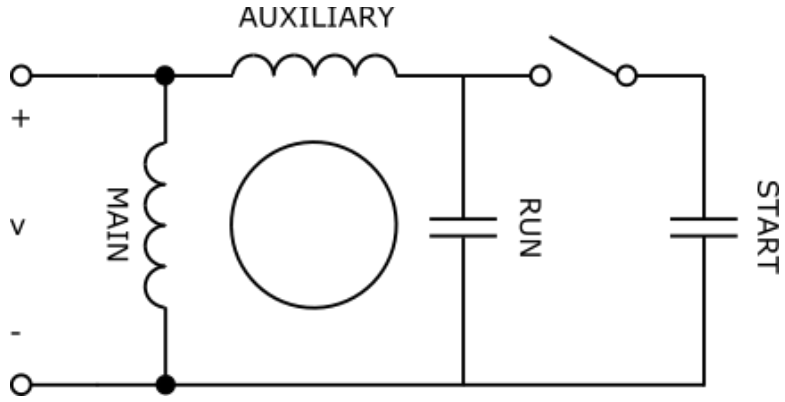

Fig. 3. Capacitor start, capacitor run induction motor diagram.

A simplified equivalent circuit for the induction motor is shown in Fig. 4. Here, the auxiliary winding and capacitors have been omitted for clarity. The prime notation (‘) indicates that the rotor leakage inductance (L_{lr}) and rotor winding resistance (r_r) have been referred to the stator winding. An important thing to note is that the rotor winding resistance (r'_r) is divided by the slip (s), which is defined as shown in EQ. 1.

$$slip\ (s) = \frac{n_s - n_r}{n_s} \qquad \text{EQ. 1}$$

Where: n_s and n_r are the synchronous speed and rotor speed for the motor, respectively.

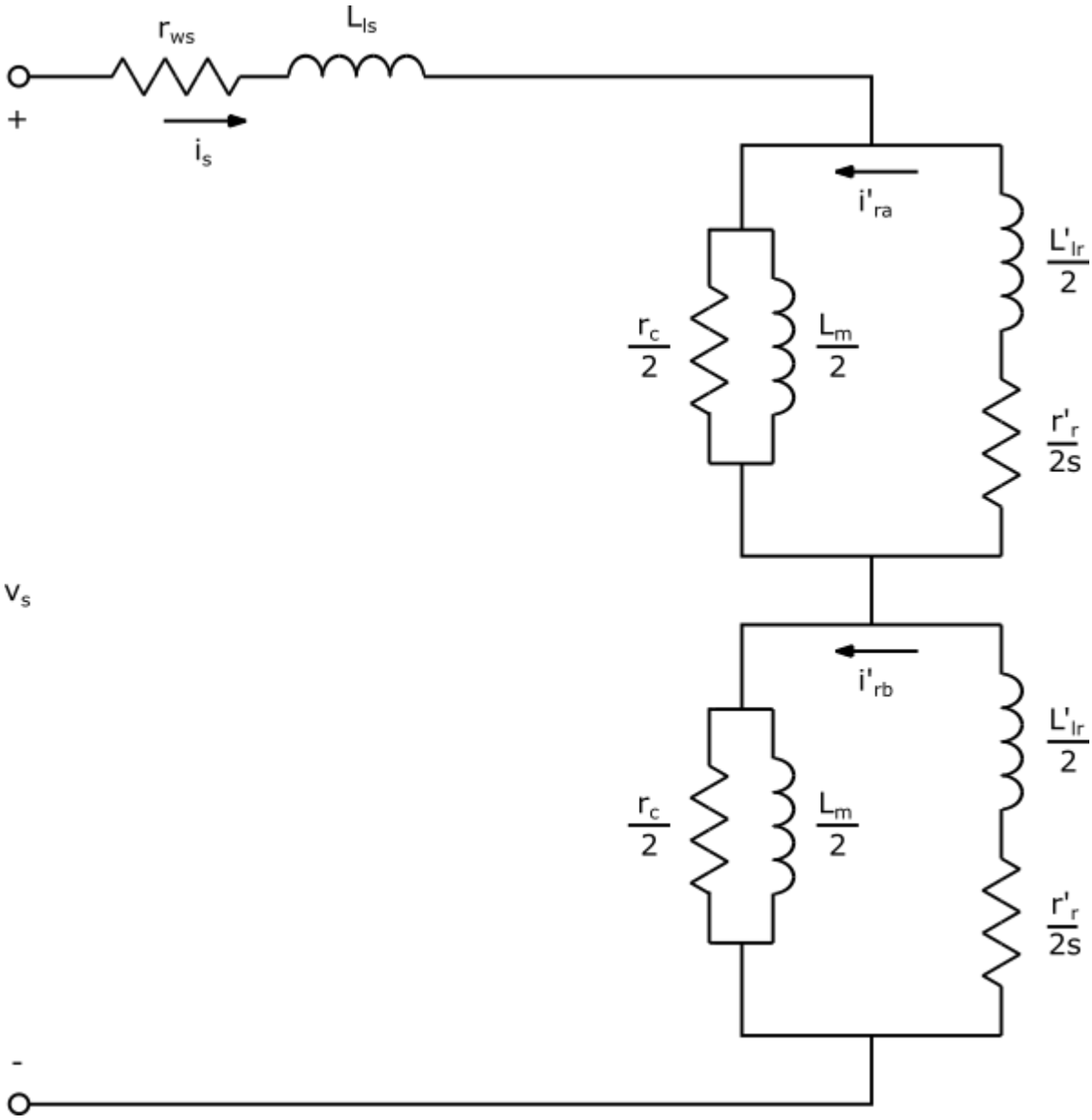

Fig. 4. Induction motor equivalent circuit (auxiliary winding omitted).

A standard test suite was conducted on the motor which consisted of: a no load test, a block rotor test, and free acceleration.

4.1 No Load Test

No load tests were conducted to determine the no load losses of the motor while it was not mechanically coupled to the mill. To achieve true no load, a second, similar motor was connected to the motor under test with a combination torque sensor/rotary encoder installed at the point where the shafts were coupled together. A photo showing this test setup with the two motors coupled together is shown in Fig. 5. The motor under test was connected to a Schneider Conext XW5548 inverter running at 50Hz. An autotransformer was used to decrease the output voltage from 240V to rated voltage (220V). The second motor was

connected to a Variable Frequency Drive (VFD); the VFD frequency was increased until the rotor speed, as measured by the rotary encoder, was equal to the synchronous frequency of the motor (i.e., 50 Hz, or 3,000 RPM). At this point, the slip was essentially zero, meaning that the rotor resistance was approximately open circuit, and the rotor current should have been near zero. In this way the magnetizing branch impedance could be isolated and measured, without being influenced by the rotor currents.

Fig. 5. Motor test setup.

This test was conducted with and without the optional run capacitor in place to estimate the contribution of the run capacitor and auxiliary winding on the no load power consumption. The results of the no load test are summarized in Table II.

Table II. Motor no load power consumption.

	Real Power [W]	Reactive Power [VAR]
With Run Capacitor	489.0	516.9
Without Run Capacitor	338.8	2110

These results indicate that with the run capacitor in place the no load power of the motor is approximately 150W (44%) greater than without; this is due to the winding resistance of the auxiliary winding, which is not present when the run capacitor is removed. The reactive power draw of the motor, however, is much greater when the run capacitor is removed. This indicates that the run capacitor is supplying roughly 75% of the reactive power requirements of the motor.

4.2 Block Rotor Test

Block rotor tests were conducted on the motor with the rotor physically blocked to prevent rotation. The Schneider Conext XW5548 was connected to the motor input terminals with

frequency set to 50Hz. The autotransformer was slowly increased from zero until the input current was measured to be near rated current (13.67A). At this point the circuit breaker connected to the inverter was opened.

The circuit breaker was closed in nine brief intervals, and the steady state, block rotor data was collected. Three of these were with both the start and run capacitors in place, three were with only the start capacitor in place, and three were with no capacitors. Because the rotor was blocked, the centrifugal switch was always closed. When both capacitors were in the system, the auxiliary winding current flowed through both capacitors in parallel. With only the start capacitor in place the auxiliary winding current flowed only through the start capacitor. With both capacitors disconnected the auxiliary winding was open-circuited, so current flowed only through the main winding.

Because the rotor was stationary, n_r was zero, therefore slip was equal to unity (1). In this way, the rotor winding resistance could be determined.

Table III. Block rotor test results.

	Real Power [W]	Reactive Power [VAR]
With Run Capacitor	550.2	294.6
Without Run Capacitor	525.1	317.8
No Capacitors	383.4	545.6

These results show that with only the main winding energized (no capacitors present), the real power was lowest, while the reactive power was highest. This matches expectations, as the auxiliary winding typically has a greater winding resistance compared with the main winding. Having the capacitors in the circuit reduced the reactive power drawn by the source, as shown by these results.

4.3 Free Acceleration Test

Free acceleration tests were conducted on the motor. The circuit breaker connecting the Schneider inverter was closed and the motor was accelerated from stall. Data collection began at or near the time when the breaker was closed and continued until after the motor had reached steady state speed.

The inrush current drawn by the motor exceeded the limits imposed by the DC power supplies acting as input to the inverter. Therefore, these tests were conducted at four different root mean squared (RMS) voltages below rated voltage: 50V, 75V, 100V, and 150V. At reduced voltage, the inrush current was lower, and the motor took longer to accelerate. This allowed the motor to be started ‘across-the-line’ (e.g., without soft starting); the reduced rate of acceleration allows for more data points to be captured during the acceleration period.

With the run capacitor, the motor would initially have both capacitors connected in parallel during starting, until the centrifugal switch opened at around 70-75% of synchronous speed. At this point, only the run capacitor would be connected to the auxiliary winding. Without

the run capacitor, the auxiliary winding would be in open circuit after the motor had reached 70-75% of synchronous speed and the centrifugal switch opened.

An example of the free acceleration results when 100V is applied is shown in Fig. 6. The high inrush current is clearly visible during the first 10 cycles. At approximately t=0.9s, the centrifugal switch opened, removing the start capacitor from the circuit. At this point, the rate of acceleration for the motor was reduced, as was the amplitude of the input current.

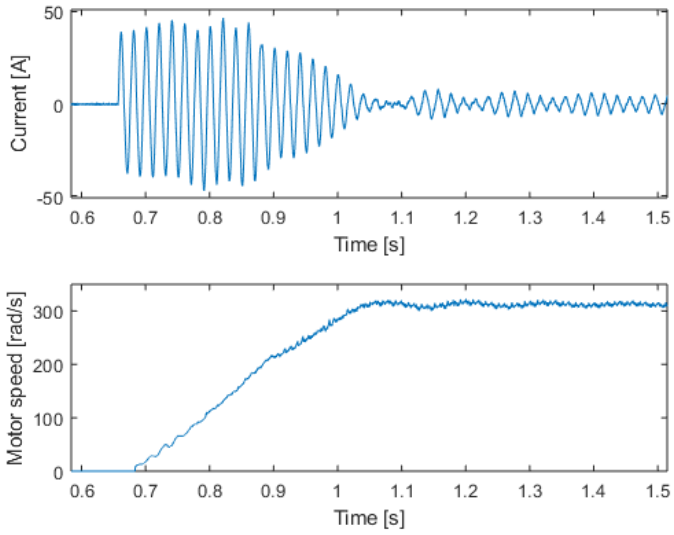

Fig. 6. Current and motor speed during free acceleration with $100V_{RMS}$ applied.

The results of the free acceleration tests are given in Table IV; the results shown in this table were taken with the run capacitor in place. When the run capacitor was removed, the results were similar, with a slightly smaller peak current (owing to the fact that only one capacitor needed to be charged, not two) and no load slip was slightly higher.

Table IV. Free acceleration test results

Applied voltage [V_{RMS}]	Peak current [A]	Acceleration time [s]	No load speed [rad/s]	No load speed [RPM]	No load slip [%]
50	23.93	2.7	307.7	2,938.3	2.0
75	35.13	0.65	311.4	2,973.7	0.9
100	46.37	0.33	312.4	2,983.2	0.6
150	68.33	0.09	313.3	2,991.8	0.3

From these results, the relationship between peak current and applied RMS voltage can be approximated by the second order polynomial given in EQ. 2.

$$I_{peak} = -8.44 * 10^{-5} * {V_{RMS}}^2 + 0.461 * V_{RMS} + 1.07 \qquad \text{EQ. 2}$$

Using this expression, the peak current at rated voltage is estimated to be 98.4A, or 7.2 times the rated full load current (13.67A). This is consistent with industry standard induction motors, which typically have an inrush current in the range of 6-7 times full load current. This high inrush current is only expected to last for roughly 6-10 cycles.

4.4 Efficiency

Motor efficiency, according to the manufacturer's data sheet, is 77%. Due to time and equipment constraints, this was not independently verified in the lab.

5 Mill Testing Description and Results

After completing motor testing, the YL90L-2 induction motor was connected to the mill and the motor/mill assembly was tested. All tests were conducted on the crusher side only due to cost and availability of unhusked rice. Tests were conducted using commercially purchased whole corn, which was obtained in 22.7kg (50lb) bags. In order to mitigate dust and particulates in the lab, a shop vacuum (shop-vac) was connected to the discharge chute of the grain mill. The volume of the shop-vac was sufficient to contain the milled output of an entire bag.

The milling side of the grain mill, as shown in the photograph of the experimental setup in Fig. 7, has both top and side hoppers. When attempting to feed the mill from the top hopper, the hammer mill tended to jam, causing the motor to draw too much current, tripping the inverter offline. The best method for feeding the mill was to fill the side hopper with grain and have an operator manually control the flow rate of whole corn into the mill.

Fig. 7. Experimental setup.

Prior to each test, the weight of a 22.7kg bag was verified using the Ohaus SD-35 digital scale. The tare weight of the shop-vac was also obtained. Next, the entire contents of the bag were fed into the grain mill as quickly as possible. In order to mitigate the high inrush current, the autotransformer was initially set to 100V and gradually increased to rated voltage (220V) at the start of each test. The input voltage, current, and motor speed were recorded during milling. Data was recorded at 1.6kHz using the NI cRIO DAQ system described in 3.11. A post-processing Matlab script extracted the average and maximum currents, the duration of the milling period, and computed the total watt-hours (Wh) consumed.

A total of 5 runs were performed, each using the entire contents of a 22.7kg bag of whole corn. Runs 1-4 were performed with the coarse (1.2mm) screen in place, while the final run (Run 5) used the fine (0.8mm) screen. The time required to process each bag was determined, and from this, the throughput in kilograms per hour (kg/hr) was extrapolated. The energy intensity in Wh/kg was also determined.

Table V summarizes some of the key data parameters which were recorded during each test. As a point of comparison, the data for when the mill was idle (not actively milling) is also included.

Table V. Mill testing performance data.

	Idle	Run1	Run2	Run3	Run4	Run5
V_{RMS} [V]	220.8	220.7	224.1	220.7	223.3	218.7
I_{RMS} (avg) [A]	4.6	10.0	12.1	11.5	10.3	13.7
P (avg) [W]	853.4	2,132.7	2,618.7	2,471.6	2,202.6	2,942.3

Q (avg) [VAR]	554.5	515.0	641.8	534.0	606.8	550.4
PF (avg)	0.836	0.969	0.969	0.977	0.964	0.982
Mass (start) [kg]	n/a	19.8	23.3	23.8	23.1	23.0
Mass (end) [kg]	n/a	18.7	23.2	22.3	21.3	20.2
Energy [Wh]	n/a	136.0	163.4	158.4	168.3	257.2
Time [s]	n/a	230.0	225.0	231.0	271.0	315.0
I_{PEAK} (steady state) [A]	4.844	14.0	14.2	14.5	12.0	19.2
P_{PEAK} (steady state) [W]	963.5	3,012.5	3,130.6	3,124.9	2,638.0	4,138.9
Milling efficiency [%]	n/a	94.44	99.74	93.66	92.30	87.75
Throughput [kg/hr]	n/a	292.70	371.20	347.38	283.48	230.86
Energy intensity [Wh/kg]	n/a	7.27	7.04	7.11	7.89	12.73

The parameters listed in Table V are defined as follows:

V_{RMS}: Root mean square (RMS) value of applied voltage for the duration of the test

I_{RMS} (avg): Average value of the RMS current drawn by the motor during the course of the test (excluding startup transient)

P (avg): Average real power drawn by the mill motor during the test (excluding startup transient)

Q (avg): Average reactive power drawn by the mill motor during the test (excluding startup transient)

PF (avg): Average power factor of the mill motor during the test

Mass (start): The starting weight of the grain prior to milling

Mass (end): The ending mass of the grain after milling

Time: The length of time required to process the entire bag of grain

I_{PEAK} (steady state): The peak current drawn by the mill motor during steady state operation (excluding startup transient)

P_{PEAK} (steady state): The peak real power drawn by the mill motor during steady state operation (excluding startup transient)

Crushing efficiency: The ratio of ending mass to starting mass. Mass loss is due to dust and grist which does not pass through the screen

Throughput: The rate of mass processed by the grain mill

Energy intensity: The amount of energy used by the mill per unit mass of grain

A 60 second excerpt of the real and reactive power that was recorded during Run 3, which used the coarse screen, is given in Fig. 8. The dotted line indicates the rated input power for the mill motor. A similar figure for the data from Run 5, using the fine screen, is included in Fig. 9.

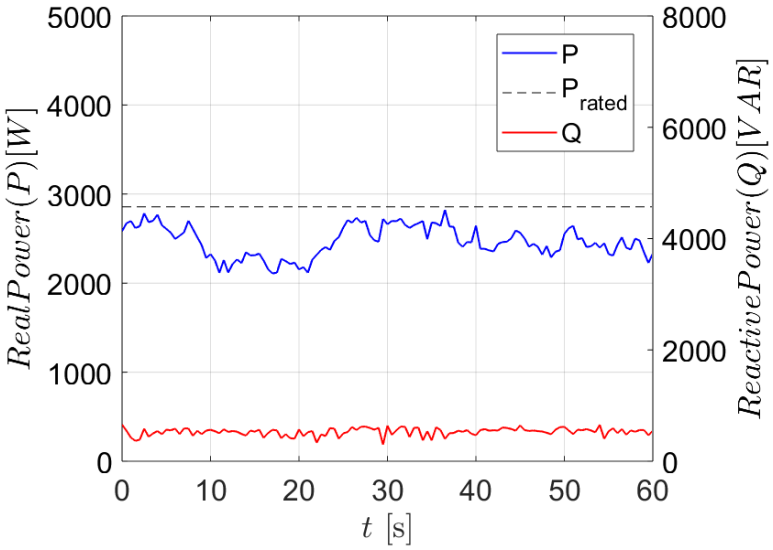

Fig. 8. Real and reactive power vs. time for Run 3.

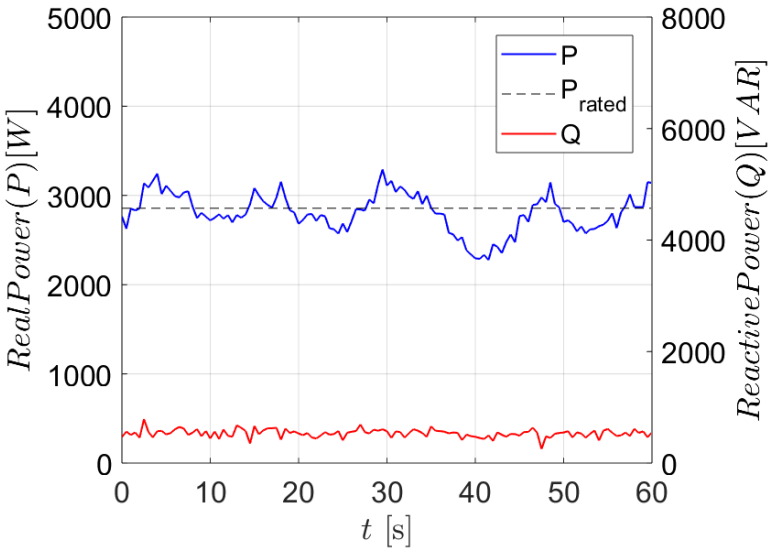

Fig. 9. Real and reactive power vs. time for Run 5.

In addition to the average and steady state data values that were recorded, a few high speed data captures of the voltage and current waveforms were performed. These were recorded at 20 kilo-samples per second (kS/s) in order to capture any high order harmonics that might be present in the waveforms. An example of the input voltage and frequency waveforms is given in Fig. 10. Voltage Total Harmonic Distortion (THD_V) was fairly low, approximately 3%, during all tests, while current THD (THD_I) was measured between 13.2-15.2%. These results are summarized in Table VI.

Table VI. Total Harmonic Distortion (THD) values for mill motor.

	THD_V [%]	THD_I [%]
Capture 1	2.9	14.4
Capture 2	3.2	13.2
Capture 3	3.0	15.2

The Fast Fourier Transform (FFT) result in Fig. 11 shows that this was predominantly third harmonic, with some fifth, seventh, and ninth harmonics as well. The likeliest culprit for this type of low order current distortion is magnetic saturation in the motor core.

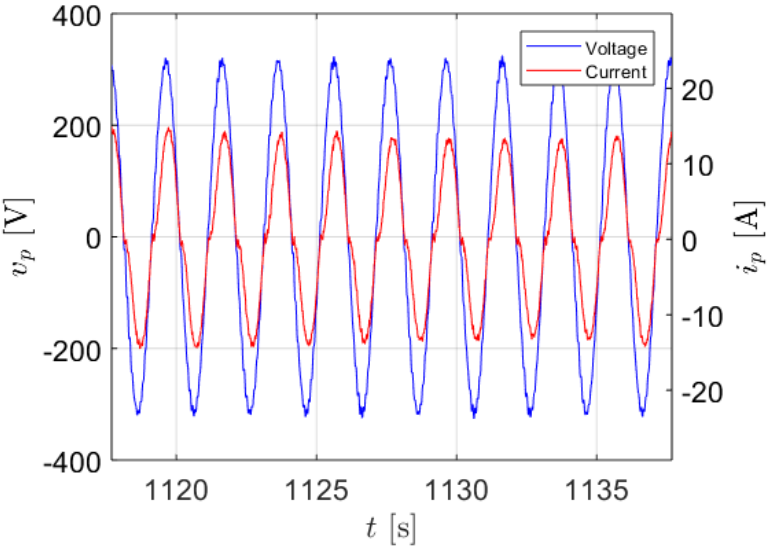

Fig. 10. Input voltage and current waveforms for the mill motor.

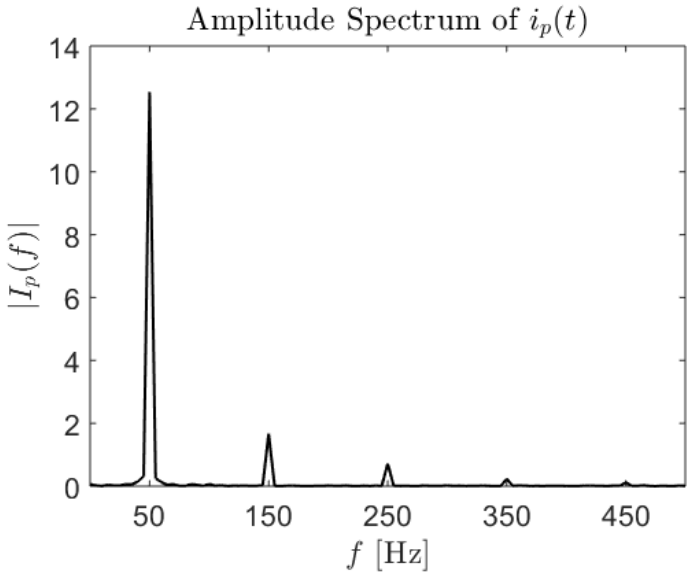

Fig. 11. FFT amplitude spectrum for mill motor current.

5.1 Grain Sieve Testing

A series of representative samples of the milled corn output from the grain mill were sifted using a US Standard sieve set, and the mass of the grain entrapped in each sieve was measured. Seven sieves were used: US sieve size #20, #40, #60, #80, #100, #140, and #200). These corresponded to diameters ranging from approximately 0.075mm to 0.85mm. A total of six samples, three from milling tests using the coarse screen, and three from milling tests using the fine screen, were evaluated using these sieves. Each sample was between 560-650 grams. The results from the sieve testing are plotted in Fig. 12.

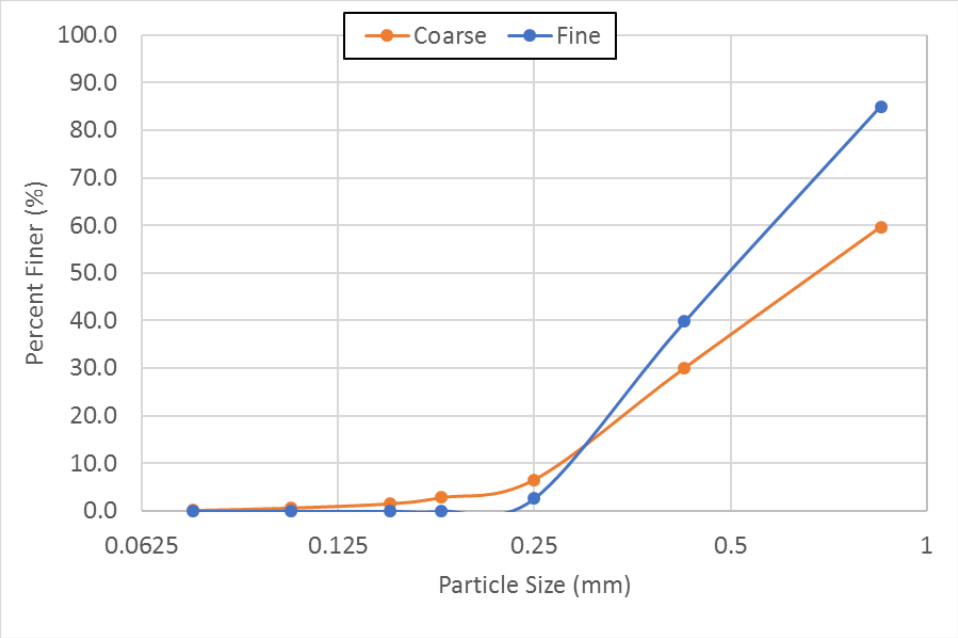

Fig. 12. Particle size distribution results for sieve testing.

A photo of the sieve testing setup is shown in Fig. 13.

Fig. 13. Photo of sieve testing setup.

5.2 Other Testing

Other tests were conducted including: audible noise, temperature rise, and tip speed. The testing and results are described below, and are summarized in Table VII.

The audible noise level of the mill was tested using the Exetech Sound Level Meter mentioned in section 3.8. First, the ambient background noise level was recorded to be around 53-54

decibels (dB). When running idle, the noise level of the mill was recorded to be 91-92dB. When actively milling, the noise level increased slightly to 94-95dB.

A temperature rise test on the milled grain was performed. Prior to milling, the surface temperature of the grain was measured to be 23.3ºC. After milling, the surface temperature of the milled output was 27.2ºC. This equates to a temperature rise of 3.9ºC.

The rated spindle speed of the crushing side of the grain mill is 5,000-5,600RPM. This was confirmed and verified using the optical speed sensor mentioned in 3.6. The hammer length was measured to be about 100mm, from which the tip speed can be calculated as 52-59 meters per second (m/s).

Table VII. Other testing result summary.

Audible noise	
Ambient	53-54dB
Idle	91-93dB
Active milling	94-95dB
Temperature rise	3.9ºC
Tip speed	52-59m/s

6 Results Discussion and Conclusion

These results show that when idling the mill drew around 4.6-4.8A, or roughly 1/3 of rated current. With the coarse screen in place, the average current drawn by the motor was around 10-12A, or 73-88% of the rated current, with brief excursions that exceeded the 13.7A rating. When running with the fine screen, the average current was approximately equal to rated current (13.7A) and regularly exceeded rated current. Therefore, when running with the fine screen for extended periods of time, the motor could potentially experience overheating due to regularly being pushed above rated current.

A common industry rule is that for every 10ºC above rated temperature, the expected working life of the motor is cut in half. Therefore, for a motor with NEMA Class A insulation (rated for a maximum temperature of 105ºC) operating at 115ºC, the life expectancy of the motor would be reduced from 15 years to 7.5 years. The manufacturer's data for the motor that was provided did not specify the insulation class, maximum allowable temperature rise, or a rated life for the motor. Conducting a winding temperature rise test fell outside the scope of this evaluation.

The real power consumption of the mill varied in proportion to the instantaneous amount of grain it was processing, and whether the coarse or fine screen was used. When idle, the real power drawn by the motor was 800-900W; with the coarse screen, the real power was about 2.3kW, but increased about 26% to 2.9kW when using the fine screen. Small fluctuations in the amount of grain being processed at any given time can be seen in the fluctuations in real power consumed by the mill.

Reactive power, unlike real power, did not change significantly with loading. However, this was extremely sensitive to voltage. When voltage was slightly above rated, such as Run 2

(224V) or Run 3 (223V), reactive power exceeded 600VAR, whereas when the voltage was closer to 220 (Runs 1, 4, and 5) reactive power was in the range of 515-550VAR. The presence of the run capacitor seems to have helped the motor supply most of its own excitation, resulting in a very high running power factor on the order of 0.97-0.98, lagging.

The mill used approximately 7.3Wh/kg of grain processed using the coarse screen and 12.7Wh/kg with the fine screen. For the coarse screen, the throughput matched the rated throughput of the datasheet, close to or greater than 300kg/hr. Mass loss using the coarse screen was negligible, leading to crushing efficiencies in the 92-99% range. With the fine screen, however, more mass was lost due to dust and grist, leading to a crushing efficiency of 88%. Rated throughput could not be obtained using the fine screen.

The high inrush current requirement of this motor (>98A) means that for most microgrid applications a soft-starter will be required. The THD could also potentially be problematic for microgrids where power quality is an issue, or situations where sensitive loads could be impacted by the low order harmonics. An isolation transformer could be used to prevent the harmonics from impacting other hardware on the distribution system.

When running with the coarse screen, the mill was able to meet the rated throughput. However, with the fine screen, rated throughput could not be achieved, and the energy intensity was about 1.7 times higher. Therefore, if a coarser grind is acceptable for the application, the coarse screen will provide increased throughput and lower energy intensity for the same mass of grain. Further investigation is required to determine the impact of a larger motor on the performance of the fine screen.

7 References

[1] *IEEE Standard Test Procedure for Single-Phase Induction Motors*, IEEE Standard 114, 2010.

[2] *IEEE Standard Test Code for Resistance Measurement*, IEEE Standard 118, 1978.

[3] M.H. Haque. “Determination of NEMA Design Induction Motor Parameters From Manufacturer Data,” *IEEE Trans. on Energy Conversion*, vol. 23, no. 4, pp. 997-1004, Dec. 2008.

[4] S. Jurkovic. “Induction Motor Parameters Extraction,” Available online: http://web.mit.edu/kirtley/binlustuff/literature/electric%20machine/motor-parameters.pdf. Accessed May 5, 2018.

[5] G. Mehos and D. Morgan. *Hopper Design Principles.* Chemical Engineering Online. Jan. 2016. Online: http://www.chemengonline.com/hopper-design-principles/

[6] O. Adekomaya and O.D. Samual. “Design and Development of a Petrol-powered Hammer mill for rural Nigerian Farmers”. *Journal of Energy Technologies and Policy*, vol. 4, no. 4, pp. 65-74, Jan. 2014.

[7] D. Armitage, T. Wontner-Smith, and R. Wilkin. *Grain Moisture – guidelines for measurement*. HGCA publications. London, England. 2008.

[8] G.C. Mrema, et. al., *Rural structures in the tropics: design and development*. Food and Agriculture organization of the United Nations. Rome, Italy. 2011.

[9] K. Koch, *Hammermills and Rollermills*, Kansas State University, May 2002. Online: https://www.bookstore.ksre.ksu.edu/pubs/mf2048.pdf

[10] D.L. King, J.A. Kratochvil, and W.E. Boyson. “Temperature Coefficients for PV Modules and Arrays: Measurement Methods, Difficulties, and Results,” presented at the 26th IEEE Photovoltaic Specialists Conf., Anaheim, USA, 1997.

[11] *Standard Specification for Wire Cloth and Sieves for Testing Purposes*, ASTM Standard E11, 2004.

[12] A. Patwa, J. Wilson, and K. Ambrose, “Particle Size Analysis of Two Distinct Classes of Wheat Flour by Sieving,” *Trans. ASABE*, no. January, pp. 151–159, 2014.

[13] “Extend the Operating Life of Your Motor”, Advanced Manufacturing Office, Energy Efficiency and Renewable Energy, U.S. Department of Energy, DOE/GO-102012-3735, November, 2012. Available online: https://www.energy.gov/sites/prod/files/2014/04/f15/extend_motor_operlife_motor_systemts3.pdf. Accessed 12/28/2018.

Appendix A: Mill Datasheet

天福®

四川省佳信机械制造有限公司

Sichuan Provincial Jiaxin Machinery Manufacturing Co., Ltd.

6N40–加宽9FC23碾米粉碎组合机

Combinational machine of grinder and rice mill

重量：65kg 纸箱包装、无电机

Net weight: 65kg

(no motor but packaged with carton)

技术参数 Technical Parameters

项目 Project / 名称 Name	粉粹机 crushing machine	碾米机 milling machine
配套动力 Matched Power KW	2.2kw	
生产率 Productivity kg	≥300kg/h	≥150kg/h
电耗 Power consumption	≤20kw.h/t	≤12kw.h/t
主轴转数 Spingdle speed	5000–5600r/min	1400–1600r/min
运转直径 Operation diameter	230mm	40mm

主 要 性 能：粉碎加工玉米、豆类、小麦等颗粒粮食，红薯、马铃薯等状物的粉碎；米机用于碾米。

Performance: Grinding process of corn, beans, wheat and other food grains as well as which similar to sweet potato and potato in shape; Mill for rice milling.

纸箱包装尺寸：700*540*350mm

Package size of carton: 700*540*350mm

Appendix B: Mill Motor Datasheet

ISO 9001:2008 CE EFF 2

YL Series

Single-phase two-value capacitor asynchronous motor technical data

Model	Rated power (kW)	Rated power (HP)	Rated voltage (V)	Rated current (A)	Frequency (Hz)	Speed(r/min)		Eff(η%)	Power Factor	IS	TS	Tmax
						50Hz	60Hz			IN	TN	TN
YL7112	0.37	0.5	110/220	5.4/2.7	50/60	2750	3300	67	0.94	5	1.8	1.8
YL7122	0.55	0.75	110/220	7.6/3.8	50/60	2750	3300	70	0.94	5	1.8	1.8
YL7114	0.25	0.33	110/220	4.2/2.1	50/60	1370	1640	62	0.9	6	1.8	1.8
YL7124	0.37	0.5	110/220	5.8/2.9	50/60	1370	1640	65	0.9	6	1.8	1.8
YL8012	0.75	1	110/220	10.4/5.2	50/60	2800	3360	72	0.92	6	1.8	1.8
YL8022	1.1	1.5	110/220	14/7	50/60	2800	3360	75	0.95	6	1.8	1.8
YL8014	0.55	0.75	110/220	8/4	50/60	1400	1680	68	0.92	6	1.8	1.8
YL8024	0.75	1	110/220	10.4/5.2	50/60	1400	1680	71	0.92	6	1.8	1.8
YL90S-2	1.5	2	110/220	19/9.5	50/60	2820	3380	76	0.95	5	1.7	1.8
YL90L-2	2.2	3	110/220	27.4/13.7	50/60	2820	3380	77	0.95	6	1.7	1.8
YL90S-4	1.1	1.5	110/220	14.4/7.2	50/60	1420	1700	73	0.95	5.5	1.7	1.8
YL90L-4	1.5	2	110/220	19.2/9.6	50/60	1420	1700	75	0.95	6	1.7	1.8
YL90S-6	0.55	0.75	110/220	9/4.5	50/60	910	1090	60	0.94	5.5	1.7	1.7
YL90L-6	0.75	1	110/220	11.9/6	50/60	910	1090	61	0.94	5.5	1.7	1.7
YL90L2-6	1.1	1.5	110/220	16.6/8.3	50/60	910	1090	64	0.94	5.5	1.7	1.7
YLX100L-2	3	4	110/220	36.4/18.2	50/60	2840	3410	79	0.95	6.5	1.6	1.7
YLX100L1-4	2.2	3	110/220	27.8/13.9	50/60	1420	1700	76	0.95	6.5	1.6	1.7
YLX100L2-4	3	4	110/220	37.4/18.7	50/60	1420	1700	77	0.95	6.5	1.6	1.7
YLX112M4	4	5.5	110/220	49.2/24.6	50/60	1420	1700	78	0.95	6.5	1.5	1.7
YLX112M2	4	5.5	110/220	48.6/24.3	50/60	2840	3410	79	0.95	6.5	1.5	1.7
YLX132S2	5.5	7.5	110/220	66.6/33.3	50/60	2840	3410	79	0.95	6.5	1.5	1.7
YLX132M2	7.5	10	110/220	89.8/44.9	50/60	2840	3410	80	0.95	6.5	1.5	1.7
YLX132S4	5.5	7.5	110/220	67.6/33.8	50/60	1440	1730	78	0.95	6.5	1.5	1.7
YLX132M4	7.5	10	110/220	90.8/45.4	50/60	1440	1730	79	0.95	6.5	1.5	1.7

Appendix C: Data file description

The complete data results that were captured during testing can be found in "Mill Test Data_CSU2018.xls". This workbook combines the data results for all testing, with one sheet per test. Data for eight tests total are included. These are:

- Run 1 – Steady state values for mill test Run 1 with 1.2mm screen
- Run 2 – Steady state values for mill test Run 2 with 1.2mm screen
- Run 3 – Steady state values for mill test Run 3 with 1.2mm screen
- Run 4 – Steady state values for mill test Run 4 with 1.2mm screen
- Run 5 – Steady state values for mill test Run 5 with 0.8mm screen
- Waveform 1 – High speed capture of voltage and current waveforms during milling with 1.2mm screen
- Waveform 2 – High speed capture of voltage and current waveforms during milling with 1.2mm screen
- Waveform 3 – High speed capture of voltage and current waveforms during milling with 1.2mm screen

The data columns for the steady state data are as follows:

- Column A – Elapsed time in seconds. Each test starts from time t=0.
- Column B – Primary electrical frequency of the input voltage waveform (50Hz nominal)
- Column C – RMS value of the line-to-line voltage applied to the mill motor ($220V_{RMS}$ nominal)
- Column D – RMS value of the line one current supplying the mill motor
- Column E – RMS value of the line two current supplying the mill motor (note that this should be equal to the line one current values in Column D)
- Column F – Power Factor, defined as the cosine of the angle between the current and voltage waveforms. Negative indicates lagging while positive indicates leading.
- Column G – Motor speed as recorded using the optical speed sensor, in radians per second.

The data columns for the waveform data are as follows:

- Column A – Elapsed time in seconds. Each test starts from time t=0.
- Column B – Instantaneous value of the line-to-line voltage applied to the mill motor
- Column C – Instantaneous value of the line one current supplying the mill motor
- Column D – Instantaneous value of the line one current supplying the mill motor (note that this should have equal magnitude to line one current in Column C but be mirrored about the x axis)

5.5. Solar Water Pump Test Methods

Test Method for Reciprocating and Rotodynamic Pumps Driven by Electric Motors

Colorado State University
Factor[e] Ventures
430 N College Ave.
Fort Collins, CO 80524
11 January 2019

Table of contents

1. Objective 1
1.1. Scope 1
2. Instrumentation 1
2.1. Voltage 1
2.2. Current 1
2.3. Power 1
2.4. Pressure 1
2.5. Flow 2
2.6. Speed 2
2.7. Torque 2
2.8. Temperature 2
2.9. Electromagnetic noise 2
2.10. Accuracy 3
2.11. Calibration 4
3. Test Configuration 5
3.1. Description of testing components 5
3.1.1. Open or closed tank 5
3.1.2. Flowmeter 5
3.1.3. Control valve for throttling suction 5
3.1.4. Thermometer 5
3.1.5. Dampening valve 6
3.1.6. Suction pressure gauge 6
3.1.7. Discharge pressure gauge 6
3.1.8. Accumulator tank 6
3.1.9. Discharge control valve 6
3.1.10. Current sensor 6
3.1.11. Voltage sensor 6
3.1.12. DC power supply 6
3.1.13. AC power supply 6
4. Motor Tests 7
4.1. Winding resistance measurement 7
4.1.1. Precision resistance meter or impedance analyzer 7
4.1.2. Bridge method 7
4.1.3. Voltage Drop Method 9
4.2. Winding temperature rise 9
4.3. Efficiency 10
5. DC Motor Tests 10
5.1. Winding inductance measurement 10
5.1.1. Shunt and compound-wound machines 10
5.1.2. Series excited machines 11
5.2. Magnetic saturation 11

5.2.1. Separately driven 11
5.2.2. Self-driven 11
5.3. Voltage vs. rotational speed 12
5.4. Speed regulation 12
5.5. Efficiency 12
5.5.1. Machine loading 12
5.5.2. Segregated loss method 13
5.6. Torque-current characterization curve 14
6. AC Induction Motor Tests 14
6.1. Locked-rotor tests 15
6.1.1. Locked rotor current and torque 16
6.2. No-load test 16
6.2.1. Separately driven 16
6.2.2. Self-driven 17
6.3. Efficiency 17
6.3.1. Machine loading 17
6.4. Power Factor 18
6.5. Speed-torque and Speed-current Characteristic 19
6.5.1. Measured output 20
6.5.2. Acceleration 20
6.5.3. Input 20
6.5.4. Direct measurement 21
7. Pump Performance Testing 21
7.1. Test methodology 22
7.2. Variable voltage DC systems 23
7.3. Efficiency 24
7.3.1. Overall efficiency 24
7.3.2. Pump efficiency 24
7.3.3. Volumetric efficiency 25
8. References 25
Appendix A: List of tests 26

List of figures

Figure 1. Test configuration diagram. 5
Figure 2. Wheatstone bridge. 8
Figure 3. Kelvin bridge. 8
Figure 4. Voltage drop method 9
Figure 5. Pump-back test system diagram. 13
Figure 6. Equivalent circuit for an induction motor (single-cage rotor model). 14
Figure 7. Induction motor locked-rotor equivalent circuit 15
Figure 8. Diagram for motor-generator slip test. 18

Figure 9. Representative speed vs. torque characteristic curve for a single-phase induction motor. 19

List of tables

Table 1. Instrument accuracy requirements. 3
Table 2. Instrument calibration intervals. 4
Table 3. Acceptable steady state test value fluctuations. 21

1. Objective

The purpose of this document is to outline the preferred method for testing reciprocating-type pumps driven by brushed or brushless Direct Current (DC) motors, or by AC induction motors.

1.1. Scope

This testing is for determining the electrical parameters and characteristics, and overall efficiency, for the motor-pump assembly only. It does not cover other testing procedures, such as hydrostatic testing, or Net Positive Suction Head Required (NPSHR) for pumps, which can be found in ANSI/HI 6.6 [1]. Methods for determining segregated motor losses are not addressed as part of this methodology. These and other miscellaneous motor tests are covered by the standards IEEE 113 for DC motors, and IEEE 112 and IEEE 114 for poly-phase and single-phase induction motors, respectively.

2. Instrumentation

It is recommended that, whenever possible, all measurements be taken using electronic instruments with analog outputs that can be read and recorded by a data logger.

2.1. Voltage

Voltage measurements should be made at or as near to terminals as possible. If, for some reason, they cannot be, then the error should be evaluated and subsequent readings corrected. Tests should be conducted at rated voltage for the pump.

2.2. Current

Current measurements can be made with in-line current sensors or current transformers if the magnitude of the measured current is too high. Hall effect sensors may also be used. For appliances with DC motors, DC compatible current sensors must be used. Current draw by instruments, such as volt and/or watt-meters, should be subtracted to obtain the net motor current.

2.3. Power

Power measurements can be made using a dedicated watt-meter. For DC motors, power can be calculated by taking the product of Voltage (as measured in 2.1) and current (as measured in 2.2).

2.4. Pressure

Pressure can be measured with a pressure gauge or pressure transducer. A dampening device, such as a needle valve or capillary tube, should be used to dampen pressure pulsations. Pressure taps should be located a minimum of two diameters of straight pipe of unvarying cross section before the suction stabilizer and after the discharge dampener following an elbow, valve, or other obstruction. Pressure measurements should not be made at or near the highest nor the lowest point of the pipe cross section. The diameter of the pressure tapping must be between 3mm and 6mm, or 1/10 the pipe diameter, whichever is smaller. The length of the pressure tapping hole shall not be less than two and a half times its diameter [1].

An accumulator tank and/or backpressure regulator may be used on the discharge side of the pump to dampen noisy or turbulent water flow.

2.5. Flow

Measurements of rate of flow may be taken using any of the methods outlined in section 6.6.7 of ANSI/HI 6.6 [1]. These include, but are not limited to:

- Measurement by weight
- Measurement by volume
- Measurement by displacement-type meters
- Measurement by head-type rate meters
- Measurement by venture meter
- Measurement by nozzle
- Measurement by thin square-edged orifice plate
- Measurement by Pitot tubes
- Other methods as allowed by ANSI/HI 6.6.

Use of rotating vane type flowmeters is discouraged because the additional load imposed on the pump can lead to inaccurate results. Ultrasonic or electromagnetic flow meters are preferred.

2.6. Speed

Pump speed measurements can be made using tachometers, frequency-responsive devices, or magnetic pickups. Stroboscopes are discouraged due to uncertainty in precision and limited accuracy.

2.7. Torque

Torque measurements may be made using transmission dynamometers, torsion dynamometers, strain gauge type torque measuring devices, calibrated motors, or other methods of acceptable accuracy.

If a dynamometer is being used, its rating should not exceed three times the rating of the pump motor, and the rated torque should not be greater than four times the maximum pump torque. Additionally, the dynamometer should be sensitive to a change in torque less than or equal to 0.1% of the rated motor torque.

2.8. Temperature

Temperature may be measured using electric or mercury thermometers, or by using thermocouples or Resistance Temperature Detectors (RTDs).

2.9. Electromagnetic noise

Electronic instruments feature higher input impedance than passive instruments, which means they draw less current, thereby reducing the need to make corrections for current drawn by the instrument. They are, however, more susceptible to electromagnetic noise.

Common noise sources include:

- Inductive or electrostatic coupling of signal leads to power circuits
- Inadequate common mode rejection
- Common impedance coupling or ground loops
- Conducted interference from power circuits

Good practices for minimizing electromagnetic noise should be adhered for all electronic instruments. These include:

- Using shielded, twisted pair wires for signal leads
- Grounding the shield at only one point
- Maintaining as much distance as is practical between signal leads and power cables
- Grounding all exposed metal parts

2.10. Accuracy

Instrument error is rated as a percentage of the full scale for the measurement instrument. For this reason, it is important to size measurement instruments appropriately such that the full scale of the instrument is close to the expected range of operating values. Instrument transformers should be avoided if possible because they can inject additional error into measured values. If instrument transformers are used, their error must not exceed ±0.3%.

Accuracy for all measurement devices must adhere to the values specified in Table 1.

Table 1. Instrument accuracy requirements.

Measured Value	**Accuracy of the instrument as a percentage of the values**
Rate of flow	±1.5%
Differential pressure	±1.0%
Discharge pressure	±1.0%
Suction pressure	±1.0%
Voltage	±0.2%
Current	±0.2%
Power	±0.2%
Frequency	±0.05%
Resistance	±0.2%
Torque	±0.7%
Motor speed	±0.3% or 1.0 rpm, whichever is less

2.11. Calibration

The recommended calibration intervals found in Table 2 should be followed for all instruments and measurement equipment, unless they differ from manufacturer's recommendations, in which case the manufacturer's recommended calibration interval shall be used.

Table 2. Instrument calibration intervals.

Rate of Flow		**Torque**	
Quantity meter		Dynamometer with scale	6 years
Weighing tank	1 year	Dynamometer with load scale	6 months
Volumetric tank	10 years	Torque bar	1 year
Rate meters		Calibrated motor	Not required
Venturi	Not required	Strain gauges	6 months
Nozzle	Not required	**Power**	
Orifice Plate	Not required	kW transducer	3 years
Weir	Not required	Watt-amp-volt meter	1 year
Turbine	1 year	Transmission gears ≤500 HP	10 years
Magnetic flow	1 year	Transmission gears >500 HP	20 years
Rotameter	5 years	**Speed**	
Propeller	1 year	Tachometers	3 years
Ultrasonic	5 years	Eddy current drag	10 years
Pressure		Electronic	Not required
Bourdon tube	4 months	Frequency-responsive devices	
Manometer	Not required	Vibrating reed	10 years
Dead weight tester	1 year	Electronic	10 years
Transducer	4 months	Photocell	10 years
Digital indicator	1 year	Stroboscopes	5 years
Temperature		**Electrical**	
Electric	2 years	Voltage	1 year
Mercury	5 years	Current	1 year

3. Test Configuration

The recommended pump test configuration is shown in the diagram in Figure 1, below.

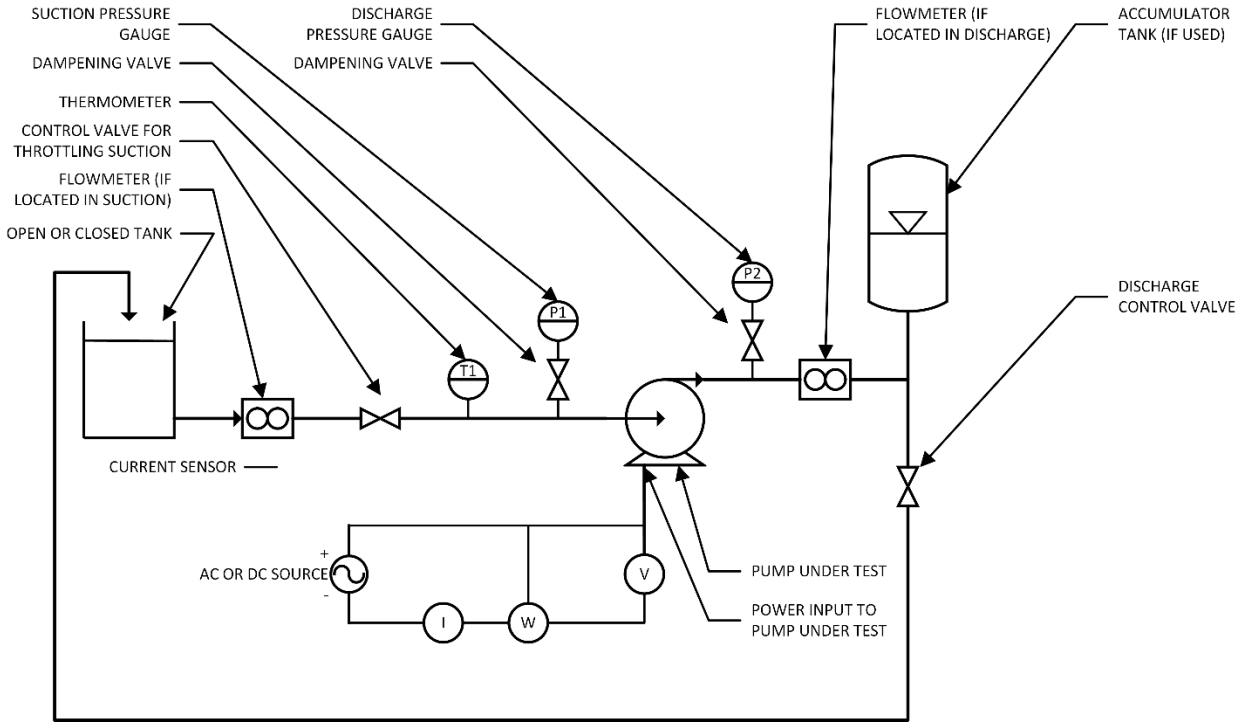

Figure 1. Test configuration diagram.

3.1. Description of testing components

This section describes the various aspects of the testing setup shown in Figure 1.

3.1.1. Open or closed tank

A tank should be provided with sufficient volume to maintain a constant flow rate and pressure in the test system. Water will be circulated into and out of this tank, maintaining a constant liquid level in the tank. This tank may be closed or open to atmosphere.

3.1.2. Flowmeter

A flowmeter that meets the requirements as defined by section 2 shall be installed on either the suction (inlet) or discharge (outlet) side of the pump under test.

3.1.3. Control valve for throttling suction

An optional valve may be installed on the suction (inlet) side of the pump to regulate the flow rate. This may be manually or operable or automated.

3.1.4. Thermometer

Thermometer (either mercury or electronic) to record the temperature of the water in the test setup. Tests should be conducted as close to 20°C as possible. The specific gravity of the water should be corrected for temperatures other than 20°C.

3.1.5. Dampening valve
A needle valve, capillary tube, or similar device for dampening pressure variations in the pressure gauge.

3.1.6. Suction pressure gauge
A pressure measurement device meeting the requirements in section 2 for determine pressure at the suction (inlet) side of the pump under test.

3.1.7. Discharge pressure gauge
A pressure measurement device meeting the requirements in section 2 for determine pressure at the discharge (outlet) side of the pump under test.

3.1.8. Accumulator tank
An accumulator tank, or other backpressure regulation device, may optionally be used to maintain constant pressure on the discharge (outlet) side of the pump.

3.1.9. Discharge control valve
An optional valve may be installed on the discharge (outlet) side of the pump to regulate the discharge backpressure.

3.1.10. Current sensor
An in-line, Hall effect, or current transformer-type current sensor meeting the requirements in section 2 shall be used to monitor AC or DC input current to the pump motor.

3.1.11. Voltage sensor
The input voltage to the pump motor shall be monitored either directly or by means of a voltage divider, or an AC or DC voltage transducer, meeting the requirements in section 2.

3.1.12. DC power supply
For pumps with DC motors, a DC fixed power supply may be used to power a pump motor. The power supply shall be capable of supplying rated voltage and power to the pump motor, and must be essentially ripple free. To be considered ripple free, the peak-to-peak value of the AC current component shall be less than 6%, or the RMS value less than 2%, of the rated current of the test motor under all test conditions.

A photo-voltaic simulator or outdoor test using the associated photo-voltaic panels may optionally be used to power a pump motor. Unlike a power supply that has infinite current, a PV simulator or panels provides power to the pump along a power curve that determines voltage and current.

3.1.13. AC power supply
An AC power supply capable of supplying the full load current of the pump motor at the rated voltage and frequency shall be provided. The voltage waveform should be as close to purely sinusoidal as possible; voltage waveform deviation should not exceed 10%. The frequency should be maintained within ±0.5% of the required testing value. When evaluating motor efficiency, the rated frequency must be within ±0.5% of the required test value.

4. Motor Tests

This section outlines test procedures for electrically characterizing electric motors used to drive a pump. This section outlines test procedures that are applicable to both DC and AC motor types. Tests methodologies that are specific to DC motors are detailed in Section 5. If the motor uses an AC induction motor, the procedures in Section 6 should be followed.

4.1. Winding resistance measurement

The electrical resistance of the motor windings should be established in order to estimate conduction (I^2R) loss in the machine, as well as determining temperature rise in the windings. Resistance measurements should be taken under "cold" conditions when the motor has sat idle for sufficient time such that the winding temperature is equal to ambient air temperature. Measured values should be corrected to a standard reference temperature of 25°C, using EQ. 1:

$$R_s = \frac{R_t(t_s + k)}{(t_t + k)} \qquad \text{EQ. 1}$$

Where:

R_s= Resistance of winding measured at specified reference temperature t_s (Ω)
R_t = Resistance of winding at measured temperature t_t (Ω)
t_s = Specified reference temperature (25°C)
t_t = Measured temperature (°C)
k = 234.5 for copper
225 for aluminum

Resistance measurements may be made using a sufficiently accurate, calibrated precision resistance meter or impedance analyzer, or by the bridge method. The voltage drop method is an acceptable alternate method.

4.1.1. Precision resistance meter or impedance analyzer

A digital precision milli-ohm or micro-ohm meter or impedance analyzer with a resolution of ≤ 0.1mΩ and an accuracy of ±0.2% may be used for resistance measurements. Four wire resistance measurements should be made to compensate for lead resistance. Resistance measurements should be made as close to the motor terminal windings as possible, with an ambient temperature at or near 25°C.

4.1.2. Bridge method

The bridge method is the preferred method for measuring low resistances with high accuracy, without the high equipment cost of a precision resistance meter or impedance analyzer. The Wheatstone bridge circuit, shown in Figure 2, is typically used for high precision measurements of resistance ≥ 1Ω.

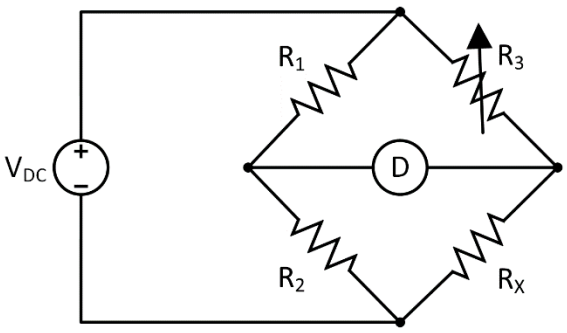

Figure 2. Wheatstone bridge.

Two known resistors, R_1 and R_2, are connected to the unknown winding resistance R_X, along with an adjustable resistor R_3. A detector (either current or voltage) is connected between the two nodes as shown. When the circuit is balanced, there will be no voltage nor current flow through the detector. When this occurs, the unknown resistance R_X can be calculated by EQ. 2.

$$R_X = \frac{R_2 R_3}{R_1} \qquad \text{EQ. 2}$$

For resistances < 1Ω the lead wire resistances should be compensated for; the Kelvin bridge, shown in Figure 3 is therefore recommended.

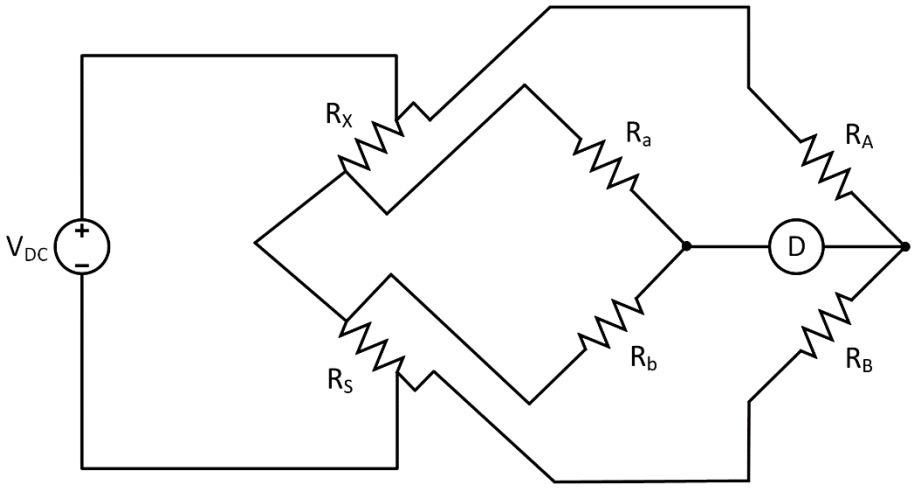

Figure 3. Kelvin bridge.

In this case, the unknown resistance R_X can be calculated by EQ. 3:

$$R_X = R_S \frac{R_A}{R_B} + \left[\frac{R_b R_y}{R_a + R_b + R_y}\right]\left[\frac{R_A}{R_A} - \frac{R_a}{R_b}\right] \qquad \text{EQ. 3}$$

Where R_y is the resistance of all the associated wires and leads (yoke). For this reason, yoke resistance should be minimized as much as possible. Assuming R_y is

negligible and R_A/R_B exactly equals R_a/R_b, EQ. 3 can be simplified and rewritten as EQ. 4:

$$R_X = R_S \frac{R_A}{R_B} \qquad \text{EQ. 4}$$

4.1.3. Voltage Drop Method

This method may be alternatively used if a precision resistance meter or bridge resistance measurement device is unavailable. The results, however, will not be as accurate relative to the aforementioned methods. In this method, a DC voltage source is connected to the motor windings. This DC source can be a switching power supply, battery, filtered rectifier, or other suitable supply, but should be relatively ripple-free. The resulting current is measured, along with the voltage across the winding, and the resistance is calculated according to Ohm's law. The current should not exceed 15% of the rated current to prevent temperature rise in the windings, which will skew the results. An optional resistor may be added in series with the winding to reduce the current flow. A diagram of the circuit for the voltage drop method is shown in Figure 4.

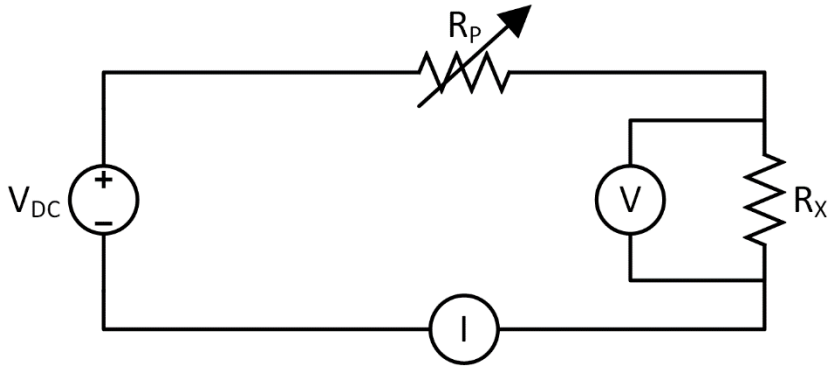

Figure 4. Voltage drop method

4.2. Winding temperature rise

In order to determine the temperature rise in the machine windings, the motor under test should be run with all covers in place, in a test environment with sufficient space for heat dissipation and no drafts. The machine should be run at rated voltage and load until winding temperature has stabilized. Readings should be taken at least once every 30 minutes, and are said to have stabilized when they do not vary more than 2% for three consecutive readings spaced at least 30 minutes apart.

Winding surface temperature is typically much lower than the internal temperature; therefore, the most reliable method of measuring temperature rise is by accurately measuring the winding resistance. Winding resistance measurements should be taken using any of the methods described in Section 4.1. Measurements should be made quickly to avoid stopping the motor for a prolonged period of time, such that winding temperature is maintained. For machines ≤ 50kW readings should be taken within 60s.

4.3. Efficiency

Efficiency refers to the ratio of output power to input power. In the case of the pump motor, it represents the percentage of electrical power that is translated to mechanical power to the pump. Efficiency may be calculated by directly measuring input and output power, and taking the ratio of them (as shown in EQ. 5), or by separately determining the individual sources of loss (as shown in EQ. 6).

$$Efficiency\ [\%] = \left[\frac{P_{OUT}}{P_{IN}}\right] * 100\% \qquad \text{EQ. 5}$$

$$Efficiency\ [\%] = \left[\frac{P_{IN} - P_{LOSS}}{P_{IN}}\right] * 100\% \qquad \text{EQ. 6}$$

Efficiency data should be determined at rated voltage and speed. Measurements should be taken after the motor has been running at rated load for sufficient time to allow the winding temperature to stabilize. See 4.2 for how to determine winding temperature rise and how temperature stabilized is determined.

Motor efficiency shall be determined at six points ranging between 25-150% of rated load. Specifically, these points shall be approximately: 25%, 50%, 75%, 100%, 125%, and 150% of rated load. Machine loading should begin with the highest loading, and points taken in descending order. Winding temperature shall be within 10% the hottest measured temperature rise as found in 4.2.

The specific parameters to be recorded at each load point differ between DC and AC motor types. Specific methods for accomplishing the machine loading also vary based on the type of motor being tested. DC motor efficiency test procedures are defined in Section 5.5 while those for AC motors can be found in Section 6.3.

5. DC Motor Tests

This section describes tests and test procedures that are unique to pumps with brushed or brushless DC motors.

5.1. Winding inductance measurement

The winding inductance may be determined directly through the use of an impedance analyzer, or analytically. If determined analytically, the methodology used varies based on the specific construction of the machine under test.

5.1.1. Shunt and compound-wound machines

For these types of machines, the unsaturated inductance can be found by applying single phase 50 Hz or 60 Hz AC to the armature circuit terminals of the motor. The shunt-field winding should be short-circuited to prevent high voltages from developing within the windings. The armature should be locked in place during testing to prevent motion.

Three values of current, equally spaced, should be applied, with the largest not to exceed 20% of the current rating of the motor. An oscilloscope is required to

measure the phase angle between the corresponding voltage and current waveforms. The inductance can be calculated by EQ. 7:

$$L = \frac{V sin\theta}{\omega I} \qquad \text{EQ. 7}$$

Where

L = Inductance (H)
V = Voltage (V)
I = Current (A)
θ = Phase angle between the voltage and current (^{o})
ω = Frequency times 2π (rad/s)

5.1.2. Series excited machines

For series excited machines, the armature circuit inductance varies widely with frequency, and with the magnitude of the DC and AC current components. Therefore, inductance values for frequencies other than the test frequency cannot be determined analytically using the method described in 5.1.1. For these machines, an impedance analyzer is recommended for characterizing the inductance over a broader frequency range.

5.2. Magnetic saturation

The no-load magnetic saturation curve for the pump motor refers to the nonlinear relationship between the terminal voltage of the armature and the field current at rated speed. The motor may be separately driven or self-driven during this test.

Data points should be taken at regularly spaced intervals from zero field current up to 125% of rated voltage, with three of the readings taken as near as possible to 90%, 100%, and 110% rated voltage. Field current, armature voltage, and machine speed readings should be recorded during the duration of the test.

In order to avoid hysteresis effects skewing the results, measurements should be taken on separate ascending and descending curves. While on the ascending curve, the armature terminal voltage should only increase from one point to the next. If the voltage exceeds the intended test point while on an ascending curve, the field current must be reduced to zero and the armature terminal voltage should be increased to the test point. Similarly, while on the descending curve, the voltage should only be decreased; it should never be taken below the intended test point and then increased. If necessary, the field current must be increased to the maximum value and the armature terminal voltage decreased to the intended test point.

5.2.1. Separately driven

For separately driven tests, the machine should be driven at rated speed by any suitable source. Field current should be supplied from a separate source to stabilize the armature terminal voltage.

5.2.2. Self-driven

In cases where an acceptable separate drive is available, a no-load saturation curve may be approximated by driving the uncoupled pump motor using a ripple-

free DC power source capable of operating between 25%-125% of the rated motor voltage. In this case, some field current will be required to maintain the machine speed, so the results will not be as exact as those obtained by the separately driven method mentioned in 5.2.1.

5.3. Voltage vs. rotational speed

For DC motors, the rotational speed is directly proportional to the input voltage. A no-load voltage vs. RPM curve should be created using an adjustable, ripple-free DC power supply. The lower boundary for the curve should be the voltage that most closely corresponds to 50% of the rated speed, and increased to 125% of rated voltage.

5.4. Speed regulation

Speed regulation refers to the effects of machine loading on the rotational speed of the motor. The test should be conducted after the motor has been running continuously at rated load for sufficient time such that the winding temperature has stabilized. The machine loading should be varied several times from full load to no load and back, and the machine speed should be recorded. Speed regulation can then be calculated by EQ. 8.

$$Speed\ regulation\ [\%] = \left[\frac{\omega_{no\ load} - \omega_{full\ load}}{\omega_{full\ load}}\right] * 100\% \qquad \text{EQ. 8}$$

Where ω is the rotational speed of the machine.

5.5. Efficiency

Efficiency characterization shall be determined at six load points as defined in Section 4.2. At each load point the following values shall be recorded:

1. Voltage input to power supply
2. Voltage input to armature circuit
3. Current input to armature circuit
4. AC component of armature circuit current
5. Power input to armature current
6. AC component of power input to armature circuit
7. Voltage input to shunt-field circuit
8. Current input to shunt-field circuit
9. Power input to shunt-field circuit
10. Speed
11. Torque
12. Armature temperature or resistance
13. Field-coil temperature or resistance
14. Ambient temperature

Machine loading can be accomplished via a brake, dynamometer, or through the Pump-back method.

5.5.1. Machine loading

Machine loading can be accomplished in a number of different ways. The first method is to use a brake and pulley to provide loading to the motor. The motor

can also be loaded using a dynamometer and torque meter. In this case, the mechanical power can be calculated from EQ. 9:

$$P_{mech} = \tau * \omega \qquad \text{EQ. 9}$$

Where τ is the measured torque in Newton-meters (Nm) and ω is the rotational speed in radians per second (rad/s).

If a dynamometer is used, it must be rated to less than or equal to three times the power rating of the machine being tested, and it must be sensitive to a torque that is at least 0.1% of the rated torque of the machine under test.

A third option is to use the Pump-back method, which requires two duplicate machines. The two machines can be coupled together and electrically connected as shown in Figure 5.

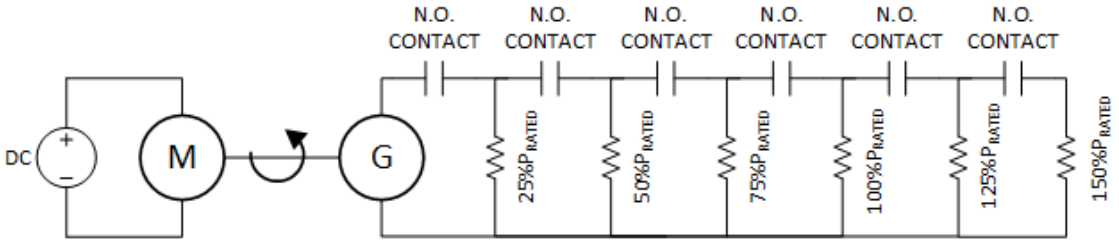

Figure 5. Pump-back test system diagram.

In this configuration, one machine is operated as a generator while the other acts as a motor. The main power produced by the generator is pumped back into the system via the motor, and the DC power supply only supplies the system losses. An optional booster generator can be used to stabilize the system voltages.
In the diagram in Figure 5, six power resistors are shown to represent the six load steps at which measurements will be taken. The normally open (N.O.) contacts can be manually or remotely operated during testing.

5.5.2. Segregated loss method

For large machines where direct calculation of machine efficiency may not be possible, efficiency can be determined by measuring each source of loss individually. These sources of loss include:

- Armature I^2R loss
- Series connected winding I^2R
- Brush contact
- Stray load
- Shunt field I^2R
- Rheostat
- Exciter
- Rotational core
- Brush friction
- Friction and windage
- Ventilating

The methods for testing and measuring each loss source is beyond the scope of this document, and can be found in IEEE-113.

5.6. Torque-current characterization curve

The torque-current characterization is the relationship between the field current drawn by a DC motor at a particular mechanical load (torque). The machine can be loaded in any of the methods described in Section 5.5.1. Data points should be gathered at the six load points used to evaluate machine efficiency. If it is anticipated that this motor might run on DC power source with a variable voltage output, such as a solar photovoltaic array, these curves should be generated for each voltage value that will be used for pump testing (see 7.2 for a description of how to determine these voltages).

6. AC Induction Motor Tests

This section describes the tests used to characterize an AC induction motor for pumps. A common equivalent circuit model for an induction motor is shown below in Figure 6.

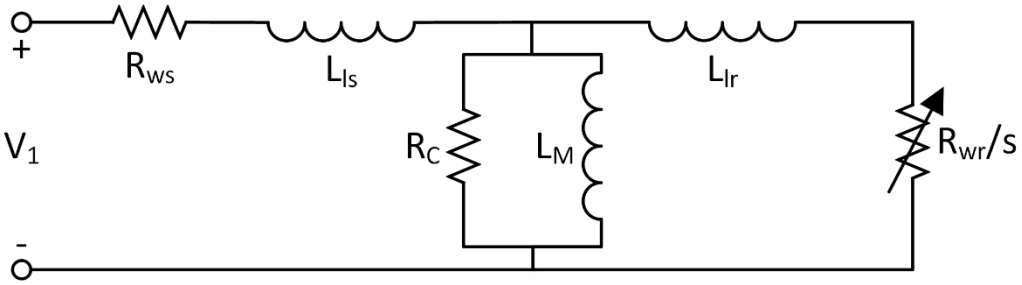

Figure 6. Equivalent circuit for an induction motor (single-cage rotor model).

The equivalent circuit shown in Figure 6 is a single-cage rotor model, which is sufficient for predicting the motor characteristics in the normal operational range. If low speed and/or motor starting characteristics are of particular interest, a double-cage model should be used (see [8]).

The key parameters of this model are:

- Stator winding resistance (R_{ws}) – the electrical resistance of the stator winding. This value contributes to load losses in the motor that increase with the square of the operating current (I^2R losses). This is found in 4.1.
- Stator and rotor winding leakage inductance (L_{ls} and L_{lr}) – this is a self-reactance in the stator and rotor windings that contributes to voltage drop, and hence loss, in the motor windings. These are found in 6.1.
- Core loss resistance (R_C) – some real power is lost in the motor core, which can be represented by a shunt core loss resistor. Core losses tend to be insensitive to motor loading, and can be assumed to be essentially constant regardless of motor load. This is found in 6.1.1.
- Magnetizing inductance (L_M) - a certain amount of reactive current is required to maintain the motor excitation, which can be represented as an additional shunt inductor. This is found in 6.1.1.

- Slip (s) – this is the difference between synchronous speed and measured rotational speed of the motor. It is typically as a per unit value relative to synchronous speed, as shown in EQ. 10.

$$s = \frac{n_{synchronous} - n_{measured}}{n_{synchronous}} \quad \text{EQ. 10}$$

- Rotor winding resistance (R_{wr}) - the electrical resistance of the rotor winding, which is inversely proportional to slip. This value contributes to load losses in the motor that increase with the square of the operating current (I^2R losses). This is found in 6.1.

6.1. Locked-rotor tests

Running the motor with the rotor locked allows winding resistance and reactance values to be determined. The rotor should be locked to prevent rotation, using any available means, such as a brake, dynamometer, or torque table. During locked rotor, the magnetizing branch can be neglected, and slip is one per unit (s=1pu), such that the equivalent circuit can be drawn as shown in Figure 7.

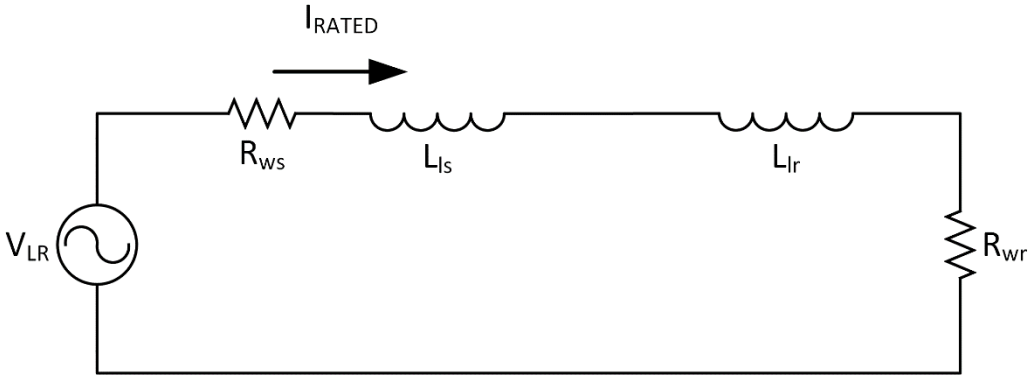

Figure 7. Induction motor locked-rotor equivalent circuit.

A variable AC voltage source with rated frequency is required. The applied voltage should start at zero, and should be slowly increased until rated current is measured. The voltage at which rated current is achieved should be noted and recorded as the locked-rotor voltage (V_{LR}). The equivalent impedance (Z_{LR}) can then be determined from EQ. 11.

$$Z_{LR} = \frac{V_{LR}}{I_{RATED}} \quad \text{EQ. 11}$$

Using this, along with the stator winding resistance found in 4.1, the rotor winding resistance can be calculated using the real part of Z_{LR} as shown in EQ. 12.

$$R_{wr} = Re\{Z_{LR}\} - R_{ws} \quad \text{EQ. 12}$$

Assuming L_{ls} is equal to L_{lr}, these can be found by from the imaginary part of Z_{LR} using EQ. 13.

$$L_{ls} = L_{lr} = \frac{1}{2\omega} Im\{Z_{LR}\}$$ EQ. 13

6.1.1. Locked rotor current and torque

The locked rotor current [also referred to as Locked Rotor Amps (LRA)] should be determined at rated frequency and within ±5% of rated voltage. Note that this test is potentially destructive, so all readings must be made as quickly as possible. All readings must be taken within 5s of applying voltage.

The locked rotor torque will vary as a function of angular position of the rotor with respect to the stator. For this reason, determining the locked rotor torque requires making several measurements, with the rotor adjusted approximately 1/8 turn between each reading. The results should then be plotted as a torque versus angular position plot. The locked rotor torque is defined as the minimum torque developed at rest in any angular position of the rotor.

6.2. No-load test

Running the unloaded motor allows the no-load losses to be determined. No load losses are the sum of stator resistive loss, rotor resistive loss, core loss, and friction and windage losses. No load testing can also be used to find R_C and L_M parameters. There are two different ways to conduct no-load testing: the separately driven method uses a separate DC machine to rotate the motor under test at rated speed, while the self-driven runs the motor runs the motor unloaded at rated frequency and voltage. Core loss is sensitive to frequency, so frequency must be maintained within ±0.5% of rated during this test.

6.2.1. Separately driven

The most accurate method for determining no-load losses is to use a separate DC machine to drive the induction motor to synchronous speed, such that slip equals zero. At zero slip ($s=0$), the rotor winding resistance R_{wr}/s term will be infinite, meaning the rotor branch can be treated as an open circuit. An AC voltage source is used to supply rated voltage and frequency. The no-load impedance (Z_{NL}) can then be calculated by from the measured no-load current (I_{NL}) as shown in EQ. 14.

$$Z_{NL} = \frac{V_{RATED}}{I_{NL}}$$ EQ. 14

From here, the core resistance and magnetizing inductance can be found from the real and imaginary components, respectively, of the no-load resistance, as shown in EQ. 15 and EQ. 16.

$$R_C = Re\{Z_{NL}\} - R_{ws}$$ EQ. 15

$$L_M = \frac{1}{\omega} Im\{Z_{NL}\} - L_{ls}$$ EQ. 16

Where R_{ws} is the stator winding resistance, as found in 4.1 and L_{ls} is the stator leakage reactance as found in 6.1.

6.2.2. Self-driven

If a separate DC motor that is sufficient to drive the induction motor to synchronous speed is unavailable, no-load losses can be approximated by the power consumed by the unloaded motor when driven at rated voltage and frequency. Note that because slip is non-zero during this test, rotor resistance and leakage reactance will affect the results, such that the results, notably the core resistance, will be less accurate than the separately driven method.

The measured no-load current (I_{NL}) can be used to find R_C and L_M using the same equations that were used for the separately driven method (EQ. 14, EQ. 15 and EQ. 16).

6.3. Efficiency

Induction motor efficiency shall be determined in accordance with the requirements in 4.3. At each of the six points the following parameters shall be recorded.

1. Electrical input power (real and reactive)
2. Input voltage
3. Input current
4. Input frequency
5. Slip
6. Output torque
7. Ambient temperature
8. Stator winding temperature and/or stator winding resistance

For item 8 the winding resistance shall be corrected to a standard temperature of 25ºC.

6.3.1. Machine loading

Machine loading can be accomplished in a number of different ways. The first method is to use a brake and pulley to provide loading to the motor. The motor can also be loaded using a dynamometer and torque meter. In this case, the mechanical power can be calculated from EQ. 17.

$$P_{mech} = \tau * \omega \quad \text{EQ. 17}$$

Where τ is the measured torque in Newton-meters (Nm) and ω is the rotational speed in radians per second (rad/s).

If a dynamometer is used, it must be rated to less than or equal to three times the power rating of the machine being tested, and it must be sensitive to a torque that is at least 0.1% of the rated torque of the machine under test.

If a suitable source of mechanical load is not available, another method for loading the motor using the motor-generator slip method can be used. This method requires two identical machines. The machines are coupled together as shown in Figure 8.

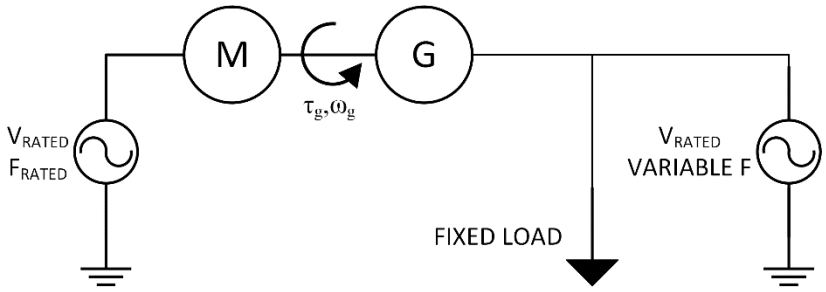

Figure 8. Diagram for motor-generator slip test.

An AC power source at rated frequency and voltage should drive one machine acting as the motor. This is coupled an identical machine that will act like a generator. Torque and speed should be calculated at the point where the machine shafts are coupled together for determined mechanical power according to EQ. 17.

The stator of the machine acting as a generator should be connected to a variable frequency AC source, such as a Variable Frequency Drive (VFD), operating at rated voltage, which will supply the necessary excitation current. A fixed load will be connected on parallel with both the generator machine and the variable frequency AC source. By adjusting the frequency of the variable frequency AC supply, the relative slip between the generator and the AC source can be controlled. The power output of the generator can thus be controlled using the slip.

The advantage to this method is that high power resistive loads and VFDs are readily available and can generally be procured for a much lower cost than a dynamometer. The other advantage is that dynamometers must be rated within 1.5-3 times the motor under test; therefore testing multiple motor sizes may require multiple dynamometers. This method, in contrast, can be easily adapted to different motor sizes. A torque meter sensitive to a change in torque of ≤ 0.1% of the rated motor torque and tachometer or other speed measurement instrument meeting the accuracy requirements in 2.10 are required.

Care should be taken to avoid reverse power flow into the variable frequency AC source if it is not rated for reverse power flow.

6.4. Power Factor

Power Factor (PF) is the ratio of real power to total apparent power.

$$PF = \frac{P}{VI} = \frac{P}{\sqrt{P^2 + Q^2}} \qquad \text{EQ. 18}$$

PF should be recorded at no load, and at the six load test points used for efficiency measurements. These points should be used to generate a PF versus loading curve.

6.5. Speed-torque and Speed-current Characteristic

The speed-torque characteristic of a motor refers to the torque delivered to a load as a function of motor speed. When plotted as a curve, key motor parameters can be identified. A representative characteristic speed-torque curve is shown in Figure 9.

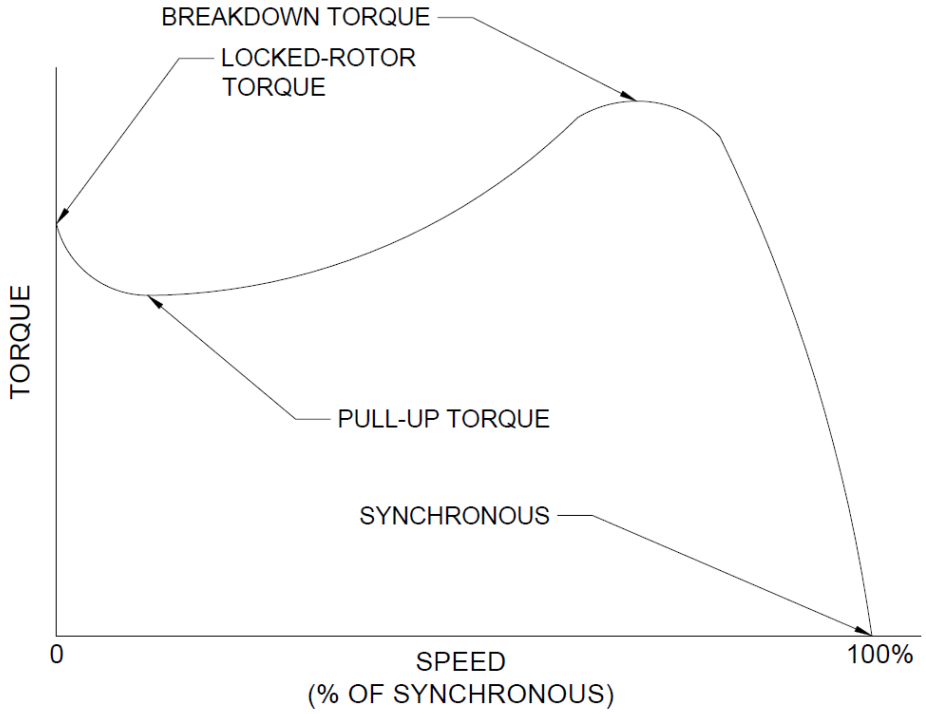

Figure 9. Representative speed vs. torque characteristic curve for a single-phase induction motor.

The key parameters of the curve include:

- Locked rotor torque – the minimum torque produced by a motor at zero speed (see 6.1.1)
- Pull-up torque – the local minimum of the curve between the locked-rotor torque and breakdown torque
- Breakdown torque – the maximum torque delivered by the motor as it accelerates from rest to synchronous speed (note that this is typically much greater than rated torque)
- Synchronous – at synchronous speed, slip and torque are both zero. In practice, the motor will always be slightly below synchronous speed, unless it is separately driven by an external source.

Similar curves can be derived for the speed-current relationship. These are often plotted together, with a common speed scale on the x-axis.

Four methods of obtaining the speed-torque and speed-torque characteristics are outlined in IEEE-114. In all methods, the motor should be driven at rated voltage and frequency.

6.5.1. Measured output

The motor is loaded via a dynamometer or any other method as defined in 6.3.1. For maximum accuracy, the friction and windage losses of the load must be known and the results must be compensated to account for them.

At least ten, equally spaced points shall be measured at speeds ranging from roughly 1/3 of the synchronous speed up to the maximum speed of the motor. At each point the input voltage and current, and output torque shall be recorded. Data shall be recorded while the motor is at steady state, such that acceleration or deceleration effects do not influence the results. The y-intercept of the curve should be the locked-rotor torque found in 6.1.1.

The corrected torque, when accounting for the load friction and windage losses, can be calculated by EQ. 19.

$$\tau_c = \frac{k(P_o - P_l)}{n} \qquad \text{EQ. 19}$$

Where:

τ_c = Torque, corrected for load losses (Nm)
k = Constant based on units of measure
P_o = Measured output power (W)
P_l = Friction and windage losses of the load (W)
n = Motor speed (rpm)

6.5.2. Acceleration

This method requires the rotational moment of inertia to be known for all rotating parts, either through calculation or via measurement. The motor is accelerated from rest to its maximum speed approaching synchronous. As the motor accelerates, simultaneous readings of input current and motor speed must be taken at regular, fixed time intervals. Torque can be calculated at each recorded speed value using EQ. 20.

$$\tau = \frac{aJ}{k} \qquad \text{EQ. 20}$$

Where:

τ = Torque (Nm)
k = $109.7 \cdot 10^{-4}$ for the units shown
a = Acceleration (rpm/s)
J = Rotational moment of inertia (kg·m^2)

6.5.3. Input

This method calculates torque by subtracting losses from the measured input power. At least ten, equally spaced points shall be measured at speeds ranging from roughly 1/3 of the synchronous speed up to the maximum speed of the motor. At each point the input voltage, current, and power shall be recorded and

plotted against speed. The y-intercept of the curve should be the locked-rotor torque found in 6.1.1.

$$\tau = \frac{k}{n}(P_i - P_l) - \tau_{fw} \qquad \text{EQ. 21}$$

Where:

τ = Torque (Nm)
k = Constant based on units of measure
n = Motor speed (rpm/s)
P_i = Input power (W)
P_l = Stator resistive loss (I^2R_{ws}, W)
τ_{fw} = Friction and windage torque at speed n (Nm)

The friction and windage torque (τ_{fw}) is defined as the torque required to rotate the de-energized motor to the specified speed n.

6.5.4. Direct measurement

The direct measurement method uses continuous data acquisition to record input current and output torque over the full range of motor speeds. Data should be recorded and plotted at chosen speeds to determine the key torque characteristics, such as the pull-up and breakdown torque. The motor should be given sufficient time to settle at each speed point such that steady state values can be obtained.

7. Pump Performance Testing

Pump performance testing should be conducted using the setup configuration shown in the diagram in Figure 1. Measurements should be taken once the system has reached steady state, equilibrium conditions at each test point. Fluctuations for each process variable should not exceed the maximum acceptable fluctuations listed in Table 3.

Table 3. Acceptable steady state test value fluctuations.

Process variable	**Acceptable fluctuation of test reading**
Rate of flow	±3%
Differential pressure	±2%
Discharge pressure	±2%
Suction pressure	±2%
Input power	±2%
Pump Speed	±1%

7.1. Test methodology

Testing shall be completed with clear water, with liquid temperature between 10-30^{o}C. Clear water is defined as water with a maximum viscosity of $1.5 \cdot 10^{-6}$ m^2/s and a maximum density of 1,000 kg/m^3. The pump should be operated at or near the known (or expected) Best Efficiency Point (BEP) for at least 20 minutes prior to evaluation to allow for break-in of the driver and other mechanical components.

The tests should follow a modified version of the test methodology described in standard IEC 62253: Photovoltaic pumping systems – Design qualification and performance measurements. There are two main pump characteristics testing: a comparison of head vs. flow over numerous constant motor speeds (H v Q) and a comparison of power vs. flow over numerous constant total differential head values (P v Q).

Regardless of the power supply type, a set of exploratory tests shall be conducted to define the range for total differential head (TDH) and rotational motor speed at standard and rated testing conditions. The TDH and motor speed intervals for the H v Q and P v Q tests are determined by at least 7 equally spaced values between and including the values that are recorded when the test configuration is fully open and just before the 'dead head' point of the pump, which is when the pump can no longer overcome the pressure applied to the outlet.

When using a PV simulator or actual PV panels, an additional set of exploratory tests shall be conducted to define the lower limit of irradiance for each TDH interval. The lower limit of irradiance at each TDH interval is defined as the solar intensity just before the pump can no longer operate. As the TDH approaches the upper limit, the corresponding lower limit of irradiance is expected to increase. For example, near TDH_{max} the lower limit of irradiance may be 500 W/m^2 but when the system is at full open, the lower limit of irradiance may be 50 W/m^2.

Refer to IEC 62253 for the methods to complete and an example of a H v Q characterization. Using a PV simulator or PV panels to complete this characterization for a pump with a DC motor is difficult given that at a fixed irradiance, voltage (thus motor speed) will fluctuate as TDH changes. This is due to a PV source having limited current along a fixed voltage curve. A H v Q characterization may be better completed by a power supply without current limitations.

Refer to IEC 62253 for the methods to complete and an example of a P v Q characterization. When using a PV simulator, tests shall be conducted at each of the TDH intervals for at least 7 equally spaced irradiance values between the respective lower limit for each TDH and 1100 W/m2. The data from the P v Q test can be used to create a min, max, or mean efficiency vs head, flow, or power curve.

At each test point the following variables should be recorded:

- Suction pressure
- Discharge pressure
- Flow rate
- Input voltage
- Input current
- Motor torque
- Motor speed

Each test point should be maintained for a minimum of 150 seconds before changing conditions. To eliminate transitions between conditions, the first and last 15 seconds of each test point should be excluded from data analysis.

7.2. Variable voltage DC systems

If the DC voltage source to the pump is variable, such as a solar photovoltaic array, and a fixed power supply is used, then a range of representative DC voltages should be applied. At least seven equally spaced DC voltage values should be chosen, with the lower boundary being the voltage that was found to correspond to a pump speed of 50% of the rated, no-load speed, as determined by the voltage vs. speed curve defined by Section 5.3. The upper voltage should be either the rated voltage of the pump motor, or the maximum anticipated input voltage from the DC source, whichever is greater. Due to the inverse relationship between photovoltaic voltage and temperature, the maximum power voltage (V_{mp}) should be calculated for the minimum anticipated ambient operating temperature (T_{min}) using EQ. 22:

$$V_{mp@T_{min}} = V_{mp@STC}[1 + \beta_V(25^oC - T_{min})] \quad \text{EQ. 22}$$

Where:

$V_{mp@Tmin}$ = Maximum power voltage at minimum temperature (V)

$V_{mp@STC}$ = Maximum power at standard test conditions (STC) [1,000 W/m^2 and 25^{o}C], according to the manufacturer's datasheet (V)

β_v = Temperature coefficient of the module voltage according to the manufacturer's datasheet (V/^{o}C)

T_{min} = Minimum operating temperature as determined by NEC 690.7 (^{o}C)

At least seven voltages, approximately equally spaced, between the maximum and minimum voltages should be applied. These voltage values will linearly correlate with motor rotational speed in DC motors.

Note that if a direct measurement of motor torque cannot be obtained while the motor is connected to the pump, the torque can be approximated by measuring the input current and/or motor speed and using the torque-current curve created in Section 5.6 (for DC motors) or the speed-torque and speed-current characterization curves created in Section 6.5.

7.3. Efficiency

From the data collected in Section 7.1, different efficiency metrics can be obtained. These include overall efficiency and pump efficiency. For reciprocating pumps, an additional metric, volumetric efficiency, can be determined.

7.3.1. Overall efficiency

The overall pump efficiency, sometimes referred to as "wire to water efficiency," is the ratio of pump output power to the total electrical input power. It requires calculating the pump output power, which is the power imparted to the liquid by the pump, and is also referred to as water horsepower or liquid horsepower. Pump output power (P_w) is calculated by Equation 23:

$$P_w = \frac{Q p_\Delta}{3600} \qquad \text{EQ. 23}$$

Where:

P_w = Pump output power (W)
Q = Flow rate (m^3/hr)
p_Δ = Differential pressure (kPa)

Using this, overall efficiency can then be calculated from EQ. 24.

$$\eta_o = \frac{P_w}{P_{mot}} * 100\% \qquad \text{EQ. 24}$$

Where:

P_w = Pump output power (W)
P_{mot} = Power delivered to pump motor (W)

7.3.2. Pump efficiency

Unlike overall efficiency, pump efficiency is looking at the pump in isolation and neglects losses in the motor. Pump efficiency (η_p) is defined by the ratio of pump output power (P_w) to pump input power (P_p) as shown in EQ. 25:

$$\eta_p = \frac{P_w}{P_p} * 100\% \qquad \text{EQ. 25}$$

Where pump input power (P_p) is the mechanical input power delivered to the shaft of the pump, and can be defined by EQ. 26:

$$P_p = \omega * \tau \qquad \text{EQ. 26}$$

Where:

τ = Torque (Nm)
ω = Rotational speed (rad/s)

7.3.3. Volumetric efficiency

Volumetric efficiency is the ratio of the flow rate of a pump to its displacement. For reciprocating pumps, the displacement is the swept area by all pistons or plungers per unit of time, and is calculated by EQ. 27:

$$D = \frac{A * L * n * M}{16.7 * 10^6} \quad \text{EQ. 27}$$

Where:

A = Swept area of the piston or plunger (mm^2)
L = Stroke length of the piston or plunger rod (mm)
n = Pump speed (rpm)
M = Number of pistons

For double-acting piston type pumps the area of the piston rod (a) should be deducted. In this case EQ. 28 should be used.

$$D = \frac{(2A - a) * L * n * M}{16.7 * 10^6} \quad \text{EQ. 28}$$

Once displacement is known, volumetric efficiency (η_v) can be calculated from EQ. 29:

$$\eta_v = \frac{Q}{D} \quad \text{EQ. 29}$$

8. References

[1] *American National Standard for Reciprocating Pump Tests*, ANSI/HI Standard 6.6, 2015.
[2] *Hydraulic Institute Standard for Methods for Rotodynamic Pump Efficiency Testing*, HI 40.6, 2016.
[3] *IEEE Guide: Test Procedures for Direct-Current Machines*, IEEE Standard 113, 1985.
[4] *IEEE Standard Test Procedure for Single-Phase Induction Motors*, IEEE Standard 114, 2010.
[5] *IEEE Standard Test Code for Resistance Measurement*, IEEE Standard 118, 1978.
[6] International Electrotechnical Commission, and Technical Committee 82, Photovoltaic pumping systems--design qualification and performance measurements. Geneva: International Electrotechnical Commission, 2011.
[7] T. Decker. *Technical Report: Income Generating Appliances*, Factor[e] Ventures, 2017.
[8] M.H. Haque. "Determination of NEMA Design Induction Motor Parameters From Manufacturer Data," *IEEE Trans. on Energy Conversion*, vol. 23, no. 4, pp. 997-1004, Dec. 2008.
[9] S. Jurkovic. "Induction Motor Parameters Extraction," Available online: http://web.mit.edu/kirtley/binlustuff/literature/electric%20machine/motor-parameters.pdf. Accessed May 5, 2018.
[10] D.L. King, J.A. Kratochvil, and W.E. Boyson. "Temperature Coefficients for PV Modules and Arrays: Measurement Methods, Difficulties, and Results," presented at the 26th IEEE Photovoltaic Specialists Conf., Anaheim, USA, 1997.

Appendix A: List of tests

The test procedures discussed in this document are very comprehensive, and some may yield more meaningful results than others for the purposes of characterization and performance evaluation. To assist users of this test method, a list of all test procedures described has been provided in Table A 1 below. A qualitative *level of importance* (1-10) and *degree of difficulty* (1-10) has been assigned, as well as a relative equipment cost, for each test. These are subjective assessments only.

Table A 1. List of test procedures.

Test Name	Section	Level of importance	Degree of difficulty	Relative cost of equipment
Winding resistance measurement	4.1	3	2	Low
Winding inductance measurement	0	2	4	Medium
Magnetic saturation	5.2	2	3	Low
Voltage vs. rotational speed	5.3	10	1	Low
Speed regulation	5.4	4	5	Medium
Motor efficiency	5.5	9	8	High
Speed-torque characterization	5.6	9	10	High
Winding temperature rise	4.2	2	5	Low
H v Q	7.1	8	10	High
P v Q	7.1	10	9	High
Overall efficiency	7.3.1	10	8	Medium
Pump efficiency	7.3.2	8	9	High
Volumetric efficiency	7.3.3	5	2	Low

5.6. Solar Water Pump Test Report

Solar Water Pump Test Report

*A study to evaluate the performance of the Futurepump SF2**

Colorado State University
Factor[e] Ventures
430 N College Ave.
Fort Collins, CO 80524
4 January 2019

*The information presented in this report was created in a lab with a simulated photo-voltaic power supply and is subject to further validation

Table of contents

1 Overview 1
2 Description of Solar Irrigation Pump System 1
3 Test and Measurement Equipment Description 1
3.1 PV Simulator 2
3.2 Voltage 2
3.3 Current 2
3.4 Pressure 2
3.5 Flow Meter 3
3.6 Backpressure Regulator 3
3.7 Data Acquisition (DAQ) 3
4 Test Description 3
4.1 PQ Characterization 3
4.2 Flow Rate versus Head 5
4.3 Calculation Methods 5
5 Testing Results 7
5.1 PQ Characterization results 9
5.2 HQ Characterization results 18
6 Discussion and Conclusion 21
7 References 23
Appendix A: SF2 Solar Irrigation Pump Datasheet 24
Appendix B: RAAJ Solar Photovoltaic Module Datasheet 27
Appendix C: Data file description 29

List of figures

Fig. 1. Pump test diagram 2
Fig. 2. The three irradiance profiles used for PQ characterization tests. 5
Fig. 3. Raaj R040P PV current vs. voltage and power vs. voltages curves. 8
Fig. 4. Experimental setup in lab. 8
Fig. 5. Time domain results for PQ test with 50mm pulley gear, H1. 10
Fig. 6. Time domain results for PQ test with 50mm pulley gear, H5. 11
Fig. 7. Time domain results for PQ test with 90mm pulley gear, H1. 12
Fig. 8. Time domain results for PQ test with 90mm pulley gear, H5. 13
Fig. 9. Annotated PV current vs. voltage curve 14
Fig. 10. Flow Rate vs. Power for 50mm pulley gear 16
Fig. 11. Efficiency vs. Power for 50mm pulley gear 16
Fig. 12. Flow Rate vs. Power for 90mm pulley gear. 17
Fig. 13. Efficiency vs. Power for 90mm pulley gear 17
Fig. 14. Average Efficiency vs. Head for both pulleys over the PQ tests 18
Fig. 15. Time domain results for HQ test with 50mm pulley gear. 19
Fig. 16. Time domain results for HQ test with 90mm pulley gear. 20
Fig. 17. Flow rate vs. Head for both small (50mm) and large (90mm) pulley gears at 1000 w/m^2. 21
Fig. 18. Efficiency vs. Head for both small (50mm) and large (90mm) pulley gears at 1000 w/m^2. 21

1 Overview

This report will describe the tests conducted to evaluate and characterize a solar irrigation pump system obtained from Futurepump. This type of solar pumping system is marketed to smallholder farmers for irrigation using shallow water sources. The purpose of this testing was to obtain basic electrical and hydraulic characteristics and provide performance benchmarks.

2 Description of Solar Irrigation Pump System

The Futurepump SF2 is a surface water pump targeted towards smallholder farmers. The system consists of three main parts: the solar photovoltaic (PV) modules, a Permanent Magnet Direct Current (PMDC) motor, and the reciprocating piston pump. The complete manufacturer's datasheet is provided in Appendix A.

The system is supplied with two Raaj R040P 40W, 36 cell, polycrystalline silicon PV modules, with provisions for an optional third module. All modules are combined in series so that the voltage is additive, but the total current is the same for all modules. The specification sheet for the PV module can be found in Appendix B.

The combined solar input provides Direct Current (DC) power directly to an Adroit Systems PMF-060-P permanent magnet DC (PMDC) brush motor. The PMDC motor is rated for 36VDC nominal, up to 60VDC maximum, with a maximum continuous current of 2.5A. One of two pulley gears is used to connect the PMDC motor to the flywheel which drives the pump: a 90mm pulley gear which provides maximum flow at low pumping heads, and a 50mm pulley gear which produces a lower flow rate but can achieve greater pumping heads.

The pulley gear connects the PMDC motor to the flywheel, which in turn drives the positive displacement, reciprocating piston pump. The pump consists of a single 104mm diameter piston with a total displacement volume of 150cm^3 per stroke. The SF2 pump is capable of up to 7m of suction lift, with a maximum total lift not to exceed 15m (when using the 50mm pulley gear). With two PV modules the maximum rated flow rate is 43 liters per minute (LPM) when using the 90mm pulley gear and 29LPM when using the 50mm pulley gear.

The SF2 solar pump system has no active voltage or current regulation, nor does it provide any Maximum Power Point Tracking (MPPT) capability. Instead, the motor was observed to draw current based on its instantaneous loading, and the input voltage varied based on the current vs. voltage relationship of the input PV module (see section 5 for more detail).

3 Test and Measurement Equipment Description

A schematic diagram of the test setup that was used for performance testing and evaluation is shown in Fig. 1.

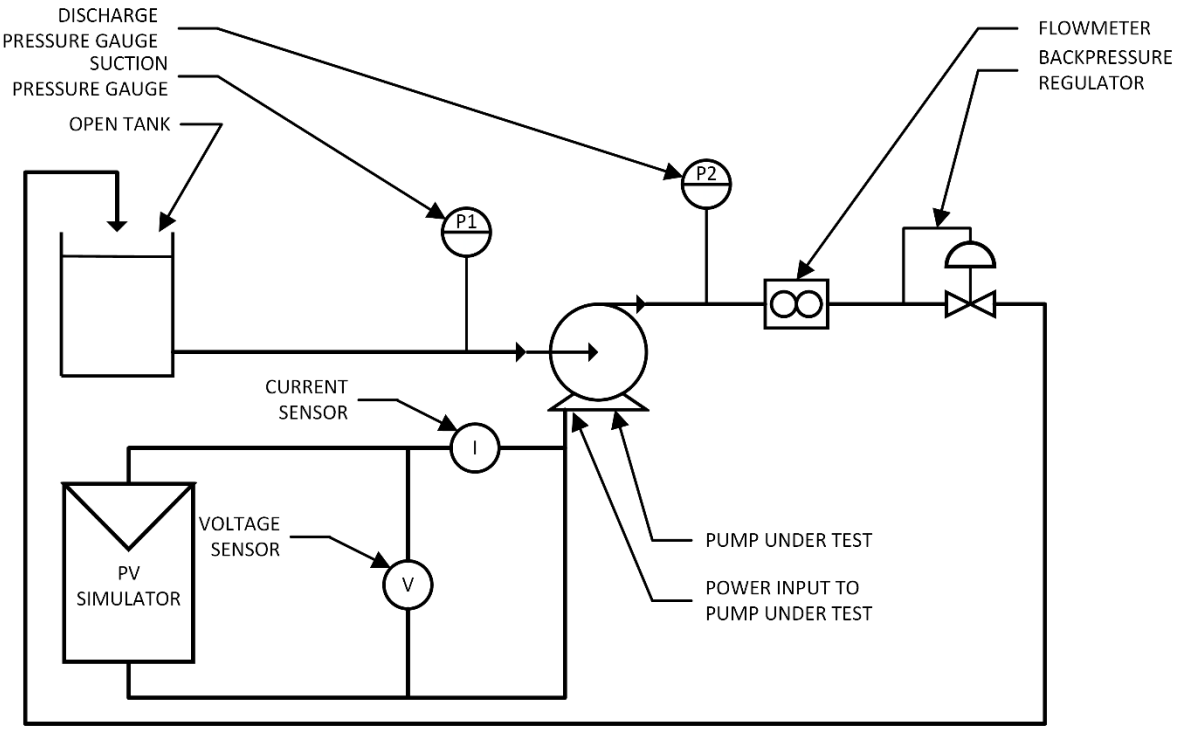

Fig. 1. Pump test diagram

The following sections describe the various pieces of test and measurement hardware that were used.

3.1 PV Simulator

In order to provide a more controlled experimental setup, two ETS60X14C Elgar ETS TerraSAS PV simulators were used in lieu of the Raaj PV modules. These PV simulators were each programmed to have the same voltage and current profile as the Raaj R040P PV modules that are supplied as part of the SF2 solar pumping system. The two outputs were combined in series and connected to the motor input power receptacle.

3.2 Voltage

A CR Magnetics CR5311-50 voltage transducer was used for DC voltage measurements up to 50VDC. Rated accuracy of this device was ±1.0%.

3.3 Current

Current measurements were recorded using a CR Magnetics CR5211-10 hall effect current transducer rated for up to 10ADC. Rated accuracy of this device was ±1.0%.

3.4 Pressure

Two pressure transducers were used, one on the suction side of the pump and one on the discharge side. The suction side pressure transducer was an Omega PX309-015CG5V with a measurement range of -15 to +15 pounds per square inch (psi). On the discharge side, an Omega PX319-V150G5V was used, which was rated for -15 to 150psi. Both transducers had a rated accuracy of ±0.25%.

3.5 Flow Meter

Liquid flow was measured using an Omega FMG-981-P insertion electromagnetic flow meter. This device was capable of measuring flow rates of 2.6-185LPM. The calibration accuracy of this device was ±1.0% of full scale. The flow meter had a pulsed output which was calibrated to produce 712 pulses per gallon (188.1 pulses per liter). This corresponded to 5.32 milliliters per pulse. By measuring the period between pulses, the flow rate could be determined.

3.6 Backpressure Regulator

Discharge head was controlled through the use of an Equilibar QPV1MANEEZ-P100PSGAXL electronic pressure regulator. This device was able to accept a 0-10V analog input to control the pressure within a GSD8PNT5-NPCP50T40G10VV precision backpressure regulator. The QPV series had a rated accuracy of ±0.25% of full scale, with resolution of ±0.01%.

3.7 Data Acquisition (DAQ)

DAQ for real time measurements of all system parameters were recorded using a National Instruments LabView application. The analog inputs were read using an NI 9201 C series analog input module at a fixed sample frequency of 1.6 kilo-samples per second (kS/s). Digital inputs were sampled using an NI 9381 multifunction I/O C series module at a rate of 100 kHz. The high frequency sampling was handled using the on-board FPGA that is integrated into the NI cRIO 9064 chassis. A real-time program aggregated the data in 0.5 second increments, computed the average and RMS for all signals, and communicated these via a network stream over TCP/IP. Finally, a host program was used to collect the data from the network stream and save to an NI TDMS file.

4 Test Description

Two different sets of tests were conducted to characterize the pump performance: flow rate versus input power (PQ) and flow rate versus head (HQ) tests.

4.1 PQ Characterization

A set of PQ curves were created with nine different values of backpressure. First, the maximum pumping head was empirically determined by running the pump with the simulated solar input at Standard Test Conditions (STC), defined as an irradiance of 1,000W/m^2 and temperature of 25^{o}C. The setpoint of the backpressure regulator was gradually increased until the flow rate fell below the minimum detectable flow of the flow meter (2.6LPM). This was repeated for both the small (50mm) and large (90mm) pulley gears, and the pressure at which flow fell below the detectable rate was noted (H_{MAX}).

The first seven backpressure values (H1-H7) were defined as 90%, 80%, 70%, 60%, 50%, 40%, and 30% of H_{MAX}, as defined by IEC 62253 [1]. Two additional points were added, one at 15% of H_{MAX}, and a final one with the backpressure regulator full open (setpoint of zero). All setpoints for both the small and large pulley are listed in both PSI and meters of head (m) in Table I.

Table I. Backpressure setpoints for PQ characterization tests.

	50mm Pulley		90mm Pulley	
	PSI	m	PSI	m
H_{MAX}	25.5	17.93	11.1	7.81
H1	23.0	16.14	10.0	7.03
H2	20.4	14.35	8.9	6.24
H3	17.9	12.55	7.8	5.46
H4	15.3	10.76	6.7	4.68
H5	12.8	8.97	5.6	3.90
H6	10.2	7.17	4.4	3.12
H7	7.7	5.38	3.3	2.34
H8	3.8	2.69	1.7	1.17
H9	0.0	0.00	0.0	0.00

Note that open loop pressure control was used; this means that the actual measured system pressure was not used to adjust the setpoint. Consequently, actual system pressure often deviated from the setpoint, and significant steady state variation was observed under certain operating scenarios.

For each value of backpressure, the available input power to the solar pumping system was reduced by decreasing the available irradiance for the PV simulator. The irradiance input was started at 110% of full sun (1,100W/m^2), corresponding to ideal solar conditions, and gradually decreased until zero flow was recorded.

For higher values of head (H1 through H6), zero flow was achieved around or before irradiance dropped to half sun (500W/m^2). For the large pulley, the irradiance had to be reduced to around 300W/m^2 to achieve zero flow, and when using the small pulley at the lowest values of head flow was still observed until irradiance was reduced to around 150W/m^2. Three profiles were therefore created: one for moderate to high head which varied the irradiance from 1,100W/m^2 to 500W/m^2 in 12 equal steps of 50W/m^2, one for low head which varied from 1,100W/m^2 to 300W/m^2 in 12 equal steps of 66.7W/m^2, and one for very low head which varied from 1,100W/m^2 to 140W/m^2 in 80W/m^2 steps. Each step was held for 150s. These three profiles are plotted in Fig. 2. Note that simulated temperature was held constant at 25^{o}C for all tests.

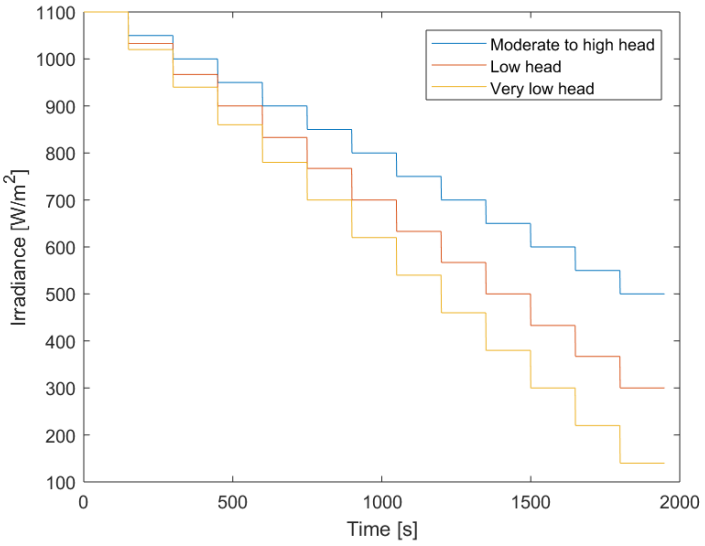

Fig. 2. The three irradiance profiles used for PQ characterization tests.

4.2 Flow Rate versus Head

In the second set of tests, the flow rate versus head characteristics for the solar pumping system were investigated. For these tests, the PV simulator was left at STC (1,000W/m^2, 25^{o}C), and the backpressure was varied from high to low. The starting pressure was selected such that no detectable flow was present, and was stepped down in 12 steps to zero. For the small pulley, the backpressure was varied from 24psi (16.9m) to zero in 2psi (1.4m) increments; for the large pulley the backpressure was varied from 12psi (8.44m) to zero in 1psi (0.7m) increments. Each step was held for 150s.

4.3 Calculation Methods

Bernoulli's equation was used to calculate the static pressure at the outlet side of the pump. The datum was set at the inlet side of the pump.

$$P_{outlet} = P_{g,dis} + \frac{1}{2}\rho_w {V^2}_{g,dis} - \frac{1}{2}\rho_w {V^2}_{outlet} + \rho_w g h_f + \rho_w g z_{g,dis} - \rho_w g z_{outlet} \quad \text{EQ. 1}$$

Where:

P_{outlet} = Static pressure at outlet side of pump (Pa)
$P_{g,dis}$ = Gauge pressure as measured on discharge side of pump (Pa)
ρ_w = Density of water (kg/m^3)
$V_{g,dis}$ = Water velocity at gauge on discharge side of pump (m/s)
V_{outlet} = Water velocity at outlet (m/s)
g = Acceleration due to gravity (9.81m/s^2)
h_f = Frictional losses between outlet side of the pump and pressure gauge
$z_{g,dis}$ = Height of discharge pressure gauge above datum (m)
z_{outlet} = Height of pump outlet above datum (m)

The discharge pressure transducer was located in line with the pump outlet, approximately 18.5cm downstream. Due to the fact that both the discharge pressure gauge and pump outlet were at the same height with respect to the datum, the $\rho g z_{gauge}$ and $\rho g z_{outlet}$ terms canceled each other out. Additionally, because of the proximity between the discharge pressure gauge and the pump outlet, the velocity at both locations was assumed to be identical, thereby canceling the two velocity terms. Finally, because of the short length of the test bench (83cm), the frictional losses were neglected. Hence, the static pressure at the discharge side could be assumed to be equal to the gauge pressure as measured by the pressure transducer ($P_{outlet} = P_{gauge}$).

From this, total discharge pressure with respect to the datum could be calculated as:

$$P_{discharge} = P_{g,dis} + \frac{1}{2}\rho_w V^2{}_{outlet} + \rho_w g z_{outlet} \quad \text{EQ. 2}$$

Similarly, static suction pressure at the inlet side of the pump using EQ. 3.

$$P_{inlet} = P_{g,suc} + \frac{1}{2}\rho_w V^2{}_{reservoir} - \frac{1}{2}\rho_w V^2{}_{inlet} + \rho_w g h_f + \rho_w g z_{reservoir} - \rho_w g z_{inlet} \quad \text{EQ. 3}$$

Where:

P_{inlet} = Static pressure at inlet side of pump (Pa)
$P_{g,suc}$ = Gauge pressure as measured on inlet side of pump (Pa)
$V_{reservoir}$ = Water velocity at surface of reservoir (m/s)
$z_{resevoir}$ = Height of the reservoir water surface above datum (m)
z_{inlet} = Height of pump outlet above datum (m)

In this case, the velocity at the reservoir surface ($V_{reservoir}$) was assumed to be zero. As the pump inlet was defined as the datum, the $\rho g z_{inlet}$ term was also zero. Again, frictional losses were neglected.

From this, the total suction pressure with respect to the datum could be calculated as EQ. 4.

$$P_{suction} = P_{g,suc} + \frac{1}{2}\rho_w V^2{}_{inlet} + \rho_w g z_{reservoir} \quad \text{EQ. 4}$$

The total differential pressure was calculated as the difference between the suction and discharge pressure, converted from Pascals (Pa) to meters (m). EQ. 7.

$$P_{diff} = P_{discharge} - P_{suction} = (P_{g,dis} + \frac{1}{2}\rho_w V^2{}_{outlet} + \rho_w g z_{outlet}) - (P_{g,suc} + \frac{1}{2}\rho_w V^2{}_{inlet} + \rho_w g z_{reservoir}) \quad \text{EQ. 5}$$

Assuming the inlet and outlet velocity are equal, this can be rewritten as:

$$P_{diff} = P_{g,dis} - P_{g,suc} + \rho_w g(z_{outlet} - z_{reservoir})$$ EQ. 6

Converting from Pascals to meters of head EQ. 6 can be rewritten as EQ. 7.

$$H_{diff} = (H_{dis} - H_{suc}) + k\rho_w g(z_{outlet} - z_{reservoir})$$ EQ. 7

Where:

H_{diff} = Total differential head (m)
H_{dis} = Discharge head (m)
H_{suc} = Suction head (m)
k = Constant to convert between pascals and meters of head ($1.02*10^{-4}$)
ρ_w = Density of water at 20°C (998.2kg/m^3)
g = Acceleration due to gravity (9.81m/s^2)
z_{outlet} = Height of pump outlet above datum (0.17m)
$z_{reservoir}$ = Height of reservoir above datum (-0.343m)

Note: temperature measurements of the water were not recorded, so the water density was not corrected for temperature. Instead, the density of water at 20°C was used for all calculations. Future testing should include a thermocouple and use recorded temperature for calculating ρ_w.

Total differential head was used in calculating the total system efficiency for the SF2 solar pump.

$$\eta = \frac{H_{diff} * Q * \rho_w * g}{V * I}$$ EQ. 8

Where:

H_{diff} = Total differential head (m) as calculated in EQ. 7
Q = Flow rate in m^3/s
V = Input voltage to the pump motor (V)
I = Input current to the pump motor (A)

5 Testing Results

Testing results for both the PQ and HQ characterization are provided here. All testing was conducted using two ETS60X14C Elgar ETS TerraSAS PV simulators connected in series. Each was programmed to mimic the current vs. voltage characteristics of a Raaj R040P PV module; the current vs. voltage and power vs. voltage curves as implemented in the PV simulator can be seen in Fig. 3. The tests were conducted with the pump fixed to a test bench circulating tap water from a 208.2 liter (55 gallon) drum through a short section (approximately 83cm) of 2.54cm (1") diameter PVC pipe. The bench, with measurement instruments integrated, is shown in the photograph in Fig. 4.

All results in raw data form are located in a separate excel file, with reference information located in Appendix C.

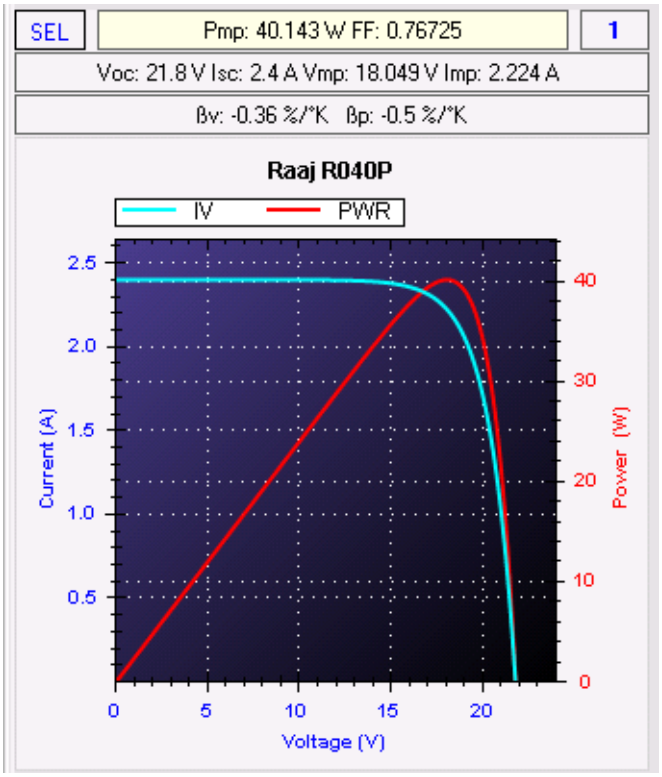

Fig. 3. Raaj R040P PV current vs. voltage and power vs. voltages curves.

Fig. 4. Experimental setup in lab.

5.1 PQ Characterization results

The pump was tested as defined in section 4.1, in which nine values of static backpressure were applied, and the irradiance was reduced until a flow rate of zero was reached. The results were collected using Labview and analyzed using Matlab.

Time domain results for all nine values of head for both the 90mm and 50mm pulley gears has not been included for space considerations. A select subset of time domain results is included in the following figures: results for the small (50mm) pulley gear with the highest backpressure (H1) are plotted in Fig. 5, and for a mid-range value of head (H5) are plotted in Fig. 6. The results for the large (90mm) pulley gear for H1 and H5 are plotted in Fig. 7 and Fig. 8.

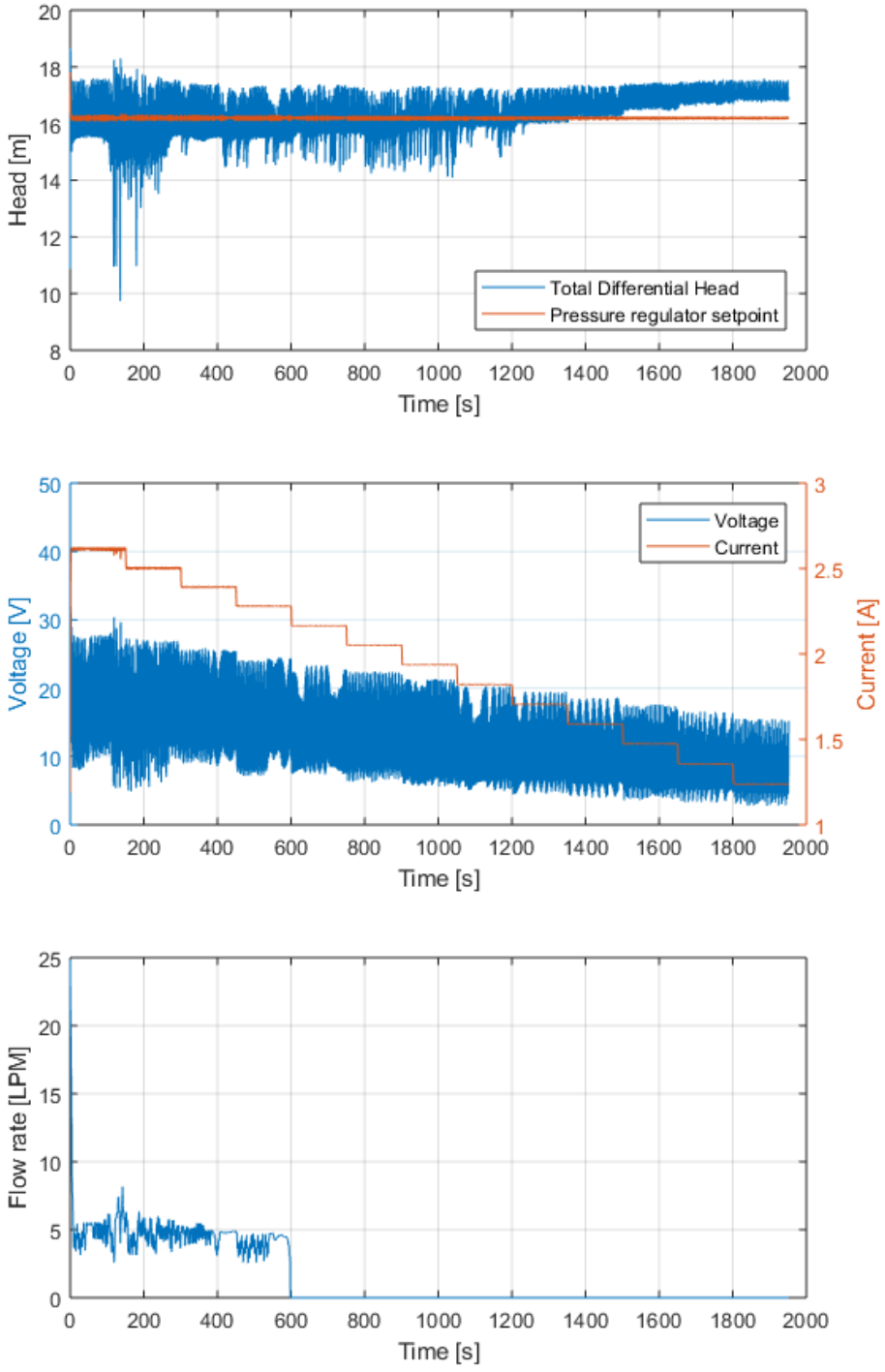

Fig. 5. Time domain results for PQ test with 50mm pulley gear, H1.

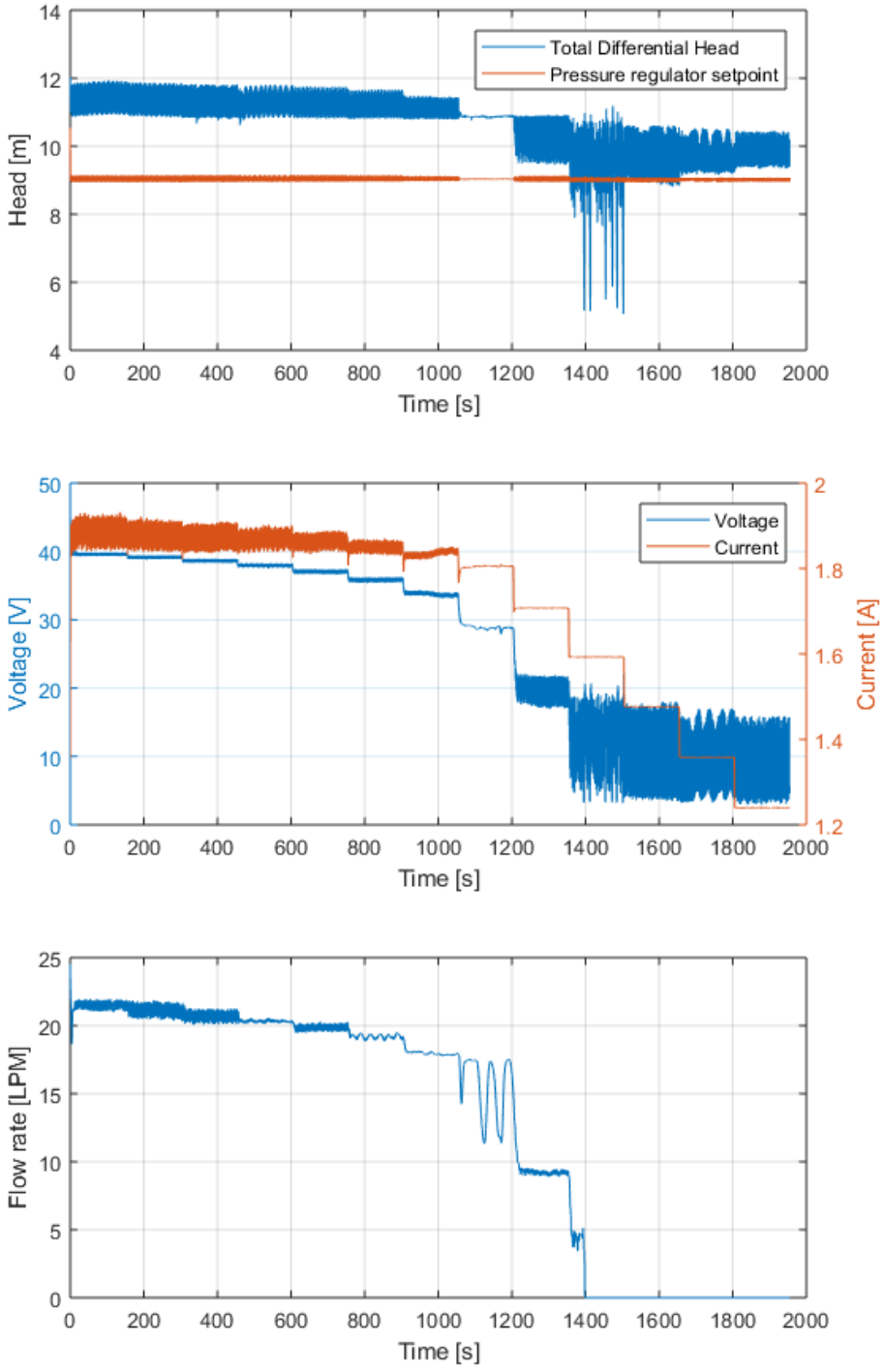

Fig. 6. Time domain results for PQ test with 50mm pulley gear, H5.

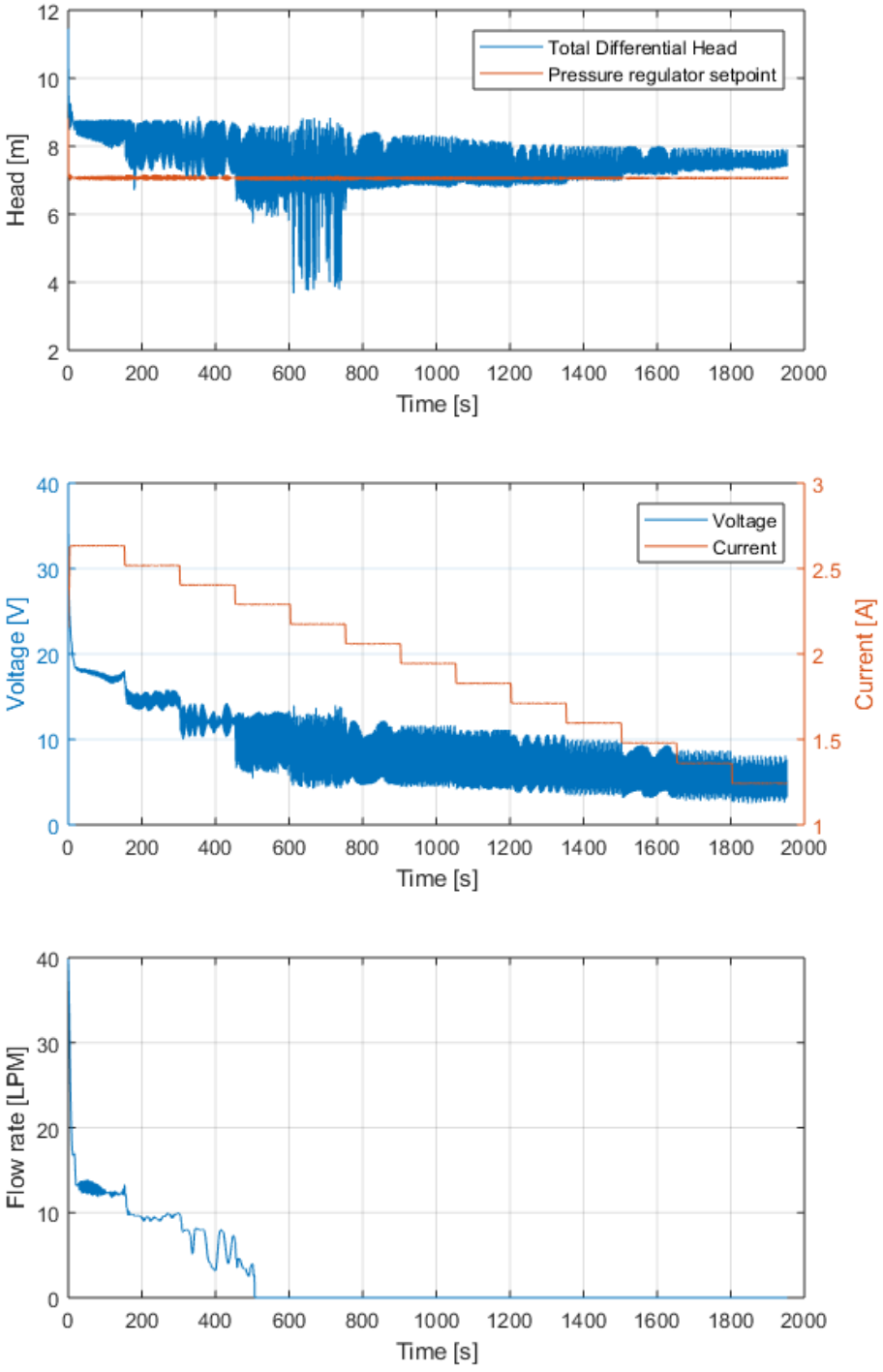

Fig. 7. Time domain results for PQ test with 90mm pulley gear, H1.

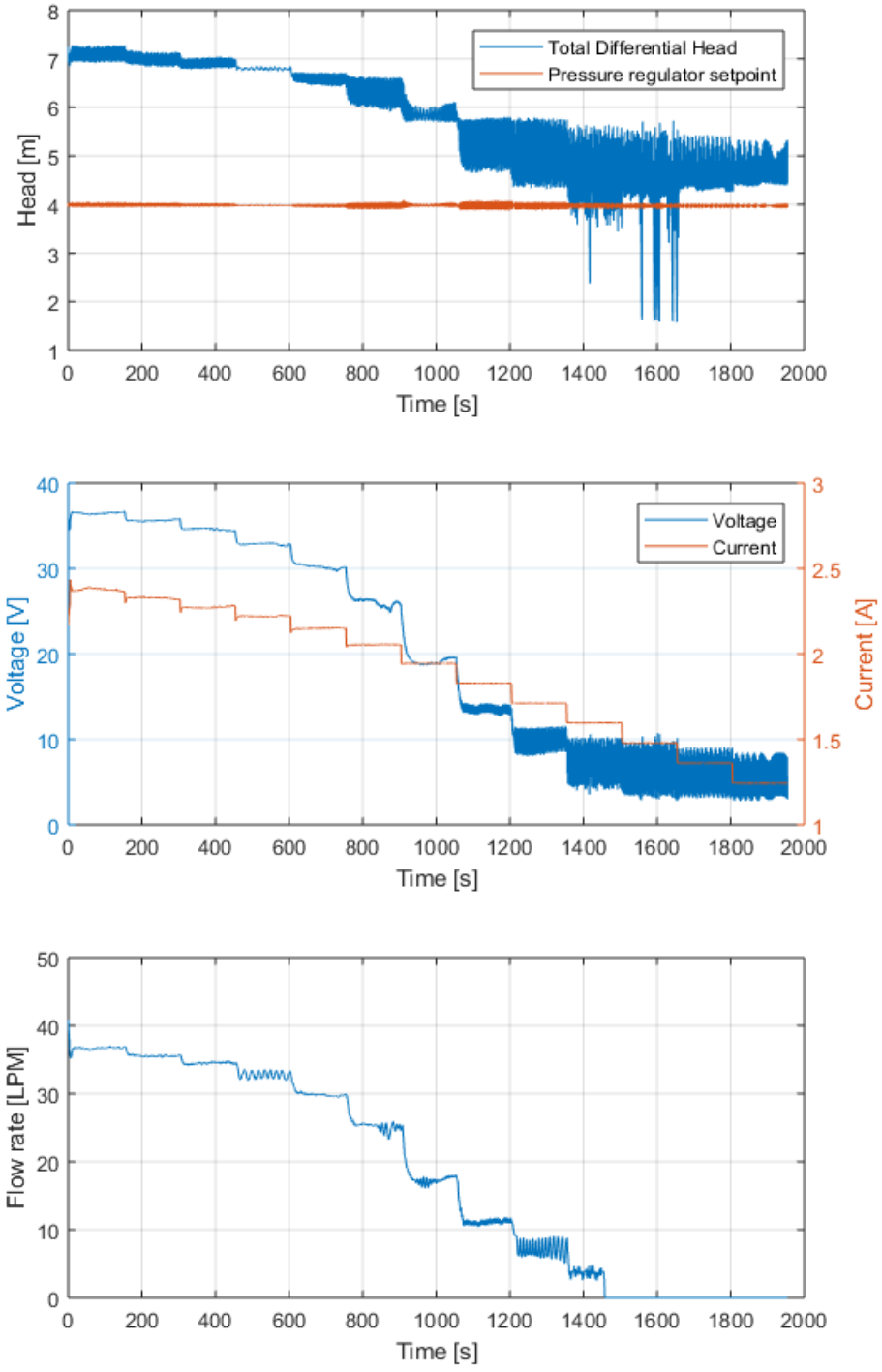

Fig. 8. Time domain results for PQ test with 90mm pulley gear, H5.

These results show that when the pump is actively moving large volumes of water the total differential head is much greater than the setpoint of the backpressure regulator; this makes sense, as the pump must overcome the backpressure between the regulator and the pressure transducer (see Fig. 1) in order to push water. The current drawn by the pump motor varies in response to the backpressure and the amount of irradiance available.

One drawback to the reciprocating piston pump is the output pressure experiences periodic ripple during each stroke of the piston. Because the SF2 uses only a single piston, this phenomenon is exaggerated. On each downstroke the output pressure peaks, while on each upstroke the pressure decreases. Using the backpressure regulator helped somewhat to minimize these periodic fluctuations.

The pressure regulator was more responsive to excursions where system pressure exceeded the setpoint than when system pressure fell below the setpoint. As a result, the maximum system pressure recorded during testing was roughly 10-30% above the average value, whereas min pressure could be 40-50+% below the average value. Additionally, there was an unexplained discrepancy between the pressure regulator feedback value and the static discharge pressure as measured by the transducer near the pump outlet. In general, the pressure transducer read 0.5-1.5psi above the pressure regulator feedback. The root cause for this discrepancy has not been investigated.

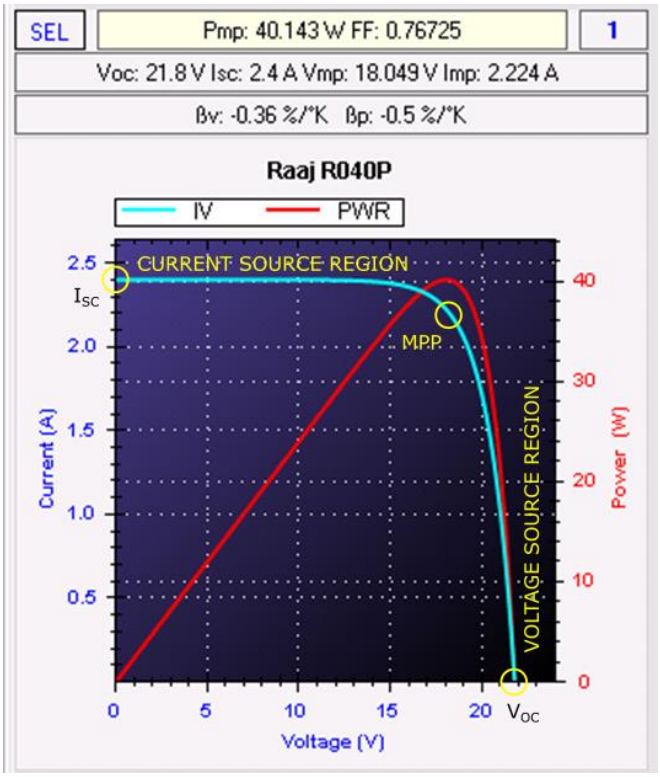

Fig. 9. Annotated PV current vs. voltage curve

The instantaneous values of current and voltage can vary significantly because there is no active regulation of current or voltage. When the hydraulic power demand is low relative

to the available power based on irradiance conditions, the motor tends to operate in the voltage source region of the PV, to the right of the Maximum Power Point (MPP) (see Fig. 9). When operating here, the input voltage to the motor is fairly constant, but there is significant ripple in the input current. A good example of this can be seen in Fig. 6 for time <1,000s. This current ripple shows up as ripple in the total differential head of the pump. This ripple is in addition to the natural pressure fluctuation that occurs due to the operating behavior of reciprocating piston pumps.

In contrast, when the hydraulic power is high relative to the power available based on irradiance, the motor tends to operate in the current source region of the PV, to the left of the MPP. In this operating region, the current tends to be fairly constant, but the voltage can vary significantly. When this happens, both pumping head and flow rate experience marked instability. As irradiance continues to decrease, voltage instability tends to increase, until eventually the measured flow rate drops to zero. Both Fig. 5 and Fig. 7 illustrate this phenomenon.

The nine flow rate vs. power (Q vs. P) curves that were created for the 50mm pulley are plotted in Fig. 10. These show that, unsurprisingly, the highest flow rates were achieved with the lowest system pressures and vice versa. The highest flow rate that was observed was 28.6LPM with the backpressure regulator full open (no applied pressure) and 1,100W/m^2 of irradiance. The highest differential head that was recorded was 17m.

The trajectory indicates that additional flow could have been achieved for all pressures had more input power been available. However, as this test was conducted with only two simulated modules (80W total), the flow rates at higher levels of input power were not investigated.

Note that the head values given in the legend are averages across the total run but, as mentioned before, differential head tended to marginally increase with flow rate at each specific head test point.

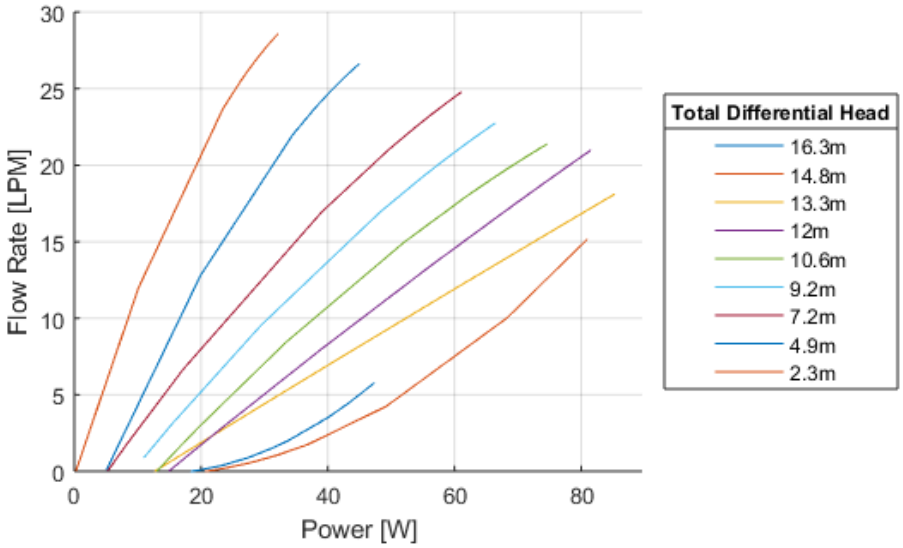

Fig. 10. Flow Rate vs. Power for 50mm pulley gear

The efficiency versus power for the pump system is plotted in Fig. 11. The Best Efficiency Point (BEP) for the test was found to be 55.2% with a differential head of 9.6m, a flow rate of 22.5LPM, and an input power of 64.2W (input irradiance was 950W/m^2).

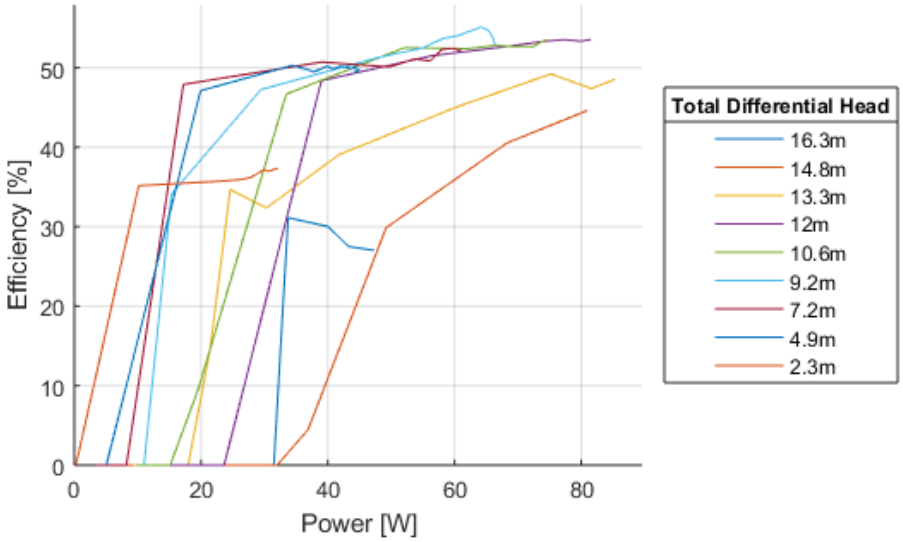

Fig. 11. Efficiency vs. Power for 50mm pulley gear

The nine flow rate vs. power (Q vs. P) curves that were created for the 90mm pulley are plotted in Fig. 12. These show a similar trend to those created using the 50mm pulley (Fig. 10). The highest flow rate that was observed was 43.1LPM, around 50% greater than the maximum flow rate that could be achieved with the 50mm pulley. However, the maximum differential head was only 8.7m, or roughly half the maximum head of the 50mm pulley.

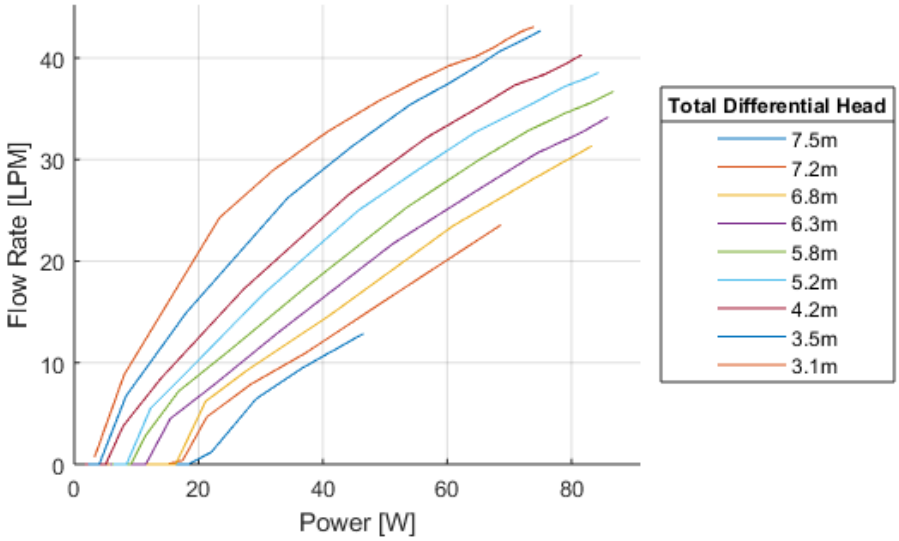

Fig. 12. Flow Rate vs. Power for 90mm pulley gear.

The efficiency vs. power for the 90mm pulley gear is plotted in Fig. 13. The BEP was found to be 51.4% with a differential head of 8.4 and a flow rate of 31.3LPM. Power input was 83.3W and corresponded to an operating point of 1,100W/m^2 and 25^{o}C.

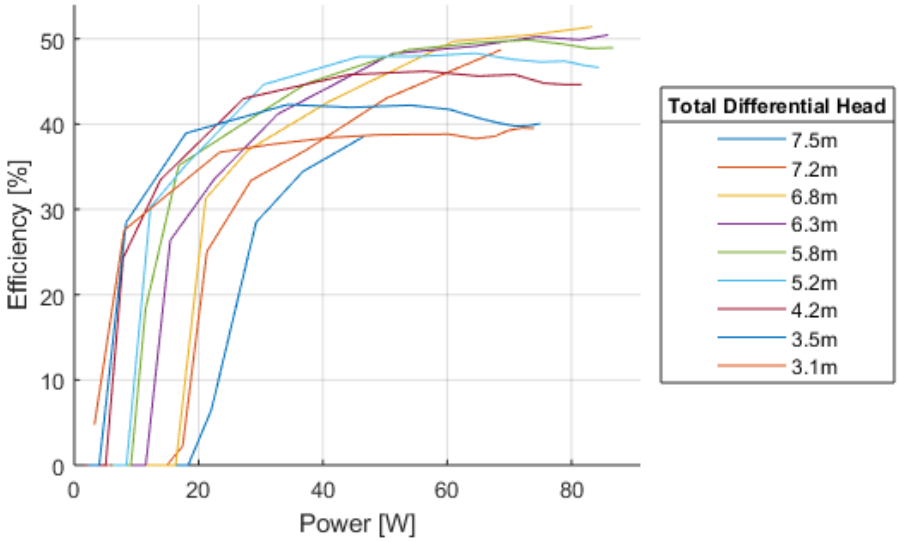

Fig. 13. Efficiency vs. Power for 90mm pulley gear

For the test points (12 points, according to Fig. 2) at each head value (H1 – H9) in the PQ test, the efficiency was averaged to generate one average efficiency for each head value. Fig. 14 displays the average efficiency curve for both pulleys during the PQ test.

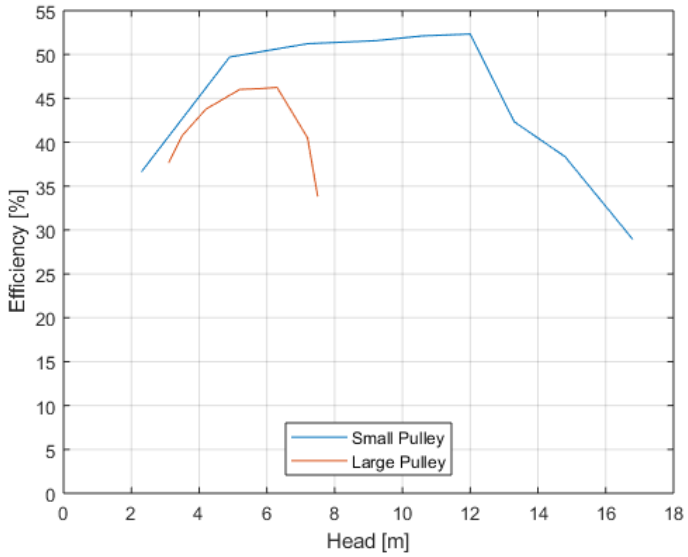

Fig. 14. Average Efficiency vs. Head for both pulleys over the PQ tests

5.2 HQ Characterization results

The HQ tests were conducted at STC as defined in section 4.2, with the backpressure initially high enough to prevent any flow. The backpressure was steadily reduced until the pump was in free flow (no applied backpressure). Data was collected using Labview and the results were analyzed using Matlab.

Total differential head and efficiency were calculated using EQ. 7 and EQ. 8.
The time domain results for the HQ characterization test using the small (50mm) pulley gear are shown in Fig. 15. At the beginning of the test, when the applied backpressure was greatest, the PV input was operating in current source mode: the current was saturated at the short circuit current and the voltage experienced large, rapid fluctuations. As the backpressure decreased the current demand of the motor decreased, and the voltage fluctuations dampened. A similar result can be seen in the results for the 90mm pulley gear, shown in Fig. 16.

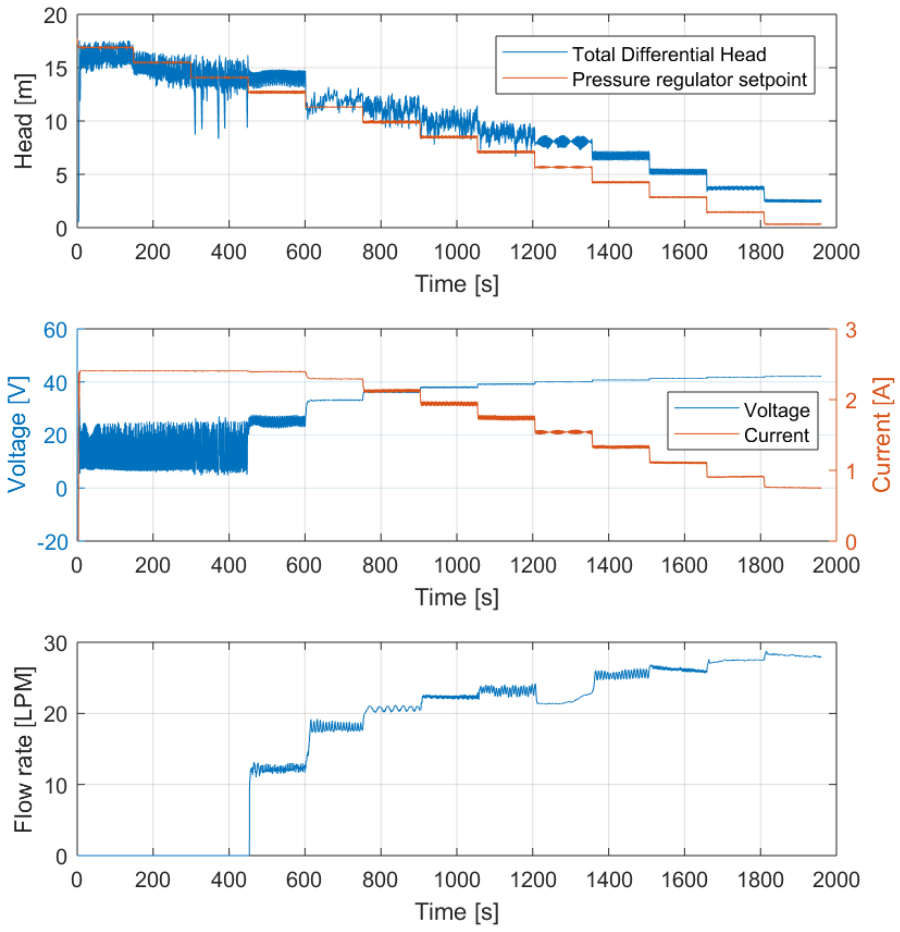

Fig. 15. Time domain results for HQ test with 50mm pulley gear.

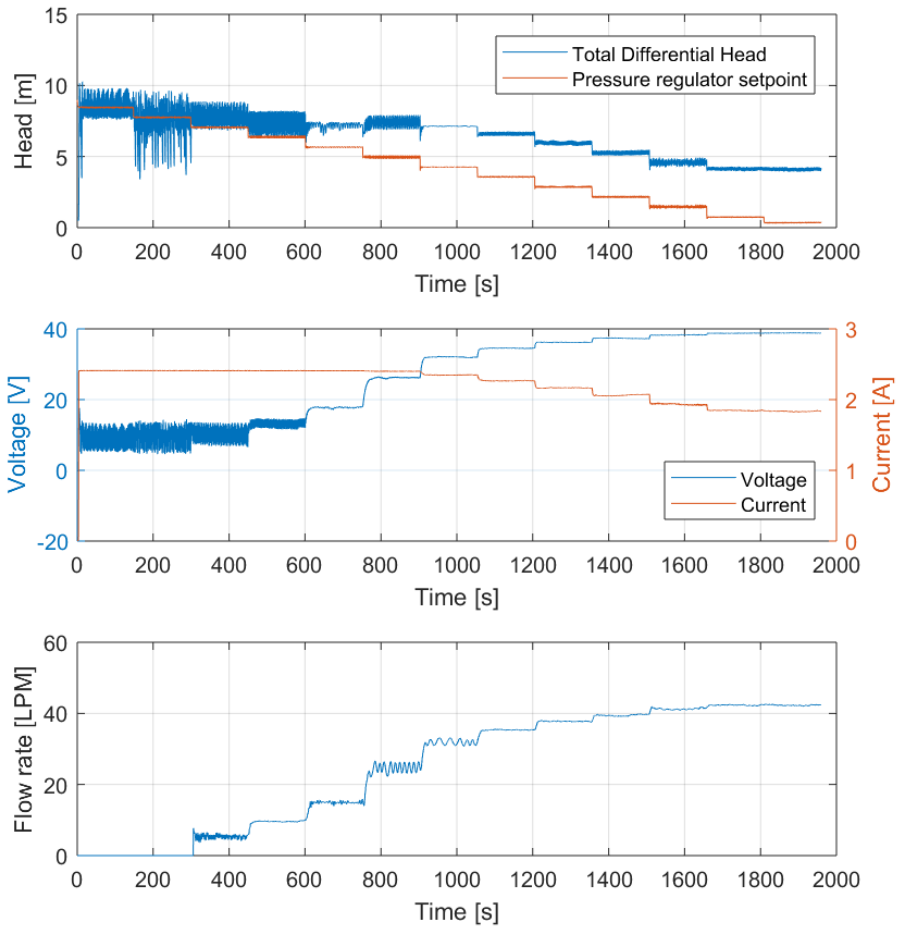

Fig. 16. Time domain results for HQ test with 90mm pulley gear.

The average flow rate versus total differential head for both the 50mm and 90mm pulley gears is plotted in Fig. 17. This figure can be compared to the figure in the datasheet (Appendix A). The highest steady state flow rate that was achieved during this testing was 28.2LPM (1,692L/hr) when using the 50mm pulley gear and 43.2LPM (2,592L/hr) when using the 90mm pulley gear; in both cases maximum flow occurred when the backpressure regulator was set to full open. Because this figure considers total differential pressure, the highest differential head when flow was present was slightly higher than when the pump was dead headed, as there was less suction pressure. The maximum heads when flow was present were 14.2m for the 50mm pulley gear and 7.8m with the 90mm pulley gear.

Peak efficiency for both pulley gears occurred when total differential head was around 7m. For the large pulley peak efficiency was 49.4% at 7.1m, then decreased sharply, reaching zero (when flow rate was zero) at 7.3m. For the small pulley, efficiency peaked at 51.8% and remained above 45% through 14m of head.

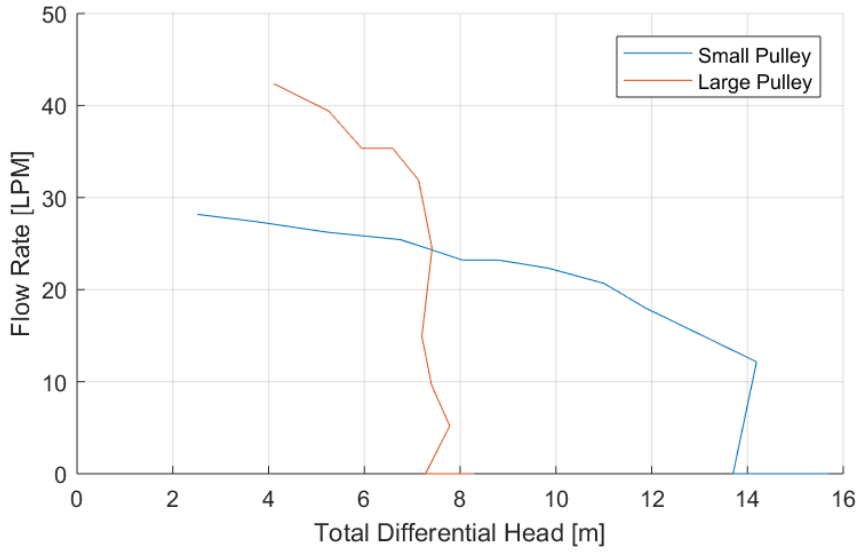

Fig. 17. Flow rate vs. Head for both small (50mm) and large (90mm) pulley gears at 1000 w/m^2.

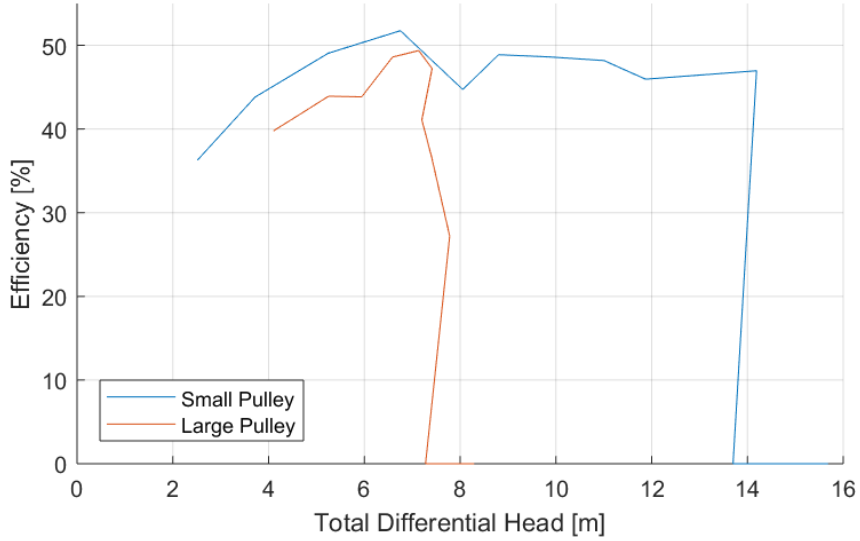

Fig. 18. Efficiency vs. Head for both small (50mm) and large (90mm) pulley gears at 1000 w/m^2.

6 Discussion and Conclusion

The SF2 solar pump system was tested according to a modified version of the test protocol outlined in IEC 62553 [1]. The pump was powered by two PV simulators each simulating a single RAAJ R040P 40W polycrystalline PV module. The test setup circulated water from a 208.2L (55 gallon) drum through a short section of 2.54cm (1") diameter PVC pipe. System pressure was maintained using an Equilibar backpressure regulator.

The PQ characterization was done over a range of backpressures from 90% of the maximum pressure to no pressure (full open). The input power was modified by incrementally reducing the simulated irradiance input of the PV simulator.

The pump motor had no voltage or current control. Instead, the motor was allowed to draw current freely based on the available input irradiance and pumping head. High pressure and/or low irradiance caused the simulated PV input to enter its current source region, which resulted in an unstable input voltage. This voltage instability led to instability in motor speed, pumping pressure, and flow rate. Adding some sort of voltage control to stabilize it in this operating region would improve pump performance in high head/low irradiance conditions.

The pump test bench setup was effective at conducting the PQ and HQ testing, but further improvements can be made. Adding a thermocouple to record water temperature will help provide a more accurate measurement of differential head and efficiency. Adding closed loop pressure control would help in maintaining a more consistent backpressure across a wide range of power values. Another potential improvement to the test configuration would be the addition of an accumulator tank, which could potentially damp out some of the pulsations in pressure and flow rate.

Other potential future work includes data validation and calibration. Pressure transducers can be validated using a manometer. The discrepancy between the recorded pressure feedback from the backpressure regulator and the discharge pressure as recorded by the pressure transducer should be investigated. Flow rate measurements can be validated using a bucket and stop watch.

Finally, testing and validation of the stock PV modules that are supplied as part of the SF2 pump system was outside the scope of this testing. Future efforts should be focused on validating the PV modules using a pyranometer and measurements of backsheet module temperature to verify the manufacturer's values for maximum power voltage and current. Tests of the pump system using the actual PV modules should be conducted, and these results should be compared against the performance recorded using the PV simulator.

A note on manufacturer rating comparison: Among the tests completed, flow rates and achievable head aligned well with Futurepump's reported performance, but efficiency did not. The discrepancies may be due to the test method or instrument precision and need to be validated further.

7 References

[1] *Photovoltaic pumping systems – Design qualification and performance measurements* IEC Standard 62253, Edition 1.0, 2011-07

[2] *American National Standard for Reciprocating Pump Tests*, ANSI/HI Standard 6.6, 2015.

[3] *Hydraulic Institute Standard for Methods for Rotodynamic Pump Efficiency Testing*, HI 40.6, 2016.

[4] *IEEE Guide: Test Procedures for Direct-Current Machines*, IEEE Standard 113, 1985.

[5] T. Decker. *Technical Report: Income Generating Appliances*, Factor[e] Ventures, 2017.

Appendix A: SF2 Solar Irrigation Pump Datasheet

Futurepump

SF2 SOLAR IRRIGATION PUMP SYSTEM

The Futurepump SF2 is a robust surface pump designed to help smallholder farmers with shallow water sources **pump up to 1 litre per second of water** to their crops using the power of the sun.

The Futurepump SF2 has three main parts: **the PV panels** which convert sunlight into electrical energy to drive **the DC motor**, a specially-designed unit coupled to a flywheel, which drives a **pump**, a reciprocating, positive displacement, high efficiency piston pump.

BENEFITS

- No fuel or electricity costs
- Robust, and farmer-fixable (as simple as a bicycle)
- Designed with easy maintenance in mind
- Pumps enough to irrigate around an acre
- Ideal with tanks, sprinklers, hoses or drip systems
- Removable, folding PV panels reduces theft risk
- Supplied with 80W panel, upgradable to 120W
- Solar panel tilting system for best performance
- No damage caused by dry pumping
- Tolerant of grid, sand, mud and debris

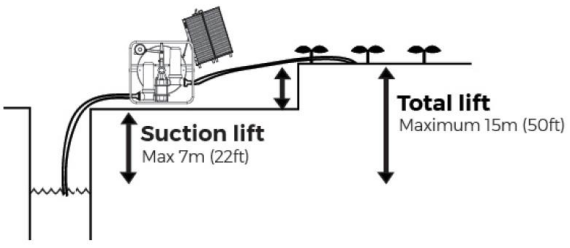

PERFORMANCE

At shallow heads, the Futurepump SF2 can deliver up to 1 litre per second, which is 3,600 litres/hour or over 21,000 litres per 6-hour pumping day (120W input).

	1 metre lift	6 metre lift
80W input	2,200 litres/hr	2,000 litres/hr
120W input	3,600 litres/hr	2,500 litres/hr

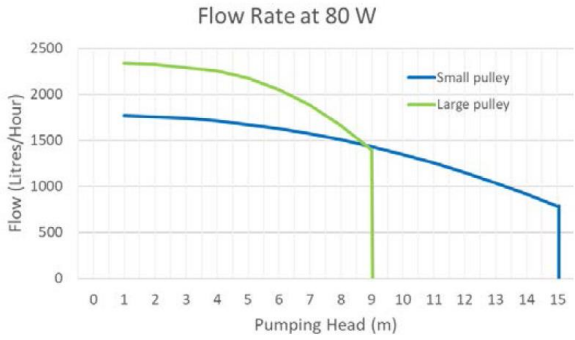

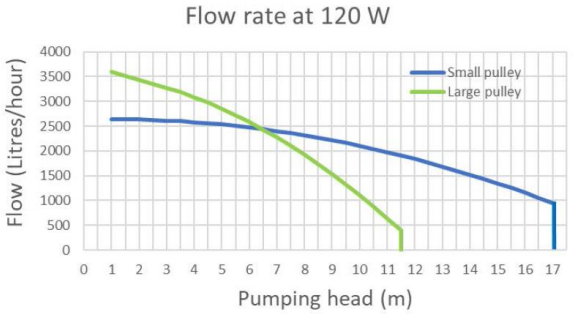

- Inlet side vertical suction limit: 7 metres
- Maximum total vertical lift: 15 metres
- Horizontal discharge: 500m+
- Peak system efficiency: 70%

ELECTRICAL / MECHANICAL

- Maximum pump voltage: 60V DC
- Maximum motor current: 5 amps DC
- Piston diameter: 104mm
- Inlet/outlets designed for $1^{1/4}$ (32mm) pipe
- Displacement volume per stroke: $150cm^3$
- Normal flywheel RPM range: 100-250 rpm
- 90mm pulley gear for 0–8m pumping heads
- 50mm pulley gear for >8m pumping heads

SF2 SOLAR IRRIGATION PUMP SYSTEM

REMOTE MONITORING

Every Futurepump SF2 pump includes remote performance monitoring at no extra cost.

- Minute-by-minute monitoring of pump vital signs - technical data displayed on a web dashboard accessible to distributors
- Monitoring of pump utilisation, including litres of water pumped, potential area irrigated, fuel savings, kWh produced,
- Pump geo-location tracking using google maps

PAY-AS-YOU-GO READY

- Ability for remote on-off switching (in seconds)
- Software integrations with leading PAYG management and billing platforms including Angaza, Lumeter and other proprietary systems.

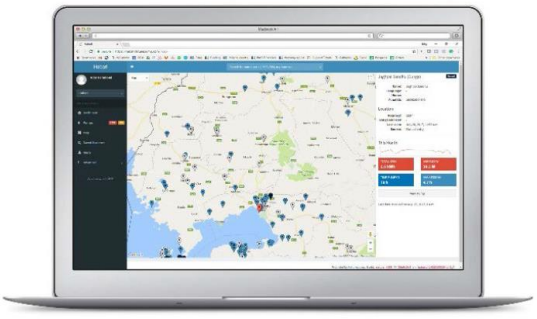

WEIGHT & DIMENSIONS

- Pump weight: 19.5kg
- Pump dimensions: 520mm x 530mm x 200mm
- Complete carton weight (including 80W PV and suction pipe): 36.7kg
- Carton volume: 0.150 CBM
- Supplied flexible inlet/suction pipe: Internal diameter of 31.8 mm, external diameter 38.8mm. 6000mm length

SPARE PARTS & TOOLS

- 3 x spare transmission belts
- 3 x spare piston seals
- 4 x adjustable hose clips
- 2 x $1^{1/4}$ inch pipe couplers
- 2 x $1^{1/4}$" -> $1^{1/2}$ inch reducers
- 1 x inlet filter/strainer
- 1 x pack stuffing box graphite packing rope
- 1 x complete set of spare o-ring seals

Toolkit: Three sizes of spanner, double ended screwdriver. Complete disassembly and reassembly possible with these tools.

STOCKISTS & PRICING

To find your nearest SF2 stockist and local pricing, please visit www.futurepump.com. For information on becoming a distributor in your country, please visit www.futurepump.com/distribute

Futurepump Ltd is proudly supported by Practica, iDE, USAID Powering Ag, AECF, REEEP and Village Capital.

WARRANTY & CERTIFICATION

The SF2 is supplied with a full five year manufacturer-backed warranty, which means servicing and parts will be provided free of charge to our customers over that period through our network of certified distribution partners.

The best support can be provided by warranty regsitration upon purchase via http://warranty.futurepump.com

The SF2 is manufactured in India by Futurepump in our factory which uses an ISO 9001:2015-certified quality management system.

Appendix B: RAAJ Solar Photovoltaic Module Datasheet

Solar PV Modules

RAAJ®

PRODUCT RANGE 020Wp to 325Wp

Poly Model	Cells	Voltage/ Wattage	Module Size [±1mm]	Packing Per MB	Weight of MB (KG)	Pmax (Wp)	Vmax (V)	Imax (Amp)	Voc (V)	Isc (Amp)	Module Eff. (%)
R020P	36	12V / 20Wp	548 x 338 x 38mm	10	34	20	17.46	1.15	21.60	1.24	10.79
R025P	36	12V / 25Wp	436 x 671 x 35mm	10	39	25	17.46	1.43	21.60	1.54	8.54
R030P	36	12V / 30Wp	436 x 671 x 35mm	10		30	17.46	1.72	21.60	1.85	10.25
R040P	36	12V / 40Wp	531 x 671 x 35mm	5	25	40	17.57	2.28	21.60	2.45	11.22
R050P	36	12V / 50Wp	636 x 671 x 35mm	5	29	50	17.57	2.85	21.60	3.06	11.71
R060P	36	12V / 60Wp	776 x 671 x 35mm	5	35	60	17.57	3.42	21.60	3.68	11.52
R075P	36	12V / 75Wp	776 x 671 x 35mm	5	35	75	17.57	4.27	21.60	4.59	14.40
R080P	36	12V / 80Wp	891 x 656 x 35mm	5	41	80	18.11	4.42	21.60	4.75	13.68
R085P	36	12V / 85Wp	956 x 671 x 35mm	5		85	18.09	4.70	21.60	5.05	13.25
R090P	36	12V / 90Wp		5		90	18.11	4.97	21.60	5.34	14.03
R100P	36	12V / 100Wp	1206 x 671 x 35mm	3	35	100	18.09	5.53	21.60	5.94	12.35
R110P	36	12V / 110Wp				110	18.18	6.06	21.60	6.51	13.59
R120P	36	12V / 120Wp				120	18.22	6.59	21.60	7.08	14.82
R150P	36	12V / 150Wp	1496 x 671 x 35mm	3	40	150	18.36	8.17	21.60	8.78	14.94
R160P	72	24V / 160Wp	1336 x 996 x 35mm	2	37	160	35.28	4.54	43.20	4.88	12.02
R175P	72	24V / 175Wp				175	35.89	4.88	43.20	5.25	13.15
R180P	72	24V / 180Wp				180	35.89	5.02	43.20	5.40	13.52
R185P	72	24V / 185Wp				185	36.72	5.04	43.20	5.42	13.90
R200P	60	20V / 200Wp	1336 x 996 x 35mm	2	37	200	30.60	6.54	36.00	7.03	15.03
R200P	72	24V / 200Wp	1496 x 996 x 35mm		40	200	36.72	5.45	43.20	5.86	13.42
R250P	60	20V / 250Wp	1640 x 990 x 35mm	2	45	250	30.60	8.17	36.00	8.78	15.39
R250P	72	24V / 250Wp				250	36.72	6.81	43.20	7.32	15.39
R260P	60	20V / 260Wp				260	30.60	8.50	36.00	9.14	16.01
R300P	72	24V / 300Wp	1960 x 990 x 35mm	2	53	300	36.11	8.31	43.20	8.93	15.46
R310P	72	24V / 310Wp				310	36.17	8.59	43.20	9.23	15.98
R315P	72	24V / 315Wp				315	36.29	8.68	43.20	9.33	16.23
R320P	72	24V / 320Wp				320	36.50	8.77	43.20	9.42	16.49
R325P	72	24V / 325Wp				325	36.72	8.86	43.20	9.52	16.75

Note: All electrical parameters specified at Standard Test Condition (STC) : 25°C, 1000W / m^2 irradiance, Spectrum Air Mass: 1.5AM

Type of Cell : Mono / Multi Crystalline Solar Cell

Power tolerance : ± 3%, Maximum

System Voltage : 1000VDC, UL - 600V

25 Years Linear Output Warranty

- 90% of rated power output for first 10 years
- 80% of rated power output for next 15 years
- 10 years warranty on materials and workmanship

Comprehensive Certificates

- UL certified IEC 61215, IEC 61730, IEC 61701
- MNRE certificate, MNRE channel partner, for grid connected
- ISO 9001 : 2008, ISO 14001 : 2004
- OHSAS 18001 : 2007

Raajratna Ventures Ltd.

A Govt. Recognized Star Export House

Manufacturer & Exporter of : Stainless Steel Fasteners | Stainless Steel Hollow Sections | Solar P V Modules

OFFICE : 1006, Sukhsagar Complex, Nr. Fortune Landmark Hotel, Usmanpura, Ashram Road, Ahmedabad 380 014, Gujarat, India

Tel : +91-79-2756 1915 / 16 / 17 **Fax :** +91-79-2756 1918 **E-mail :** sales@raajsolar.com **Web : www.raajsolar.com**

Appendix C: Data file description

The complete data results that were captured during testing can be found in "Solar Water Pump Test Data_CSU2018.xls". This workbook combines the data results for all testing, with one sheet per test. Data for 20 tests total are included. These are:

- 50mm Pulley PQ H1 through 50mm Pulley PQ H9 – Results from the flow rate versus power (PQ) characterization tests using the small (50mm) pulley gear for nine values of applied head H1-H9
- 90mm Pulley PQ H1 through p0mm Pulley PQ H9 – Results from the flow rate versus power (PQ) characterization tests using the large (90mm) pulley gear for nine values of applied head H1-H9
- 50mm Pulley HQ – Results from the flow rate versus head (HQ) characterization tests using the small (50mm) pulley gear
- 90mm Pulley HQ – Results from the flow rate versus head (HQ) characterization tests using the large (90mm) pulley gear

The data columns for the steady state data are as follows:

- Column A – Elapsed time in seconds. Each test starts from time t=0.
- Column B – DC voltage applied to the pump motor
- Column C – DC current applied to the pump motor
- Column D – Discharge gauge pressure as measured by the pressure transducer, in pounds per square inch (PSI)
- Column E – Suction gauge pressure as measured by the pressure transducer, in pounds per square inch (PSI)
- Column F – Feedback signal from backpressure regulator, in pounds per square inch (PSI)
- Column G – Motor pulley speed as recorded by optical speed sensor, in radians per second
- Column H – Flow rate in liters per minute (LPM)
- Column I – Constant value for Eqn. 7 in meters (m)